Experimental Investigations on Natural Gas-Diesel Dual Fuel Combustion

Garcia, Pablo

2018

Document Version:
Publisher's PDF, also known as Version of record

Experimental Investigations on Natural Gas-Diesel Dual Fuel Combustion

Experimental Investigations on Natural Gas-Diesel Dual Fuel Combustion

by Pablo García Valladolid

LUND
UNIVERSITY

Thesis for the degree of Doctor of Philosophy

Thesis main advisor: Dr. Per Tunestål
Thesis co-advisor: Dr. Öivind Andersson
Thesis co-advisor: Dr. Antonio García (CMT, Spain)

Faculty opponent: Dr. Jesper Schramm (DTU, Denmark)

To be presented, with the permission of the Faculty of Engineering of Lund University, for public criticism in the MA:3 lecture hall at the Annexet-Building, LTH on Friday, the 15th of June 2018 at 10:00.

Organization	Document name
LUND UNIVERSITY Department of Energy Sciences Box 188 SE–221 00 LUND Sweden	**DOCTORAL DISSERTATION** Date of disputation 2018-06-15 Sponsoring organization
Author(s) Pablo García Valladolid	

Title and subtitle

Experimental Investigations on Natural Gas-Diesel Dual Fuel Combustion

Abstract

Natural gas has been traditionally applied in spark-ignited combustion engines due to similar combustion characteristics for methane gas and gasoline. However, spark ignition requires a low compression ratio to avoid knock problems and therefore, gas engines have lower efficiency than diesel engines. A combustion concept that has been successfully applied on large stationary engines and to some extent on heavy duty engines is dual fuel combustion, where a compression ignited diesel pilot injection is used to ignite a homogeneous charge of natural gas and air. This dual fuel combustion concept is well established for large stationary engines and exists as an after-market solution for heavy duty engines but does not exist at all for light duty engines. This concept offers a high degree of flexibility for the engine operation because dual fuel combustion does not require heavy modifications of the original diesel engine architecture, so diesel operation could remain unaltered. The scope of this thesis is to explore the implementation of this dual fuel concept on different types of applications using the diesel injection system as an alternative ignition system for lean natural gas mixtures. The main objectives are the identification of pathways to increase combustion efficiency at low loads, improve the understanding of how pilot injection should be controlled over the entire operating range and finally, analyze the interaction between the pilot and main air-gas charge. Experiments resulted in robust and efficient high gas fraction dual fuel operation from 5 bar $IMEP_g$. Below this load, insufficient exhaust energy limits the applicability of this concept. The pathways explored to increase combustion efficiency at low load resulted in a minimum gross indicated efficiency of 40% from 3 bar $IMEP_g$. Moreover, the use of alternative pilot injection strategies allow a simultaneous reduction of TUHC and NO_x emissions and knock-free operation. Under certain conditions, operation without NO_x after-treatment system is possible. This requires operation near the lean limit, which has been experimentally evaluated and a gas equivalence ratio of 0.44 is proposed, considering methane emissions and exhaust temperature levels.

Key words

Dual Fuel, Diesel, Natural Gas, Pilot Injection, Combustion Efficiency, Methane, Nitrogen Oxides, Lean Operation, Ignition

Classification system and/or index terms (if any)

Supplementary bibliographical information	Language
	English
ISSN and key title 0282-1990	ISBN 9789177536970 (print) 9789177536987 (pdf)
Recipient's notes	Number of pages 202 / Price
	Security classification

Experimental Investigations on Natural Gas-Diesel Dual Fuel Combustion

by Pablo García Valladolid

LUND
UNIVERSITY

Funding information: The thesis work was financially supported by the Swedish Energy Agency, grant number 35721-1, and the KCFP Engine Research Center

Faculty of Engineering, Department of Energy Sciences

ISBN: 9789177536970 (print)
ISBN: 9789177536987 (pdf)
ISSN: 0282-1990
ISRN: LUTMDN/TMHP-18/1138-SE

Printed in Sweden by Tryckeriet i E-huset, Lund University, Lund 2018

Dedicado a mis padres, María y Ángel...

Contents

List of publications

This thesis is based on the following publications, which will be referenced by roman numericals in the body text of this thesis. The papers are appended in the order listed below:

I **Experimental Investigation on CNG-Diesel Combustion Modes under Highly Diluted Conditions on a Light Duty Diesel Engine with Focus on Injection Strategy**

P. García, P. Tunestål

SAE Int. J. Engines 8(5):2177-2187, 2015, 2015-24-2439

II **Effects of Intake Manifold Conditions on Dual Fuel CNG-Diesel Combustion in a Light Duty Diesel Engine Operated at Low Loads**

P. García, P. Tunestål

SAE Technical Paper 2016-01-0805, 2016

III **Analysis of Dual-Fuel CNG-Diesel Combustion Modes Towards High Efficiency and Low Emissions at Part Load**

P. García, P. Tunestål

Proc. 36th FISITA World Automotive Congress, 2016, Busan, South Korea

IV **Impact of Diesel Pilot Distribution on the Ignition Process of a Dual Fuel Medium Speed Marine Engine**

P. García, P. Tunestål, J. Monsalve-Serrano, A. García, J. Hyvönen

Energy Conversion and Management, 149:192-205, 2017

Other non-related publications:

Lift-off Lengths in an Optical Heavy-Duty Engine Operated at High Load with Low and High Octane Number Fuels

M. Lundgren, A. Matamis, Z. Wang, **P. García**, M. Richter, O. Andersson, A. Andersson

SAE Technical Paper 2018-01-0245, 2018

Acknowledgements

Back in 2013, I decided to start this journey. Honestly, I must admit now that I had no idea about the real task I had in front of me. These years have consisted of several *ups* and *downs* which sometimes really made me enjoy my work and time here, but on other occasions, I have been quite tempted to give up and go back home (the *sunny one*). Fortunately, that was not the case.

First of all, I would like to thank my supervisor Per Tunestål for his unconditional support and for the freedom he gave me during my studies to explore my own interests and ideas. I think I have evolved as a researcher but also as a person during our collaboration and I do believe he has had an impact on both aspects.

I would like to express my gratitude to all the other "seniors" from Lund University who have somehow had an impact on this work. Special thanks to Öivind Andersson, Martin Tuner, Bengt Johansson and all the laboratory managers that I have worked with during these years. I would also like to acknowledge the daily support that the administration and IT groups (Catarina, Elna, Gity, Krister, Robert, etc.) provide to the rest of employees of the Division of Combustion Engines. *Tack!*

I am really grateful to Jari Hyvönen and the rest of the Wärtsilä team for their active support during our 2 years of collaboration. *Kiitos!*

I would like to thank Antonio García for his active supervision during the last stage of my Ph.D. studies and for being a good friend. Many thanks also to Javier Monsalve-Serrano for his contribution to this work. *Muchas gracias*!

I have spent many hours (probably too many) setting up and commissioning engine test cells and setups. Thanks to all technicians who have contributed throughout this process. I think I have learned a lot from all of you. Special thanks go to Anders Olsson, Mats Bengtsson and Tomas Linden for all their support and the nice chats we have had during these years. I would also like to thank Tommy Petersen for having such a nice music taste, for his unconditional help and for being a good friend.

I would like to thank all my colleagues and friends from the Division of Combustion Engines. The list would be too long to mention you all. In particular, I would like to thank Marcus Lundgren, Slavey Tanov, Nhut

Lam, Guillaume Lequien and Lianhao Yin for the good times we had at and outside work.

It would be difficult to understand these 5 years without you, Sonia. I will keep it simple: *Te quiero. Gracias por todo.*

Last but not least, "*mi familia*". My apologies to all the ones who cannot read it, but I must write these last words in Spanish. *Es difícil de expresar lo agradecido que estoy a todos vosotros. Me siento un privilegiado por tener una familia como la que tengo y no cambiaría ni un solo ápice de ella. Mis decisiones me han llevado, hasta el momento, a vivir el día a día lejos de vosotros durante los ultimos 12 años y por eso os quiero pedir perdón. De corazón, gracias. Os quiero.*

Abstract

The general objective of this thesis is to contribute to the understanding of how the pilot ignited natural gas dual fuel combustion process should be optimized for its implementation in different fields of application. Natural gas has been traditionally applied in spark-ignited combustion engines due to similar combustion characteristics for methane gas and gasoline. However, spark ignition requires a low compression ratio to avoid knock problems and therefore, gas engines have lower efficiency than diesel engines. A combustion concept that has been successfully applied on large stationary engines and to some extent on heavy duty engines is dual fuel combustion, where a compression ignited diesel pilot injection is used to ignite a homogeneous charge of natural gas and air. This dual fuel combustion concept is well established for large stationary engines and exists as an after-market solution for heavy duty engines but does not exist at all for light duty engines. This concept offers a high degree of flexibility for the engine operation because dual fuel combustion does not require heavy modifications of the original diesel engine architecture, so diesel operation could remain unaltered.

The scope of this thesis is to explore the implementation of this dual fuel concept on different types of applications using the diesel injection system as an alternative ignition system for lean natural gas mixtures. The main objectives are the identification of different potential pathways to increase combustion efficiency at low loads, improve the understanding of how pilot injection should be controlled over the entire operating range and finally, analyze the interaction between the pilot and main air-gas charge.

Experiments resulted in robust and efficient high gas fraction dual fuel operation from 5 bar $IMEP_g$. Below this load, insufficient exhaust energy limits the applicability of this concept. The pathways explored to increase combustion efficiency at low load resulted in a minimum gross indicated efficiency of 40% from 3 bar $IMEP_g$. Moreover, the use of alternative pilot injection strategies allows a simultaneous reduction of TUHC and NO_x emissions and knock-free operation. Under certain conditions, operation without NO_x after-treatment system is possible. This requires operation near the lean limit, which has been experimentally evaluated and a gas equivalence ratio of 0.44 is proposed, considering methane emissions and exhaust temperature levels.

Populärvetenskaplig sammanfattning på svenska

Naturgas har traditionellt använts i gnistantända förbränningsmotorer på grund av liknande förbränningsegenskaper som bensin. Detta medför emellertid generellt att gasmotorer har lägre verkningsgrad än dieselmotorer. Ett förbränningskoncept som framgångsrikt har tillämpats på stora stationära motorer och till viss del även på tunga motorer är att använda två bränslen, så kallat Dual Fuel Combustion. Principen innebär att en pilotinsprutning med diesel används för att antända en homogen blandning av naturgas och luft. Detta förbränningskoncept är väl etablerat för stora stationära motorer och existerar som en eftermarknadslösning för tunga motorer men finns inte alls för mindre motorer till t.ex, personbilar. Detta koncept ger en hög grad av flexibilitet för motordrift eftersom Dual Fuel inte kräver omfattande ändringar av den ursprungliga dieselmotorarkitekturen, så dieseldriften kan förbli oförändrad.

Syftet med denna avhandling är att undersöka implementeringen av Dual Fuel på olika typer av motorer, då med dieselinjektion som ett alternativt tändsystem till tändstift för magra naturgasblandningar. De viktigaste målen är identifiering av olika potentiella vägar för att öka förbränningsverkningsgraden vid låga belastningar, förbättra förståelsen för hur pilotinsprutningen med diesel ska styras över hela arbetsområdet och slutligen analysera samspelet mellan pilotinsprutningen och det huvudsakliga bränsleförhållandet mellan naturgas och luft.

Genomförda motorexperiment visar på höga verkningsgrader vid motorlaster överstigande 5 bar IMEP_g. Vid lägre laster räcker inte energin i avgaserna till för att möjliggöra detta driftläge. Undersökningar med syftet att öka förbränningsverkningsgraden vid låga laster resulterade i att den indikerade verkningsgraden (brutto) var som sämst 40% vid laster över 3 bar IMEP_g. Dessutom kan alternativa strategier för pilotinjektioner reducera utsläppen av både oförbrända kolväten och kväveoxider samtidigt som problem med motorknack kan undvikas. Vid vissa driftspunkter är utsläppen av kväveoxider tillräckligt låga för att helt eliminera behovet av avgasrening av dessa utsläpp. För att uppnå låga kväveoxider-utsläpp krävs att motorn körs med en bränsleblandning som är nära magergränsen. Experimentella studier visar att denna gräns är vid 0.44 i bränsle/luft-förhållande (relativt stökiometrisk bränsle/luftblandning) när utsläppen av metan och nivåerna på avgastemperaturen beaktas.

Abbreviations and Symbols

ICE	Internal combustion engine
1D	One-dimensional
ATDC	After top dead center
BDC	Bottom dead center
BTDC	Before top dead center
CA05	Crank angle degree at 5% fuel mass burnt
CA10	Crank angle degree at 10% fuel mass burnt
CA50	Crank angle degree at 50% fuel mass burnt
CA90	Crank angle degree at 90% fuel mass burnt
CAD	Crank angle degree
CCM	Cylinder control module
CDC	Conventional diesel combustion
CDF	Conventional dual fuel
CFD	Computational fluid dynamics
CI	Compression ignition
CN	Cetane number
CNC	Conventional natural gas combustion
CNG	Compressed natural gas
COV	Coefficient of variation
DF	Dual fuel
DI	Direct injection
ECA	Emission control area
ECM	Engine control module
EGR	Exhaust gas recirculation
EHVA	Electro hydraulic valve actuation
EOI	End of injection
EPA	US Environmental protection agency
ESC	European stationary cycle
ETC	European transient cycle
FPGA	Field-programmable gate array
FS	Full scale
GF	Gas fraction
GHG	Greenhouse gases
GWP	Global warming potential
H/C	Hydrogen-to-carbon ratio
HC	Hydrocarbon
HCCI	Homogeneous charge compression ignition
HD	Heavy duty
HRF	High reactivity fuel
HT	High temperature
ID	Ignition delay
IMEP	Indicated mean effective pressure
IMO	International maritime organization
IMPG	Integral modulus of pressure gradient
IVC	Intake valve closing
LD	Light duty
LHV	Lower heating value

LNG	Liquified natural gas
LRF	Low reactivity fuel
LT	Low temperature
LTC	Low temperature combustion
MCP	Medium combustion plant
MN	Methane number
MOC	Methane oxidation catalyst
NMHC	Non-methane hydrocarbon
OEM	Original equipment manufacturer
PFI	Port fuel injection
PI	Positive ignition
PM	Particulate matter
PN	Particulate number
PPCI	Partially premixed compression ignition
RCCI	Reactivity controlled compression ignition
RoHR	Rate of heat release
RON	Research octane number
RPM	Revolutions per minute
SCR	Selective catalytic reduction
SI	Spark ignition
SOC	Start of combustion
SOI	Start of injection
STP	Standard temperature and pressure
TDC	Top dead center
TUHC	Total unburnt hydrocarbons
TWC	Three-way catalyst
WHSC	World harmonized stationary cycle
WHTC	World harmonized transient cycle
WTW	Well-to-wheel
λ	Lambda
θ	Mean value
ϕ	Equivalence ratio
σ	Standard deviation
$\mathbf{CH_4}$	Methane
CO	Carbon monoxide
$\mathbf{CO_2}$	Carbon dioxide
$\mathbf{H_2O}$	Water
$\mathbf{N_2}$	Nitrogen
$\mathbf{NH_3}$	Ammonia
$\mathbf{NO_x}$	Nitrogen oxides
$\mathbf{O_2}$	Oxygen
$\mathbf{SO_x}$	Sulphur oxides

CHAPTER 1

INTRODUCTION

1.1 Introduction

1.2 Framework of Internal Combustion Engines

The development of the modern internal combustion engine (ICE) by Étienne Lenoir, Nikolaus Otto or Rudolf Diesel, among others, during the last decades of the 19^{th} century has been one of the major contributions to the economic development of contemporary societies. Owing partly to its high power-to-weight ratio, the ICE can be found in several different types of applications, such as transportation of people and goods via both land and waterways, power generation, or industrial applications.

The most common working principle for ICEs is the 4-stroke cycle. The term *stroke* corresponds to the motion of the piston between its upper and lower positions in the cylinder. The lowest position is normally referred to as *bottom dead center* (BDC), while the highest is named *top dead center* (TDC). The classical direct injection (DI) diesel engine operating principle is explained here as example of simplified 4-stroke engine operation. The cycle is divided into 4 different phases. It begins with the intake stroke, where the piston moves from TDC to BDC while the intake valve is open and air is pulled into the cylinder. Once the

intake valve is closed, the second stroke starts with the compression of the air as the piston moves from BDC to TDC. This causes an increase of pressure and temperature in the combustion chamber. Then, near the TDC position, a certain amount of liquid fuel is introduced in the combustion chamber via a fuel injector. This fuel mass vaporizes, mixes with the surrounding air and finally auto-ignites, resulting in a combustion event. This translates into a fast increase of pressure and temperature in the combustion chamber, which transfers mechanical work to the crank mechanism consisting of the piston, the connecting rod and the crankshaft. The piston moves from TDC to BDC during this expansion stroke until the exhaust valve is opened. Here, the exhaust stroke starts and the piston returns from BDC to TDC while the exhaust valve is open to expel the remaining exhaust gases from the cylinder. Finally, the exhaust valve is closed, the intake valve opened and the cycle is repeated.

The ICE is normally based on the oxidation of carbon-based fuel molecules in a combustion process. Consequently, all fuel would be converted to carbon dioxide (CO_2) and water in an ideal cycle. However, incomplete combustion and the presence of other molecules such as nitrogen or sulphur promote the formation of other species. The major ones are total unburned hydrocarbons (TUHC), carbon monoxide (CO), nitrogen oxides (NO_x), soot and sulphur oxides (SO_x).

The full deployment of the ICE in society and the steady increase in world population have caused an increase of oil consumption for transportation purposes, as depicted in Figure 1.1 [1]. This has resulted in an increase of the global emissions of green house gases (GHG)

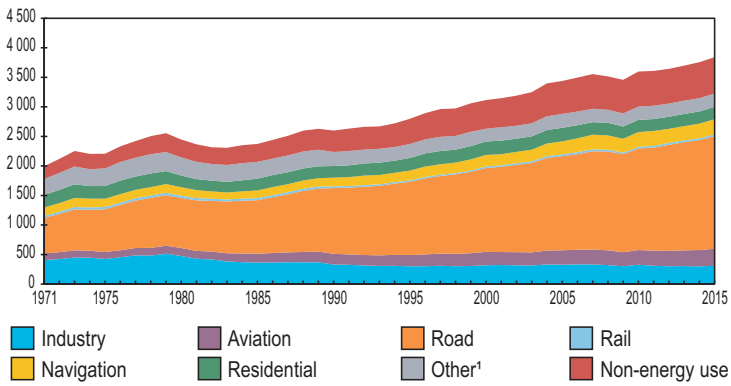

Figure 1.1: World oil total final consumption evolution by sector, in Mtoe units. Source: IEA

from fossil fuel combustion during recent decades. Currently, the transportation sector accounts for roughly 24% of the total world CO_2 emissions from fuel combustion [2]. In addition to this global effect, the use of ICEs also implies local threats due to the negative effects of NO_x, TUHC, CO and particulate matter (PM) on human health. As a result, these topics motivated the implementation of the first emission legislations during the last decades of the 20^{th} century. Since then, stringent emission legislation has driven the development of the ICE, resulting in more efficient and cleaner combustion engine applications, while maintaining engine performance.

However, the overall transportation sector is currently facing new challenges. Concerns about the effective local pollution impact of ICEs in large cities and recent OEM emission control scandals have forced authorities to implement, in some cases, countermeasures for directly reducing the use of ICE powered vehicles. Simultaneously, the development of electrical vehicles, the global policy of less dependence on fossil fuels and the appearance of new emission legislations on previously unregulated sectors are likely to substantially change the transportation sector in the future. Nevertheless, the ICE is still expected to be part of future technology solutions [3] and consequently, more efforts on efficiency maximization and pollutant emission minimization will be required. This scenario has increased the interest in low-carbon fuels and alternative combustion modes and natural gas fits particularly well in this transition due to its potential well-to-wheel (WTW) CO_2 benefits, particularly if produced from local bio-sources [4].

Natural gas has been traditionally applied in spark-ignited (SI) combustion engines due to similar combustion characteristics for methane gas and gasoline. However, spark ignition requires a low compression ratio to avoid knock problems and therefore, gas engines have lower efficiency than diesel engines. A combustion concept that has been successfully applied on large stationary engines and to some extent on heavy duty engines is dual fuel combustion, where a compression ignited diesel pilot injection is used to ignite a homogeneous charge of natural gas and air. This dual fuel combustion concept is well established for large stationary engines and exists as an after-market solution for heavy duty engines but does not exist at all for light duty engines. This concept offers a high degree of flexibility for the engine operation because dual fuel combustion does not require heavy modifications of the original diesel engine architecture so diesel operation could remain unaltered.

1.3 Research Scope

The scope of this thesis is to explore the implementation of the dual fuel concept in different types of applications using the diesel injection system as an alternative ignition system for lean natural gas mixtures.

The first part of the research presented in this thesis is focused on *light duty applications*. No commercial light duty engine applications exist to date. For that reason, this stage of the research aimed to identify the main limitations of the combustion concept for light duty applications. The extended use of natural gas to diesel engines for passenger vehicles can provide a short-term solution to the recent problems associated with diesel engines, such as concerns about local air pollution in large cities, but also benefits in terms of well-to-wheel emissions. For these reasons, studies were carried out in a modern Volvo D4 light duty multi-cylinder diesel engine (82 mm bore, 0.49 liters displacement per cylinder) modified for dual fuel operation. Special focus was put on CH_4 emissions and the feasibility of the after-treatment system.

The previous investigations pointed out the importance of the ignition delay on the overall performance of dual fuel combustion. For that reason, further focus was put on the ignition process. In particular, there is still no consensus about the characteristics of the ignition process on *medium speed marine engines* running in dual fuel mode. Moreover, the lack of validation data limits the applicability of the existing computational fluid dynamics (CFD) dual fuel models. On top of the previous facts, stringent emission legislation in this sector is forcing industry to find alternative solutions to diesel operation. Consequently, the main goal of this stage was to provide deeper insights about the ignition process and interaction between diesel and natural gas fuels in dual fuel combustion. For that reason, studies were carried out in a single-cylinder Wärtsilä 20DF research engine (200 mm bore, 8.8 liters unitary displacement). The tests were complemented with simulations of diesel sprays, which were performed in collaboration with the CMT-Motores Térmicos research center (Valencia, Spain). Special focus was put on NO_x emissions and potential operation without after-treatment system. Unfortunately, optical investigations were severely limited by different technical problems derived from an optical engine design in early development and preliminary outcomes are here only introduced as part of future work (see Appendix A).

1.4 Thesis Contributions

The studies presented in this thesis contribute to the fundamental knowledge and understanding of the combustion process in pilot-ignited dual fuel combustion engines. The main contributions are listed below:

- An experimental evaluation of the lean limit of natural gas mixtures ignited via pilot injection has been carried out considering TUHC emissions and the requirements of efficient CH_4 after-treatment.
- The relative impact of intake manifold conditions on the dual fuel combustion process has been evaluated to understand trends in performance and emissions.
- Alternative injection strategies for simultaneous minimization of TUHC and NO_x emissions have shown potential benefits over traditional pilot-ignited dual fuel combustion.
- Effects of pilot fuel equivalence ratio distribution at the start of combustion plays a key role in dual fuel combustion and simulations have allowed the creation of a link between the pilot fuel distribution and the main combustion characteristics.
- A large increase of the ignition delay can allow knock-free operation at high load conditions under high gas fractions without the need of NO_x after-treatment system.

1.5 Document Content and Structure

This thesis is organized into 8 different chapters, including the present introduction. A short description of the contents of each chapter is provided here.

Chapter 2 is divided into two sections. Firstly, natural gas is defined as fuel for transportation applications and an overview of the single-fueled combustion technologies for diesel and natural gas applications is presented. After that, the dual fuel natural gas concept is described in detail and the main challenges are presented. Accordingly, motivation and objectives for this investigation are finally defined.

Chapter 3 and Chapter 4 include information about the experimental and computational tools used in this study respectively. This work is mostly an experimental investigation based on two different research engines and consequently, exhaustive explanation of their characteristics is provided in Chapter 3. Secondly, the methods to perform the combustion analysis of experimental data are presented in Chapter 4.

Chapter 5 explores how engine settings can be simultaneously optimized to maximize combustion efficiency at low loads, considering the difficulties of methane oxidation in the after-treatment system and high gas fraction operation. Then, part load operation is analyzed for evaluating alternative injection strategies and their effects on NO_x emissions. These studies are performed within a light duty application context.

Chapter 6 includes deeper insights into the interaction between the diesel and natural gas fuels. This study is performed within the context of marine medium speed engine applications. Diesel fuel distribution in the combustion chamber is simulated using a 1-D simulation tool in collaboration with CMT Research Center (Valencia, Spain) and the results are coupled to experimental data.

Chapter 7 summarizes all the results presented in the previous chapters. Moreover, suggestions for future work on this research topic are provided in Chapter 8. Due to technical limitations of a novel setup, initially planned optical investigations in a marine optical single cylinder engine have not been performed and included in this thesis despite the efforts of the author. However, a brief description is provided in Appendix A as part of possible future activities.

The line of argument followed throughout this thesis is presented in Figure 1.2.

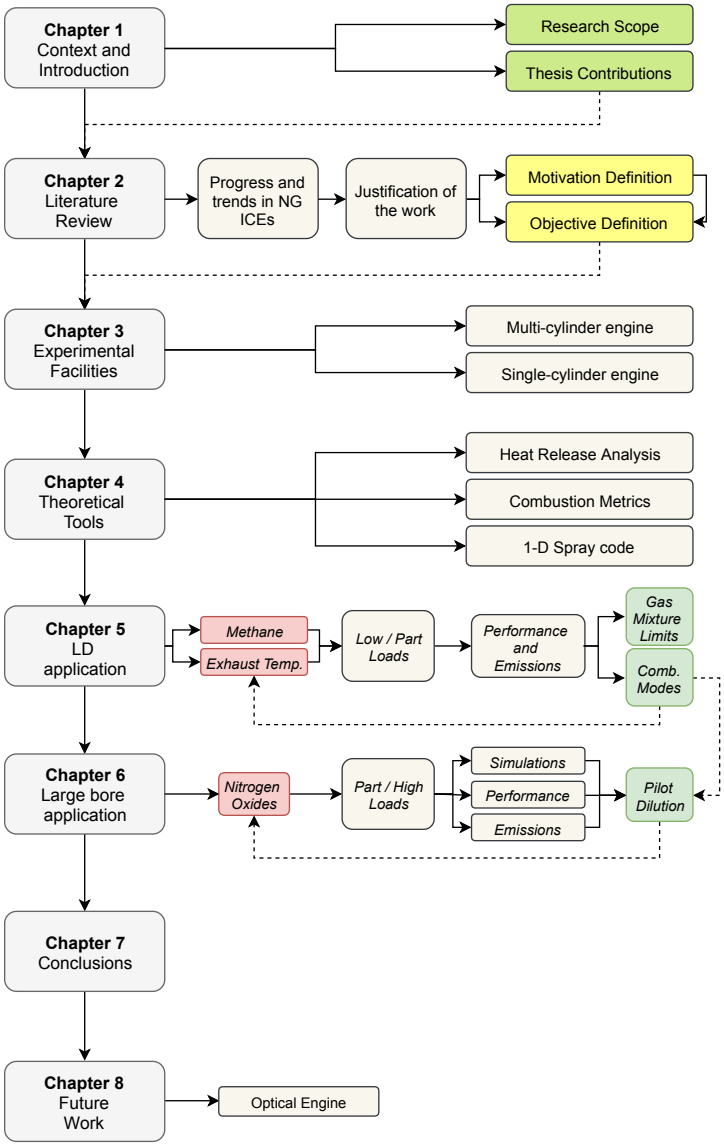

Figure 1.2: Line of argument of the work presented in this thesis

CHAPTER 2

NATURAL GAS IN DUAL FUEL COMBUSTION

This chapter aims to provide an overview of the use of natural gas in 4-stroke dual fuel applications. For this purpose, single fuel combustion concepts are firstly introduced and described in an attempt of providing enough background information before introducing the dual fuel natural gas-diesel combustion concept. After that, a discussion about emission legislation, applications and challenges of dual fuel combustion is presented.

2.1 Natural Gas as Engine Fuel

2.1.1 Fuel Definition

Natural gas is a mixture of gases which is normally found under high pressure in the porous rocks above the liquid zones of oil reservoirs. Natural gas also appears naturally in coal beds, shale gas or methane hydrates. The uses of natural gas include heating, cooking, electricity generation, transportation and organic chemicals and plastics manufacturing. Natural gas is cleaned before being used as fuel by removing impurities such as water, mercury, nitrogen, carbon dioxide, sulphur, etc. As a result, natural gas mainly consists of methane, although traces of other components might be present. The composition of natural gas varies widely depending on its source and production

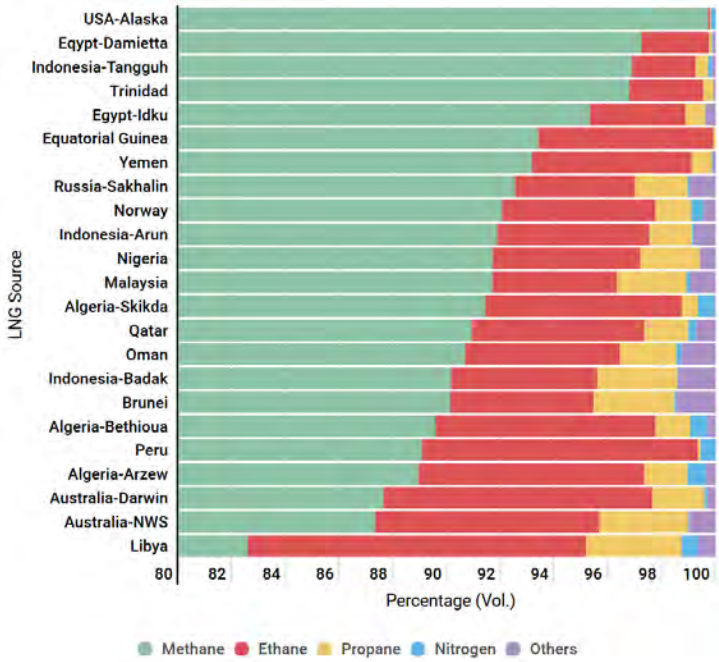

Figure 2.1: Sample of LNG compositions by source (Source: GIIGNL 2017)

process, as observed in Figure 2.1 [5]. Normally, it is composed by about 90% methane and the rest is usually traces of ethane, propane, butane, nitrogen or carbon dioxide, among others.

Methane molecules are composed of four atoms of hydrogen per atom of carbon (CH_4) and, consequently, a hydrogen-to-carbon (H/C) ratio of 4, which results in potential CO_2 reductions when natural gas is used as fuel for combustion processes. However, this greenhouse gas reduction potential is sometimes masked by the direct effect of methane on global warming since methane molecules absorb more heat per unit of mass than carbon dioxide. The specific global warming potential (GWP) of methane varies greatly among studies, although it is typically reported around 25 over a 100-year period [6]. Unburned methane emissions are normally referred to as *methane slip*.

Natural gas is considered a non-renewable resource unless it is artificially produced from biosources. In that case, it is normally referred to as biogas and it is considered a renewable resource. The term biogas is used to describe gaseous products generated during thermal (direct combustion, gasification or liquefaction) or biological (anaerobic

digestion) decomposition of biomass. These gaseous products contain methane, hydrogen, carbon monoxide, nitrogen or simple hydrocarbons, with percentages varying between the different types of processes and feedstocks. Typically, biogas methane content by volume is 50-80% and carbon dioxide represents 15-45%.

Natural gas is usually characterized by the methane number (MN), in the same way as octane (RON) or cetane (CN) numbers are used for gasoline or diesel-like fuels respectively. The MN is a measure of the resistance of fuel-air mixtures to knock (uncontrolled detonation) and it is usually an indicator of the quality of the natural gas. The difference between RON and MN is the reference fuel used for comparison. RON is referenced to iso-octane, which has a RON value of 100. However, natural gas normally has a higher resistance to auto-ignition than iso-octane, which translates into natural gas RON between 115 and 130, depending on composition. Hence, it is convenient to use another indicator which varies between 0 and 100 and is directly referenced to the characteristics of natural gas. The derived indicator is named *methane number*. A 100 MN is given to pure methane while pure hydrogen corresponds to 0 MN. Thus, the MN number of a certain natural gas composition is given by the mixture of methane and hydrogen which has the same auto-ignition characteristics when using the test fuel under certain operating conditions specified by the corresponding legislation.

2.1.2 Fuel Storage

Due to the gaseous nature of natural gas at ambient conditions, it takes roughly 0.93 m^3 of natural gas to match the energy content of 1 liter of gasoline.Consequently, its use for transportation at ambient conditions is unviable and it is necessary to use methods to increase its energy density [7]. Hence, natural gas can be stored and supplied to the engine in two different ways depending on its state: Liquefied natural gas (LNG) or compressed natural gas (CNG). LNG is the term applied to natural gas in its cryogenic liquid form, which means that it is stored at -162°C at atmospheric pressure. On the other hand, CNG consists of pressurized natural gas up to 200-300 bar in gaseous state. In both cases, CNG and LNG have lower power density than traditional petroleum-based liquid fuels. This factor particularly limits the implementation of natural gas in the transportation sector.

2.2 Single Fuel Combustion Engines

2.2.1 Conventional Diesel Combustion (CDC)

2.2.1.1 Description

As opposed to spark ignition engines, where an external device causes the ignition of the air-fuel charge, in compression ignition engines, or merely diesel engines, a highly pressurized liquid fuel is introduced in the combustion chamber late in the compression stroke near TDC, it mixes with the high pressure and high temperature air charge and finally autoignites. Despite the fact that different diesel engine concepts exist, only the modern and widely applied four-stroke direct injection compression ignition diesel engine is described here.

The diesel combustion process is a complicated turbulent, unsteady, highly heterogeneous and three-dimensional event. In an attempt to globally describe the process, the combustion process can be analyzed by means of the associated heat release rate. For that purpose, a typical heat release rate for a conventional diesel combustion event is presented in Figure 2.2.

- The process starts with the start of injection (SOI) event. This causes the fuel to absorb energy from the surroundings and consequently a quick decrease of the energy released is observed. This phenomenon is known as the evaporation phase, where the

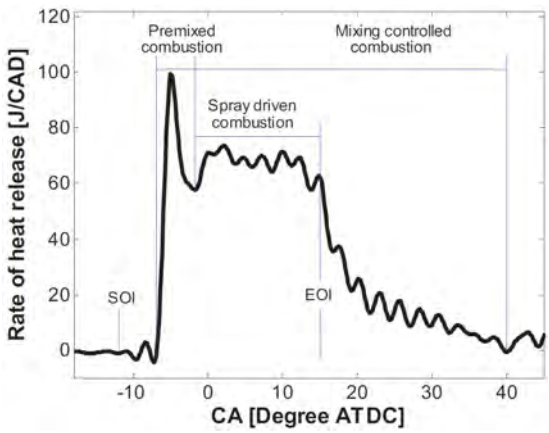

Figure 2.2: Typical rate of heat release for a conventional diesel combustion event. Reproduced from [8]

atomized fuel droplets change to vapor phase. The fuel continues to mix with the charge (air and trapped exhaust gases) and certain pre-reactions, resulting in cool flames, occur before the start of combustion (SOC). Due to the characteristics of the injected fuel, the main combustion event starts shortly after SOI in those regions where temperature and fuel-air equivalence ratio allow ignition. The time between SOI and SOC is normally referred to as *ignition delay*.

- The main combustion process starts with the *premixed* combustion phase. It is characterized by a rapid increase of heat release rate and it is greatly controlled by chemical kinetics and, consequently, ignition delay. This event results in an increase in pressure and temperature in the combustion chamber and it triggers the ignition in other regions. It is important to highlight that this phase and the fuel injection event can occur simultaneously.

- The next stage is named *spray driven* combustion phase. A diffusion flame is established while the fuel injected is being atomized, vaporized, mixed and ignited. The heat release rate is limited by the mixing rate and this stage finalizes at the end of the injection (EOI).

- The last stage is normally referred to as *late mixing-controlled* combustion and the remaining unburned fuel ignites while the heat release rate gradually decreases.

This heat release model provides global information about the combustion process but it does not explain the fundamental processes behind the diesel jet which determine the combustion characteristics. In recent decades, diagnostics on optical engines have enabled fundamental understanding of the diesel combustion process. One of the most accepted phenomenological diesel combustion models was presented by John Dec in 1997 based on laser-based experiments performed in a heavy duty diesel engine [9]. Basically, a diesel combusting jet is made of different fuel lean and rich zones which burn simultaneously and where different types of species such as soot or nitrogen oxide are formed. The model is depicted in Figure 2.3 and it should be interpreted from left to right. The process starts at the injector nozzle, where liquid diesel fuel penetrates into the combustion chamber and progressively mixes and vaporizes within the ambient charge. This forms a rich vapor fuel-air mixture inside the jet (soot formation area) which is surrounded

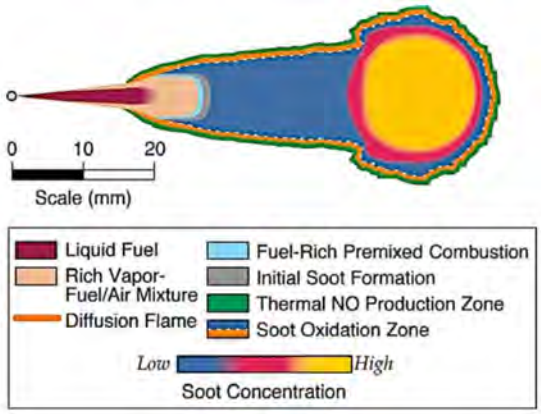

Figure 2.3: 1997 John Dec's conceptual model of a quasi-steady diesel spray during its mixing-controlled phase. Reproduced from [9]

by a diffusion flame burning close to stoichiometric conditions in the periphery of the jet (nitrogen oxides formation area). This presents the typical trade-off between soot and nitrogen oxide emissions related to diesel combustion engines.

This trade-off is represented via ϕ-T diagrams, which were first introduced by Kamimoto and Bae in 1988 [10]. An example of this technique is presented in Figure 2.4. This map links in-cylinder conditions with regions where pollutant formation occurs. As observed in the figure, the diesel combustion process normally crosses both soot and nitrogen oxide formation areas during the cycle. Several strategies have been studied for reducing these two pollutant formations during diesel combustion processes. However, it is well-proved that a trade-off between soot and nitrogen oxides is inherent to diffusion diesel combustion [11].

It is clearly observed in Figure 2.4 that simultaneous local reduction of maximum temperature and maximum equivalence ratio could potentially result in lower soot and nitrogen oxide formation rates. This strategy has motivated the appearance during the last decades of alternative combustion modes, commonly named *low temperature combustion (LTC)* modes. Generally, ignition delay is prolonged in order to obtain longer fuel mixing time for achieving lower local equivalence ratios before ignition, which avoids the soot formation region, and, simultaneously, increased exhaust gas recirculation (EGR) rates reduce oxygen availability in the combustion chamber and result in lower maximum flame temperatures, thus limiting the NO formation rate.

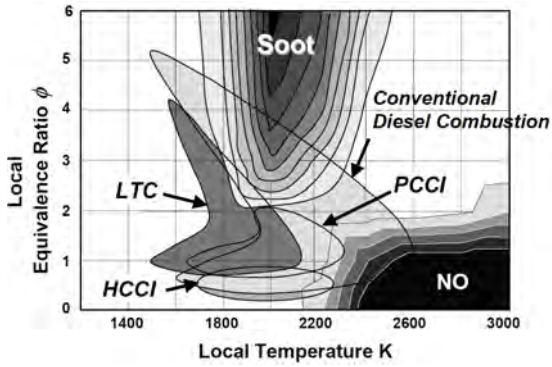

Figure 2.4: Distribution of soot and NO formation regions as a function of local equivalence ratio ϕ and temperature T for different diesel fuel based combustion modes. Reproduced from [12]

2.2.1.2 Applications

Diesel compression ignition engines have overall featured superior performance over gasoline spark-ignited engines in the last century. This is proved by the diversity of its successful applications. Fuel efficiency benefits have boosted the use of diesel engines in road transport applications, particularly for heavy duty trucks and different types of public transportation. The light duty passenger vehicle sector has been another successful area of application, although in the recent years different scandals within emission legislation compliance of certain vehicle manufacturers have damaged society's perception and acceptance of the diesel engine as a clean and sustainable engine platform for the future. Additionally, diesel engines have been widely used in stationary applications and industrial duties, such as electricity production, mining, driving pumps, etc. Finally, it is also possible to find applications within military and agricultural activities, as well as in rail propulsion and marine systems.

2.2.2 Conventional Natural Gas Combustion (CNC)

2.2.2.1 Description

Natural gas combustion has been traditionally applied in spark-ignited combustion engines where a mixture of port fuel injected (PFI) natural gas and air is admitted during the intake stroke, it is compressed during the compression stroke and, finally, the homogeneous mixture is ignited

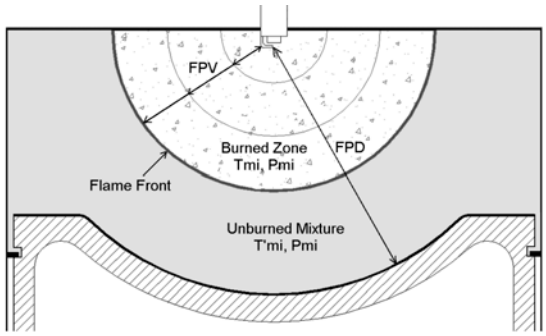

Figure 2.5: Simplified two-zone combustion model for SI natural gas combustion. Reproduced from [13]

close to TDC by means of an electric discharge created by a spark plug. This event triggers the combustion process and a propagating flame front in the vicinity of the spark plug starts. This process can be represented by a simplified two zone ignition model, as depicted in Figure 2.5.

Natural gas combustion engines can be categorized as lean burn or stoichiometric combustion engines depending on gas-air equivalence ratio. While stoichiometric natural gas combustion in combination with three-way catalyst after-treatment systems results in low exhaust emission levels [14], reduced thermodynamic efficiency and increased knock tendency, among others, limit fuel economy. For these reasons, lean burn combustion emerged as a potential alternative approach for natural gas usage in combustion engines. In this case, the fuel-air mixture is diluted either with excess air or EGR. This approach translates into an increase of the ratio of specific heats [15] (excess air), throttle-less operation and a reduction of combustion temperatures, which result in higher thermodynamic efficiency and lower NO_x emissions. However, lean operation is normally restricted by the *lean-limit*, as measured by the air-fuel ratio above which ignition is impossible or combustion is incomplete [16].

Beyond the lean-limit, the burning rate is severely reduced, potentially resulting in increased combustion duration, low combustion efficiency due to instability with high cycle-to-cycle variations (high HC emissions), reduced flame propagation velocity and misfiring [17, 18]. Regular single-pole spark plugs generate approximately 10-30 mJ electrical energy. This amount of energy normally becomes insufficient for robust and sustained ignition of homogeneous lean mixtures, while increased ignition energy can result in severe electrode erosion [19]. Hence, alternative ignition methods have been investigated

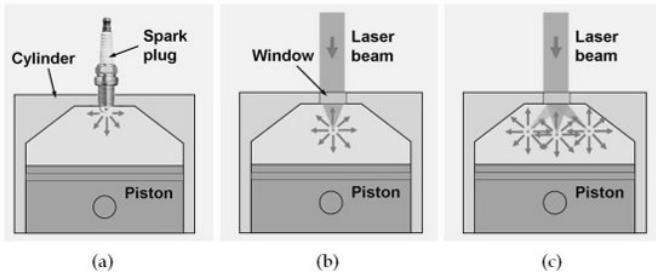

Figure 2.6: Schematics of the combustion engines ignited by (a) spark plug, (b) single-point laser ignition, (c) multi-point laser ignition. Reproduced from [20]

for effectively extending the lean-limit of natural gas combustion engines. Several different ignition systems have been developed and proposed for increasing the burning rate of lean mixtures. However, the description of all different types is outside the scope for this document, but here the two most attractive ones are presented: Laser-induced and pre-chamber ignition systems.

Laser-induced ignition has captured attention of the research community to some extent during the last decades. A laser beam is highly focused at an area in the combustion chamber and it transmits enough electromagnetic radiation for igniting a combustible mixture. Figure 2.6 shows a comparison between spark plug and laser-induced ignition methods. Larger spark volume, capability for multipoint ignition sites and lower heat losses to surrounding metallic elements are some of the main benefits of laser-induced ignition [21]. The main drawback of this technique is related to the complexity and cost of laser systems which are scalable for commercial applications. Light scattering, particle deposits and stability of the optical window are some of the technical limitations which have restricted its commercialization [22, 23].

In contrast, pre-chamber ignition systems have been effectively implemented in natural gas combustion engines for commercial applications. In these cases, the spark electrode is located inside a chamber, which results in two separate volumes: the pre-chamber, where the spark electrode is located, and the main chamber, which contains the main air-fuel mixture. The pre-chamber is connected to the main chamber via orifices on the nozzle, whose number, size, geometry and distribution may vary between different designs. An example of fueled pre-chamber assembly is depicted in Figure 2.7. A relatively small amount of air-fuel mixture is present inside the pre-chamber (fuel

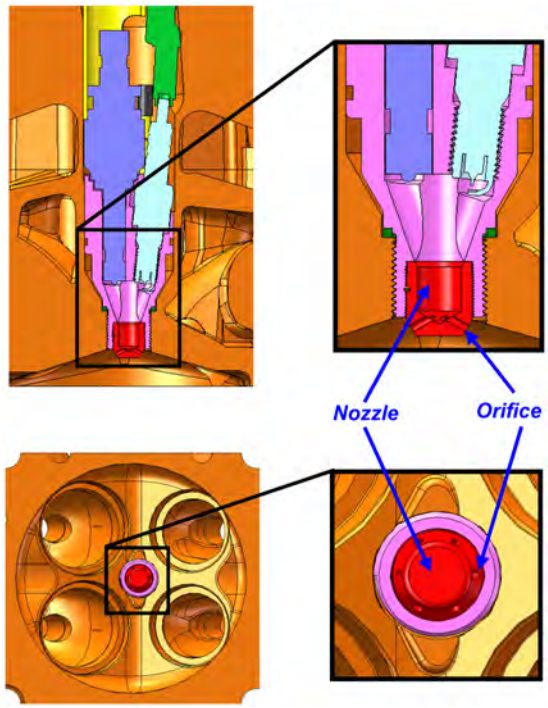

Figure 2.7: Example of pre-chamber assembly and pre-chamber details. Reproduced from [26]

is either pushed in from the main chamber or directly injected) and it is ignited by the spark plug near TDC. This combustion process causes an increase of pressure inside the pre-chamber and, consequently, chemically active flame jets flow out through the orifices. As a result, distributed ignition sites around the main combustion chamber increase the combustion robustness over a broader range of air-fuel ratios, particularly in the case of fueled pre-chambers [24]. Some of the topics that require further development are mixture formation inside the pre-chamber and the relationship between pre-chamber volume and nozzle diameter [25].

In recent years, natural gas direct injection spark-ignited combustion engine applications have been developed for minimizing some of the classical limitations of homogeneous port fuel injected natural gas engines. Direct injection during the compression stroke allows a partially stratified air-fuel mixture prior to spark ignition, which reduces premixed zones, thus reducing end-gas knock probability [27]. Consequently, higher efficiencies are obtained at full load conditions through more optimal combustion phasing and therefore, CO_2 emission

reductions [28]. Moreover, volumetric efficiency is increased by avoiding air displacement due to port fuel injection of natural gas and its associated power density loss. This technology is still under intensive development by the research community.

2.2.2.2 Applications

Natural gas engines are widely used for stationary applications such as power generation, mining or co-generation sets. In these fields, pre-chamber SI gas engines have shown superior performance over traditional SI engines. However, its implementation to mobile applications is somewhat more limited, although it is common to find natural gas powered heavy duty trucks, urban buses or public transportation fleets, particularly those with low mileage requirements. Marine applications are increasing, especially due to the increased availability of LNG. Light duty natural gas vehicles are also available, either in dedicated (natural gas only) or bi-fuel (gasoline or natural gas) configurations. Vehicle range, lack of fueling stations or diesel fuel price fluctuations are some of the factors that have limited the deployment of natural gas vehicles into the current world vehicle fleet. However, recent projects such as the LNG Blue Corridors aim for establishing natural gas as a real alternative for medium and long distance transport in Europe by improving the fueling infrastructure.

Figure 2.8: LNG Blue Corridors in Europe (Source: NGVA Europe)

2.3 Dual Fuel Combustion Engines

2.3.1 Pilot Ignited Dual Fuel Combustion (CDF)

2.3.1.1 Introduction

The concept of dual fuel combustion is far from novel. Already back in 1901, Rudolf Diesel obtained a U.S patent [29] where the use of a secondary fuel for the ignition of primary fuel was described:

> *"...It follows from the foregoing that if a given mixture is compressed to a degree below its igniting-point, but higher than the igniting-point of a second or auxiliary combustible, then injecting this later into the first compressed mixture will induce immediate ignition of the secondary fuel and gradual combustion of the first mixture, the combustion after ignition depending on the injection of the igniting or secondary combustible..."*

In the last century, the use of natural gas in dual fuel applications has varied heavily depending on the availability and price fluctuations of liquid fuels. However, the systematic development of modern dual fuel engines started with the first implementation of air pollution legislations, the general rise of fuel costs and the increased availability of natural gas (especially in LNG form) due to the development of dedicated infrastructure.

In the vehicle industry, natural gas has been traditionally used in SI engines due to its similar characteristics to gasoline-like fuels (high RON), where a fairly simple PFI gas injection system is added and the engine is operated in bi-fuel mode. In the medium speed engine industry, pre-chamber ignited gas engines are widely exploited. However, the reduced compression ratio of the widespread SI engine limits the theoretical maximum thermodynamic efficiency. For this reason and in an attempt to take advantage of the higher RON value of natural gas, the interest of natural gas combustion in CI engines has steadily increased over the last decades. The most common use of natural gas in CI engines is via pilot-ignited dual fuel combustion, where a small amount of diesel fuel is used to ignite a homogeneous natural gas and air mixture. Compared to ignition methods in SI engines, ignition energy

is increased several orders of magnitude despite the low mass of the pilot fuel and multiple ignition locations are created, which improves ignitability near the lean limit.

Consequently, this conventional dual fuel combustion concept can be analyzed as a dual fuel hybrid between SI and CI combustion processes, where multiple mechanisms overlap and influence each other. The conventional pilot-ignited dual fuel combustion (CDF) process can be analyzed in 4 different stages, as depicted in Figure 2.9:

- **Stage 1**: Firstly, natural gas is introduced into the combustion chamber. Normally, a mixture of natural gas and air (stoichiometric or lean) is admitted during the intake stroke, which results in a homogeneous mixture by the end of the compression stroke, before pilot SOI.
- **Stage 2**: The second one consists of the period between the start of pilot injection and the start of combustion, named ignition delay. Here, the pilot fuel mixes with the surrounding fuel-air mixture until self-ignition takes place. The duration of this stage depends on diesel fuel distribution and thermodynamic conditions (temperature, pressure and oxygen concentration) in the combustion chamber [30]. In most cases, the pilot injection ends before the onset of combustion. Pilot injection timing, pressure and fuel mass heavily affect this stage due to their effects on evaporation and mixing [31].
- **Stage 3**: The third stage is mainly linked to combustion of the pilot fuel and it is usually characterized by a high premixed peak

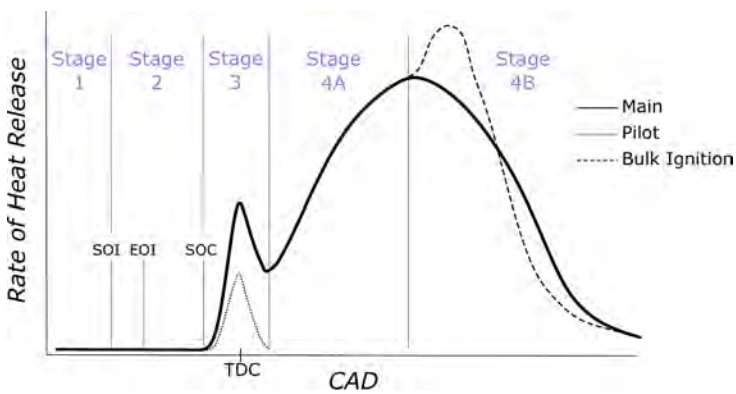

Figure 2.9: Simplified heat release rate for a pilot-ignited natural gas combustion event

and ignition of the entrained gas into the pilot injection and the gas mixture in the vicinity of the pilot spray [32].

- **Stage 4**: Lastly, natural gas combustion takes place in the remaining gas-air mixture (stage 4a) and it depends on its reactivity and thermodynamic conditions, since its flammability is highly affected by these parameters [33]. This stage is also severely influenced by the interaction between diesel and natural gas fuels during the ignition delay period. Ignition of the bulk charge (stage 4b) can occur due to excessively high reaction rate of the gaseous fuel-air mixture [34].

The previous categorization is adapted from the combustion model described by [35]. The importance and contribution of each stage to the total energy release depends on operating conditions and several different combustion modes are possible. In the following sections, a more detailed description of some of the most important aspects of pilot-ignited dual fuel combustion is discussed.

2.3.1.2 Gaseous Fuel Admission

The method with which natural gas is introduced in the combustion chamber can be categorized depending on the location of the gas fuel injector.

- **Gas Fumigation**: Natural gas is supplied upstream the engine intake manifold for mixing with the incoming air, maintaining a constant air-fuel ratio. Fuel flow is independent from the valve action of the different cylinders and the mixture tends to be highly homogeneous. Carburetors and mixers are examples of this type.
- **Port Fuel Injection**: A fuel injector is mounted in the intake port, as close as possible to the intake valves, and supplies fuel to the combustion chamber during the gas exchange process.
- **Direct Injection**: In this case, natural gas is directly injected into the combustion chamber. Both low pressure and high pressure direct injection systems exist, although both are still under development. In the low pressure system, natural gas is directly injected into the combustion chamber no later than approximately 120 CAD bTDC, while the high pressure system

relies on gas injection closer to TDC. This method generates a much higher degree of fuel stratification in the combustion chamber than fumigation or PFI systems.

Most natural gas dual fuel applications are based on indirect injection systems such as fumigation or PFI due to their simplicity. However, these indirect injection methods are usually associated with high unburned hydrocarbon emissions unless operation and combustion chamber geometry are optimized for dual fuel operation [36, 37]. Blow-by losses, piston crevices or bulk combustion loss due to excessively lean fuel mixtures are some of the most important mechanisms which have boosted the development of direct injection natural gas systems [38]. In engines without EGR or with low back-pressure levels, methane blow-through, also named *short-circuiting*, can also severely contribute to unburned hydrocarbon emissions [39]. Direct injection systems approach these issues by increasing the natural gas fuel stratification levels in the combustion chamber. There are several possible injection strategies available when using direct injection for both natural gas and diesel fuels [40] but this topic is outside the scope of this thesis. Direct injection systems provide better tolerance to knock and these engines inherently benefit from increased volumetric efficiency compared to indirect injection natural gas engines. However, the technology is still under development and only a few solutions are available. Increased complexity and cost of the DI injection system (either a separate gas direct injection system or an integrated bi-fuel injector) and cylinder head are the main limiting factors.

2.3.1.3 Pilot Injection

The diesel injection process is highly influenced by three injection system control settings: injection pressure, timing and duration. These parameters determine the fuel mass injected and the moment in the process when the fuel enters the combustion chamber and, therefore, the thermodynamic conditions which it is exposed to and the dilution level reached before self-ignition. Consequently, the diesel injection process plays a key role in dual fuel combustion. For that reason, the effects of these settings are summarized in the following points.

- **Injection Timing**: This parameter controls combustion phasing. It is often mentioned in literature that advancing pilot injection timing results in a reduction of HC emissions and higher NO_x levels under lean operation and, consequently, a trade-off between these two groups of species exist [41, 42, 43], as described in Paper I. This behavior is explained by the improvement of combustion efficiency due to the increased mixing of pilot fuel vapor with the premixed mixture. However, this trend does not apply for mixtures closer to stoichiometric conditions. As presented in Paper II, the unburned hydrocarbons trapped in the cylinder crevices are released during the early stages of the expansion stroke. Since combustion efficiency is not a limiting factor as for lean mixtures, the relative effect of crevices on HC emissions increases and retarded combustion phasing turns out in lower HC emissions due to the oxidation of fuel released from crevices [37]. Further advancements of pilot injection timing cause longer ignition delays, which dramatically change the pilot combustion mode and these trends no longer apply [44]. This topic is analyzed and discussed in Paper III and IV.

- **Injection Pressure**: Variations in pilot injection pressure have a direct effect on the dispersion and location of the diesel fuel vapors in the combustion chamber. For the same amount of fuel, higher injection pressure results in shorter injection duration, which increases the mixing time of the pilot fuel with the premixed charge. Consequently, the equivalence ratio at which diesel fuel autoignites is reached earlier and ignition is advanced. Even then, since temperature and pressure of the mixture are high around TDC, ignition delay is often short and this effect is reduced. However, if thermodynamic conditions in the combustion chamber cause long enough ignition delay, it is possible to over-dilute the pilot fuel prior to ignition. In that case, the relation between injection pressure and ignition delay is inverted [41]. This topic and the use of pilot over-dilution for combustion phasing control is analyzed and explained in detail in Paper IV.

- **Injection Duration**: The largest impact on pilot size is governed by the injection duration. Given a fixed pilot injection timing and injection pressure, longer injection duration and consequently higher pilot fuel mass injected results in earlier combustion phasing and higher peak cylinder pressures [45]. In general terms, it is preferable to reduce the size of the diesel fuel mass in relation

to the natural gas fuel mass. This is mainly due to economical reasons since diesel fuel price is normally higher than natural gas. However, there are some limiting aspects. Firstly, reduced pilot mass means lower ignition energy, which in the case of cold starts or excessive lean operation results in high HC emissions and reduced combustion stability [46]. Besides, load increments are normally beneficial for increased combustion efficiency due to the higher temperature and pressure present in the combustion chamber. This suggests that pilot mass can be reduced as load increases. However, overheating of the pilot injector tip may occur [47]. Lastly, the accuracy and repeatability of the diesel injector for small pilots (below 5% of total fuel energy) may be reduced since the required short injection duration can result in ballistic behavior of the injector [45]. For these reasons, some dual fuel engines have a dedicated pilot injection system, independent from the main diesel injection system.

2.3.1.4 Combustion Modes

Although the conventional approach for pilot-ignited dual fuel engines is based on a pilot injection close to TDC as ignition source for lean premixed mixtures, other strategies have emerged as potential alternatives. The different variations normally differ between each other in ignition delay, gas fraction or gas-air equivalence ratio selected.

- **Ignition Delay**: The combustion mode in which the pilot fuel is burned has a direct impact on the combustion process. While late pilot injection timing results in a highly reactive stratified pilot fuel zone and its associated initial premixed peak, early pilot injection timing promotes mixing and, consequently, possible over-dilution of the pilot fuel with the gas-air mixture prior to the start of combustion, which results in a more homogeneous auto-ignition of the pilot fuel. The ignition delay controls the magnitude of stage 2 defined in the CDF introduction section. This topic is introduced in Paper III and extensively analyzed and discussed in Paper IV.
- **Gas Fraction**: The gas fraction (GF) is defined as the ratio between the fuel energy from the gaseous fuel and the total fuel energy required for the combustion process. Given a constant

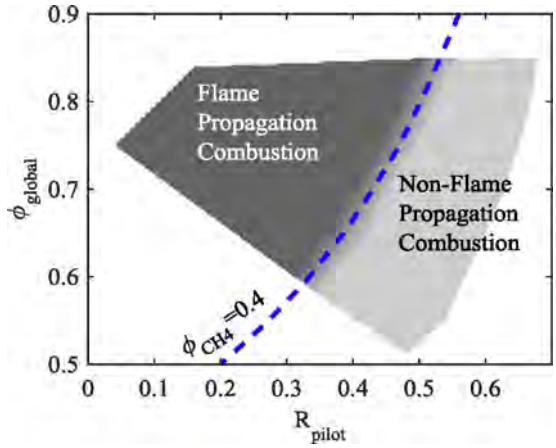

Figure 2.10: Operating modes as a function of global equivalence ratio and diesel fraction. Reproduced from [48]

total fuel energy input, low gas fraction results in more diesel-like combustion and non-flame propagating combustion, while high gas fraction uses diesel merely as ignition source and correct flame propagation combustion depends on gas-air mixture properties, as shown in Figure 2.10. Consequently, this parameter controls the ratio between stages 3 and 4 defined in the CDF introduction section. This topic is further discussed in Paper I and III.

- **Gas-air Equivalence Ratio**: As depicted in Figure 2.10, the gas-air equivalence ratio plays a key role in the combustion characteristics, since it establishes a limit for the flame propagation combustion mode. Given a constant pilot fuel mass, increasing gas-air equivalence ratio promotes a transition from "highly skewed" to "bell-shape" heat release profiles [49]. This behavior is further developed in Papers I, II and III.

2.3.1.5 Conversion of Diesel Engines to Dual Fuel Operation

There are two different techniques for conversion of CI engines to dual fuel operation: OEM dedicated or retrofit. In the first case, OEMs design an optimized combustion system for dual fuel operation [50]. This approach is mostly used on stationary engines with precise requirements in terms of load and engine speeds. This is the case of the Wärtsilä 20 DF engine used in Paper IV. In the second case, the OEM diesel CI engine is equipped with a natural gas port fuel injection system which allows operation in dual fuel mode. This results in fewer modifications

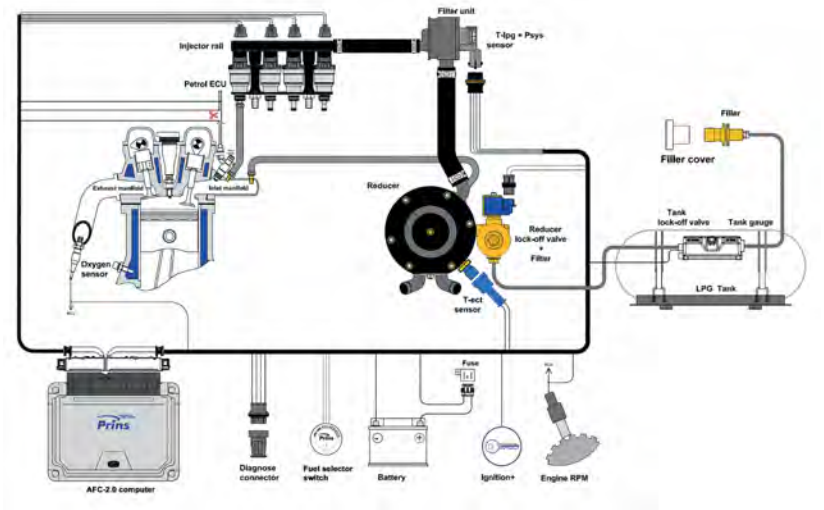

Figure 2.11: Example of retrofit kit for natural gas engine conversion. Reproduced from Prins Alterative Fuel Systems

of the original base CI engine and diesel operation remains unaltered when there is no gas supply available. These retrofit kits usually consist of a gas tank, valves, filter, pressure regulator and set of injectors. Additionally, a separate ECM which controls the dual fuel combustion strategy is required. Figure 2.11 shows an example of retrofit kit for natural gas engine conversion. A retrofitted diesel engine is used in Papers I, II and III.

2.3.2 Reactivity Controlled Compression Ignition (RCCI)

Pilot-ignited natural gas combustion is not the only dual fuel concept that has captured attention from the research community. In the last decade, and in an attempt of achieving high engine efficiency with low emissions simultaneously, *Reactivity Controlled Compression Ignition* has emerged as a promising combustion concept. The appearance of LTC modes, as described in the CDC section, resulted in combustion strategies with high thermal efficiency and low NO_x and soot levels. However, some LTC modes suffer from controllability challenges and rapid rate of pressure rise, which limits the maximum operating load. In this line, several investigations have shown how the simultaneous use of two fuels with different reactivities can result in acceptable combustion

control by means of controlling the proportion between them [51, 52], which results in extended heat release periods by the staged use of the two different fuels. These studies describe that, in RCCI combustion, the high reactivity fuel is controlled in order to generate a certain degree of mixing with the low reactivity fuel, which results in a stratified blend of two fuels prior to ignition. This in-cylinder fuel blending strategy leads to reductions in the maximum pressure rise rate compared to single fuel premixed combustion [53], which allows more efficient high load operation. Consequently, RCCI relies on local fuel reactivity stratification and equivalence ratio for improving the controllability of LTC combustion regimes.

Initial studies were carried out using diesel-like and gasoline-like fuels as low and high reactivity fuels respectively. Alternatively, due to the higher RON number of natural gas over gasoline, investigations about the effect of a larger reactivity gradient between the two fuels have been performed using natural gas as low reactivity fuel [53, 54, 55]. Similarly to pilot-ignited dual fuel combustion, operation at low load is limited due to high hydrocarbon emissions while overall engine efficiency is slightly reduced at high load compared to gasoline/diesel RCCI due to higher heat transfer losses possibly caused by the higher adiabatic flame temperature of methane.

The main difference between CDF and RCCI relies on the purpose of the high reactivity fuel. In CDF combustion, the high reactivity fuel is used as ignition source of the low reactivity fuel and it is usually desirable to minimize the pilot size due to economical reasons. By contrast, RCCI relies on the formation of a mixture with a certain reactivity which is varied depending on the different requirements of each operating point. Consequently, higher ”pilot” fuel mass is allowed if required to fulfill the system boundaries and its use is intended for other purposes rather than just ignition source. The RCCI combustion concept is still under development by the research community.

2.4 Emission Legislation and After-treatment

The requirements regarding pollutant emissions from natural gas CI combustion engines vary widely depending on the type of application. Marine and stationary applications have a well defined legislation, while OEM certification of a natural gas CI light duty engine is still difficult

due to the lack of specific legislation. In the next sections, an overview of the emission legislation by sector is provided and, lastly, a description of after-treatment solutions used in dual fuel engines is presented.

- **Marine Applications**: The International Maritime Organization (IMO) is the United Nations agency responsible for the prevention of marine pollution. The first IMO anti-pollution protocol was created in 1978, during the International Convention for the Prevention of Pollution from Ships (MARPOL). This protocol effectively entered into force in 1983. However, it did not include any air pollution protocol at that time. MARPOL has been updated via amendments throughout the years. It includes not only limits on pollutant emissions but also strategies and regulations to inhibit and decrease pollution from ships.

  In 1997, the Annex VI to MARPOL (TIER I) introduced new regulations focused on sulphur oxides (SO_x) and NO_x which entered into force in 2005. After that, successive revisions have been applied to MARPOL Annex VI, which have strengthened the emission limits in special emission control areas (ECA). These include the Baltic Sea, the North Sea, North American Sea and the EEUU Caribbean Sea area. In these locations, more stringent pollutant emission requirements apply. Lately, TIER II (for ships constructed after 1st January 2011) and TIER III (for ships constructed after 1st January 2016) regulations have introduced more severe limits. Actual MARPOL Annex VI NO_x limits are depicted in Figure 2.12 [56]. At the same time, SO_x in ECAs has

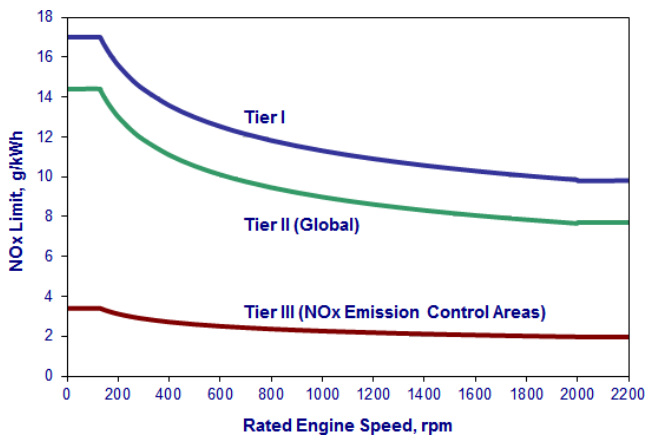

Figure 2.12: MARPOL Annex VI NO_x emission limits [56]

been also reduced to a value of 0.1% (mass by mass), while the global limit is set to 3.5%, which it is planned to be decreased to 0.5% in 2020. However, the opposition of some countries to the TIER III NO_x limits has resulted in an uneven implementation. So far, IMO TIER III limits have only entered into force from 2016 in the North American and US Caribbean sea areas.

Currently, IMO does not establish any specific limit on HC (including CH_4) CO and PM emissions, although regulation of the first two is expected if natural gas becomes more widely used [57]. However, in the US, the Environmental Protection Agency (EPA) has regulated HC, CO and PM emissions separately from IMO regulations. In Europe, inland waterway vessels emission legislation is harmonized with US marine standards and its Stage V has significantly tightened emission limits, including CO, HC, NO_x and PM. Finally, China has set specific CH_4 limits (from 1 to 2 g/kWh depending on unit displacement and power) in marine engine emission standards, apart from CO, HC, NO_x ad PM, which should enter into force in 2018 and 2021 sequentially [56].

- **Stationary Applications**: In Europe, one of the most stringent regulations is the *Technische Anleitung zur Reinhaltung der Luft*, usually referred to as *TA Luft*. The latest revision was published in 2002. Although introduced and enforced by the German Environment Ministry BMU, it has been adopted by several other European markets. TA Luft NO_x limit for CI dual fuel engines is set to 0.5 g/Nm^3 [56]. This emission limit is referenced at standard temperature and pressure (STP) conditions and 5% oxygen content. This usually translates into limits below 1 g/kWh, depending on engine operation.

  In the latest years, other regulatory frameworks have imposed stringent limits for stationary applications. This is the case of the Medium Combustion Plant (MCP) Directive in Europe, which was adopted in 2015 for plants in the power range between 1 and 50 MW. Compliance for new plants will start in 2018, while existing power plants below and over 5 MW are targeted for 2030 and 2025 respectively. This new regulation sets a limit of 0.25 g/Nm^3 (0.5 g/Nm^3 for existing engines) [56], referenced at 5% oxygen concentration, which would usually result in NO_x limits below 0.5 g/kWh. In Europe, no limits on HC and CH_4 are normally set, although specific HC limits depending on average gas fraction over

Table 2.1: EURO VI emission legislation for heavy duty road engines [59]

Test	CO	THC	NMHC	CH_4	NO_x	NH_3	PM	PN
			g/kWh			ppm	g/kWh	10^{12}/kWh
WHSC (CI)	1.5	0.13	-	-	0.4	10	0.01	0.8
WHTC (CI)	4.0	0.16	-	-	0.46	10	0.01	0.6
WHTC (PI)	4.0	-	0.16	0.5	0.46	10	0.01	0.6

the proposed certification cycle will be set for non-road generator sets above 560 kW from 2019.

- **Heavy Duty Road Applications**: The framework for heavy duty natural gas engines in Europe is provided by the EURO VI regulation [58], which entered into force in 2013. Euro VI european emission standards for heavy-duty engines are provided in Table 2.1. Nowadays, the World Harmonized Transient Cycle (WHTC) and the World Harmonized Stationary Cycle (WHSC) are used for heavy duty engine certification [59], in replacement of the European Transient Cycle (ETC) and European Stationary Cycle (ESC) which were in use until the EURO V legislation.

  The current specific limit on CH_4 emissions is set to 0.5 g/kWh and it applies only to positive ignition (PI) engines (The legislation defines PI engines those in which combustion is initiated by a localized high temperature in the combustion chamber produced by energy supplied from a source external to the engine). However, in 2014 and in an attempt of adapting the regulation framework to the technological progress made on dual fuel applications, amendments to the legislation introduced the concept of the "dual-fuel" working principle in Euro VI [60]. The dual fuel working principle is divided into 3 different types depending on the average gas fraction over the WHTC and the purpose of diesel operation. The type of certification test applied depends on this dual fuel categorization and consequently, a dual fuel engine can in some cases either be certified as a PI or a CI engine, which translates into different CH_4 emission requirements.

- **Light Duty Road Applications**: EURO VI legislation established a limit for HC and NMHC emissions from SI engines running on natural gas but this limit does not apply for compression ignition engines. The absence of specific regulation of CH_4 has forced OEMs to use special after-treatment systems (higher content of precious materials) for fulfillment of the HC limit when natural gas is used as fuel [61].

Moreover, there is no definition of light duty dual fuel engine, as opposed to heavy duty regulations. Therefore, there is no specific legislation for dedicated dual fuel light duty engine certification in Europe.

Consequently, the assessment of CH_4 emission measured in the light duty engine tests presented in this thesis is made assuming the heavy duty engine regulated CH_4 limit.

The previous points briefly exemplify the diversity and complexity of emission legislation for internal combustion engine applications. The fulfillment of these limits most often requires the use of emission after-treatment systems. Consequently, several efforts have been made to develop after-treatment systems which provide high conversion efficiency.

In stoichiometric gas engines, three-way catalysts (TWC) are used to simultaneously convert HC, CO and NO_x to CO_2, H_2O and N_2. Platinum, palladium and rhodium are the most used precious metals in TWC catalysts [50]. This type of catalyst only works effectively within a narrow band around stoichiometric conditions. and, therefore, requires accurate air-fuel ratio control for maintaining high conversion efficiency during the different modes of engine operation. Recent research has shown that the optimal CH_4 conversion does not correspond to the nominal stoichiometric point but slightly richer conditions due to inhibition from competing reactions involving CO and NO [62, 63], as observed in Figure 2.13.

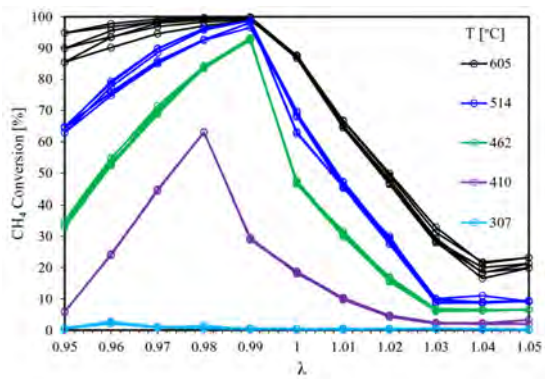

Figure 2.13: CH_4 conversion in TWC for lambda and temperature sweep. Reproduced from [63]

However, lean burn operation resulting in excess air conditions prevents the use of TWCs. In this case, dedicated methane oxidation catalysts (MOC) are required. The most common precious metal used is palladium [50]. In some cases, platinum is used since it prevents the catalysts from water and sulfur deactivation, which are the two main challenges of MOC over long term operation [64, 65]. If required, NO_x emissions are usually controlled separately via Selective Catalytic Reduction (SCR) systems.

Another aspect indicated by Figure 2.13 is the effect of temperature on the CH_4 conversion rate. Methane is a very stable gas and it is more difficult to oxidize than other lighter hydrocarbons. The required light-off temperature is normally over 400°C, although below 350°C is possible through optimization and increased cost [66].

2.5 Dual Fuel Engine Applications

The use of dual fuel engine technologies is common in dedicated medium speed engines and stationary applications with narrow requirements in terms of operating load and speed. For example, Wärtsilä introduced its first dual fuel engine in 1987 (Wärtsilä 32GD), although the modern and widely used 4-stroke low pressure gas dual fuel engine did not appear until 1995 (Wärtsilä 32DF). For road vehicle applications, most applications are of CI engines retrofitted for natural gas operation. Several companies around the world, such as NGV Motori, Clean Air Power or Bosch, offer conversion kits for diesel engines which allow dual fuel operation. These kits are mainly targeted for buses and heavy duty trucks running with LNG. However, some dedicated heavy duty dual fuel engines have been commercialized in recent years, such as the Volvo FM MethaneDiesel. Lastly, dedicated applications for light duty engines are not available yet.

2.6 Approach of the Study

2.6.1 Motivation of the Study

Based on the previous sections, the motivations that support the investigations performed on natural gas-diesel dual fuel combustion can be categorized as:

- **To extend the load range**: Combustion efficiency at low loads have been traditionally limited by the lean-limit of natural gas-air mixtures. This is particularly true for light duty applications, where low load and transient operation are essential. Consequently, evaluation of different methods for improving low-load operation is necessary.
- **To decrease CH_4 and NO_x emissions**: Due to the high GWP and direct effect on operational costs, methane slip should be minimized. This inherently means that combustion efficiency must be optimized for an efficient use of the gas fuel. Combustion chamber geometry, valve timings and thermodynamic conditions are some of the characteristics of the combustion process in internal combustion engines which might have an effect on methane slip. However, under certain circumstances, increasing combustion efficiency results in a parallel increase in nitrogen oxide emissions. This is particularly true for retrofitted dual fuel engines where pilot injection is not optimized for dual fuel operation. Therefore, it is necessary to improve the general understanding in this area and try to decouple these two characteristics.
- **To reduce after-treatment cost**: As mentioned, methane is a very stable molecule which is difficult to oxidize at low temperatures. Consequently, it is crucial to maximize the operational window where hydrocarbon emissions are below the legislated limits. On the other hand, allowed NO_x emission levels require expensive after-treatment systems to be installed. Operation with NO_x exhaust levels already below legislation limits would results in a clear cost advantage over after-treatment technologies.

2.6.2 Objective of the Study

The previous three areas represent the context where the investigations presented in this thesis contribute with experimental and simulation results. Based on the information available in the literature, the general objective of this work is *to contribute to the understanding of how the pilot ignited natural gas dual fuel combustion process should be optimized for its implementation in the different fields of application.* Consequently, this general objective is divided into specific objectives as follows:

- **Objective 1**: *Identify the potential of different pathways to increase the combustion efficiency of the dual fuel concept at low loads.* This includes thermodynamic conditions, such as mixture temperature, pressure and composition, and interaction between the PFI and DI fuels (pilot pre-mixing and gas fraction)
- **Objective 2**: *Improve the understanding of how the pilot injection should be controlled over the entire operating range.* This study aims to analyze the potential of different pilot injection strategies for fulfilling the operational boundaries depending on the specific application.
- **Objective 3**: *Analize the interaction between the pilot and main air-gas charge.* The main mechanisms behind the ignition process in pilot ignited dual fuel combustion and the effect of pilot injection on the combustion of the main charge are crucial aspects for achieving efficient combustion.

2.6.3 General Methodology and Research Development

The general approach considered for achieving the previously described objectives is based on a combination of experimental and theoretical tools.

The results presented in this thesis come from experiments performed in different engine platforms, as described in Chapter 3. During the experimental tests performed, several parameters are recorded and some of them are used to feed theoretical models which help to understand the results obtained from engine tests. In this case, a zero-dimensional thermodynamic model, which is defined in Chapter 4, has been selected

as the main theoretical tool. Apart, a one-dimensional diesel spray model has provided extra insights on topics that could not be explored with the available experimental resources or combustion analysis tools. This model is presented and briefly described in Chapter 4.

Chronologically, experiments within the light duty on-road engine context have been performed firstly. They resulted in Papers I, II and III and covered objectives 1 and 2. Research was mainly performed at low and part loads and with a focus on CH_4. However, the focus shifted towards the marine and stationary sectors because of project funding related issues. This new stage allowed to explore the interaction between the pilot fuel and main charge and, therefore, perform experiments for covering the objective 3 using a medium speed marine engine. Moreover, simulations were incorporated for a better understanding of the experimental results. These studies were captured in Paper IV and the boundaries included part and high load operation and NO_x emissions. After this, optical investigations were planned and initial optical tests were performed. However, the project schedule was heavily affected by technical problems with the optical setup. For that reason, only an introduction to this phase is proposed as future work in appendix A.

CHAPTER 3

EXPERIMENTAL FACILITIES

The work presented in this thesis is mostly based on experiments performed in different engines and configurations. In the next sections, information about each experimental facility used is provided, as well as information about fuel specifications. The test cells used for the investigations presented in this document are located in the laboratories of the Division of Combustion Engines at Lund University

3.1 Wärtsilä 20DF Single-Cylinder Engine

3.1.1 Specifications

Single-cylinder metal engine experiments have been performed in a medium speed 4-stroke Wärtsilä 20DF engine. This engine is a dedicated dual fuel engine used as primary mover in marine applications or for electricity generation. The engine is operated in single-cylinder mode,

Table 3.1: Single-cylinder engine specifications

Bore x Stroke [mm]	200 x 280
Connecting Rod Length [mm]	510
Displacement per Cylinder [l]	8.8
Geometric Compression Ratio [-]	13.4:1
Number of Valves	4

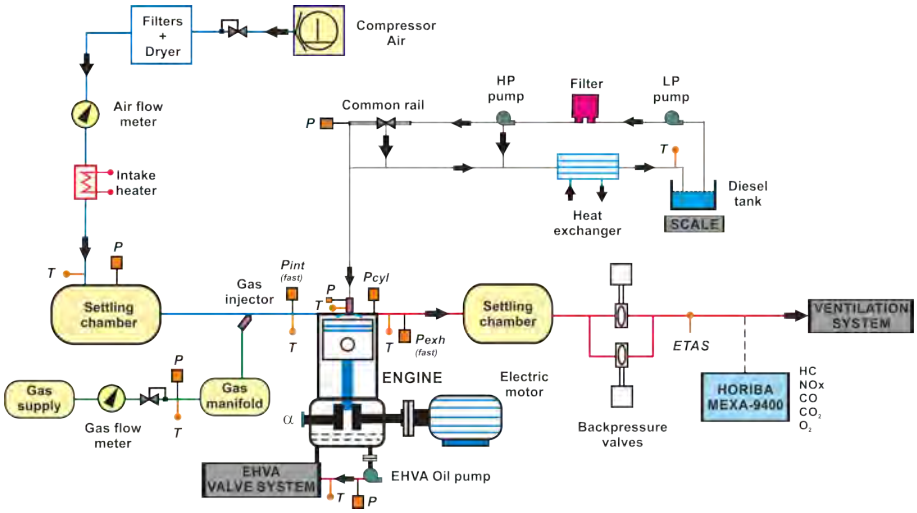

Figure 3.1: Wärtsilä 20DF engine test cell layout

which means that combustion only happens in one cylinder, while the others are "de-activated". In this case, the cylinder located closer to the flywheel has been used. Main engine specifications are depicted in Table 3.1 and Figure 3.1 shows a diagram of the different subsystems present in the test cell.

3.1.2 Electro-Hydraulic Valve Actuation (EHVA)

The engine is equipped with electro-hydraulic valve actuation (EHVA) in order to allow variable valve timing, lift and opening and closing profiles. The EHVA system is based on two industrial Parker D3FP direct-operated proportional DC valves [67], which are controlled via a dSpace-based software provided by Wärtsilä. Two different linear position sensors continuously monitor the positions of the hydraulic pistons and provide real time valve position feedback.

High pressure oil is supplied via an oil pump coupled to the engine crankshaft. This means that both intake and exhaust valves remain closed for some revolutions during engine start, before high pressure oil is available for EHVA operation.

Table 3.2: Main characteristics of the W20DF diesel injector

Type	Solenoid
Steady Flow Rate @ 100 bar [ml/min]	4940
Number of Holes [-]	9
Hole Diameter [μm]	295
Spray Angle [°]	156

3.1.3 Fuel Injection Systems

3.1.3.1 Common Rail Direct Injection System

The engine was originally equipped with diesel fuel jerk pumps. The engine had two different diesel fuel injectors. The main injector was present for full diesel operation, while dual fuel operation was provided via the use of a smaller diesel pilot injector. For this research, only the main injector is used and the jerk pumps are replaced by a modern common rail injection system. The system is based on a Scania XPI high pressure fuel pump coupled to an electric motor run at a constant speed of 500 rpm. Since the fuel pump was not designed for pilot ignition engine operation, a high-pressure valve is installed in the common rail in order to increase the fuel flow through the fuel pump and avoid overheating. A L'Orange VTO-G255 diesel injector is used and its main characteristics are described in Table 3.2.

3.1.3.2 Port Fuel Injection System

The original port fuel injection system has remained unaltered. It consists of a Woodward SOGAV 43 solenoid operated gas admission valve, which injects the fuel directly into the intake port. Gas supply pressure is approximately 4.8 bar and the gas manifold pressure is controlled via a Tescom electronic regulator ER5000 coupled to a pneumatically actuated valve which maintains 1 bar pressure drop over the gas admission valve. Gas injection timing is kept at 330 CAD bTDC, always occurring while the intake valves are open.

3.1.4 Lubrication and Cooling Systems

The lubrication system is based on an oil pump driven by gears located at the free end of the crankshaft, which collects oil from the engine oil

sump and sends it to the different engine components. Lubricating oil temperature and pressure are monitored by the test cell control system. The system is equipped with a thermostat valve for regulating oil temperature since this parameter has great impact on the performance of the EHVA system. Therefore, all experiments are performed under steady oil temperature conditions.

To provide lubrication during start and stop procedures, an electrically-driven pre-lubricating pump guarantees filling of the engine lubricating system. This is particularly necessary due to the increased weight of the engine flywheel required for single-cylinder operation, which increases the need for lubrication of crankshaft bearings during start and stop events.

Regarding the cooling system, a high temperature circuit (HT) and a low temperature circuit (LT) are present. The HT circuit is the one responsible for cooling the cylinder and the cylinder head, while the LT circuit is responsible for oil cooling. Due to the reduced heat flux generated by single-cylinder compared to multi-cylinder engine operation, an external electrical pre-heater and pre-heating pump are installed for reducing warm-up periods and avoid excessively low oil temperatures during engine start. The entire cooling system is pressurized at 2 bar via the use of an expansion tank and pressurized air.

3.1.5 Air Supply System

The engine is not equipped with the original turbo-charging system. Instead, compressed air is used to provide the desired boosting levels. Intake pressure is regulated via a Spirax Sarco two port control valve coupled to a Spirax Sarco SP500 electro-pneumatic smart positioner, which automatically controls valve opening percentage as function of the setpoint provided by the test cell control system. After filtering and drying incoming air, air flow is measured via a Coriolis mass flow meter. Then, air flow continues through an OhmEx electric process heater, controlled by an industrial PID controller, for adjusting intake temperature as desired via the test cell control system. Finally, a 2 m^3 settling chamber is installed just before the engine for reducing the flow pulsations inherent to single-cylinder engine intake events. At this point, the system is equipped with a pressure relief valve calibrated at 6 bar for safety purposes. Finally, both temperature and pressure are

monitored as close as possible to the intake ports. This overall structure allows the operator to manage intake conditions independently of engine operating settings and consequently adds a high degree of flexibility during experiments.

3.1.6 Exhaust System

In order to reproduce turbocharged conditions, the exhaust system is also modified for single-cylinder engine operation. Firstly, both pressure and temperature are measured as close as possible to the exhaust ports. Secondly, a 120 liter settling chamber located in the exhaust line reduces the pulsating waves generated at exhaust valve opening and closing events. At this point, a pressure relief valve calibrated at 6 bar is installed for safety purposes. After this, two electro-pneumatic valves, controlled by a PID controller, are mounted after the exhaust settling chamber for controlling exhaust pressure and, consequently, simulate the degree of back-pressure which is present in the original turbocharged engine. Finally, measurement of emissions and exhaust oxygen content takes place and the exhaust line is redirected towards the ventilation system of the test cell.

3.1.7 Engine Speed Regulation System

An electrical motor ABB M3BP-160-MLB-4 is used to maintain the engine at the desired rotational speed. Nominal power output and speed are 15 kW and 1470 rpm respectively. The electrical motor is controlled via a dedicated ABB control system based on variable-frequency drive and regulator with a precision of ± 1 rpm. A remote is used for introducing stop and start commands and the desired engine speed. This solution allows cranking of the engine without fuel injection enabled, so characterization of the engine can be performed via motored tests.

3.1.8 Data Acquisition and Control System

Data acquisitions systems are required for collecting all available data from measuring equipment and sensors. The control system regulates and commands the behavior and safety of the engine test cell. In this case, three different computers are used, which interact with the

other elements of the engine test cell. Depending on signal acquisition sampling frequency, the signals can be divided into high frequency signals (up to 30 kHz, engine crank angle based) and low frequency signals (up to 50 Hz, time based).

A general diagram of the acquisition and control systems is presented in Figure 3.2. Firstly, a host PC is installed for data visualization of the combustion process and test cell status, and for sending control commands. These commands are sent to the target PC, which processes and adapts the data to the specific needs of the application. Additionally, low sampling frequency data from pressure transducers, temperature sensors and flow meters is fetched to the host PC via an Agilent 34970A sequential logger.

In this case, the target PC communicates with a Wärtsilä cylinder control module (CCM-20) which controls the injection system. The target PC also receives high sampling frequency data, such as encoder signals, in-cylinder pressure or injector current profiles via a PCI-7851R FPGA card. At the same time, commands for controlling valves and actuators, gas exchange pressures and other signals for safety purposes are transferred using the FPGA card input and output channels.

Both host and target computers are part of an in-house developed LabVIEW control system which manages all input and output paths, real-time calculations and safety and emergency shut-down procedures.

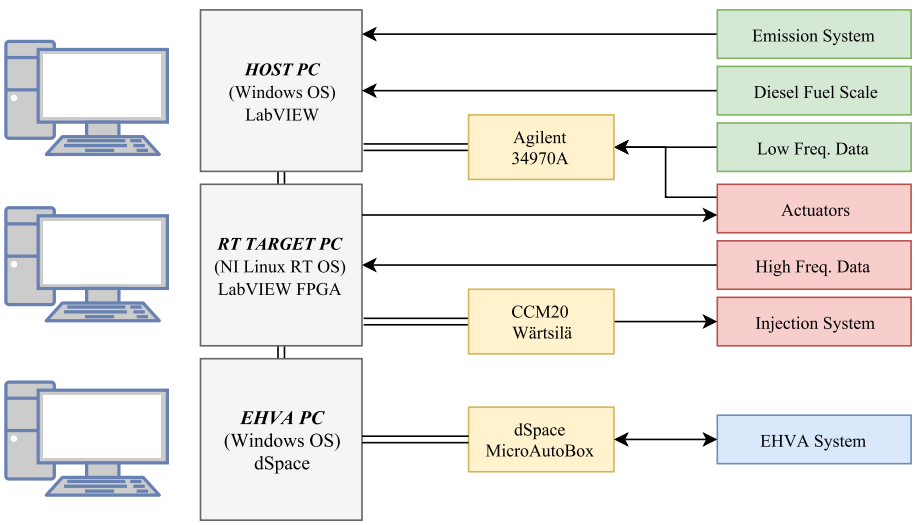

Figure 3.2: Description of Wärtsilä 20DF test cell acquisition and control system layout

Finally, a third computer is dedicated only for interaction with the EHVA system, which is governed by a control system implemented in a rapid control prototyping dSpace MicroAutoBox. Both software and hardware are provided by Wärtsilä.

3.1.9 Instrumentation and Measurement Equipment

3.1.9.1 Piston Position and Speed

The high sampling frequency control system is based on a Kistler 2614CK crank angle encoder located on the crankshaft. It provides two different output signals. The encoder produces digital pulses which trigger the acquisition of high sampling frequency signals every 0.2 CAD. On the other hand, the encoder sends one pulse per revolution in a separate channel, which is used for detecting completed engine revolutions and for engine speed calculation. This signal is synched with the mechanical engine TDC position.

3.1.9.2 High Sampling Frequency Data

In-cylinder pressure sensing is commonly the most important data required for engine combustion analysis. For this purpose, a flush-mounted water-cooled Kistler 7061B piezoelectric pressure sensor in combination with a Kistler 5011B10 charge amplifier is installed in the combustion chamber. The sensor has a measuring range between 0 and 250 bar and it is statically calibrated before each experimental campaign.

Two different water-cooled Kistler 4075A10 piezoresistive absolute pressure sensors are used in intake and exhaust ports respectively. They are mounted on Kistler 737 switching adapters and they have a measuring range between 0 and 10 bar. The pressure signals are conditioned by means of Kistler 4618A0 amplifiers.

Fuel pressure and temperature before the injector nozzle are measured via a Kistler 4067C3000A2 piezoresistive sensor. The signals are conditioned by means of a Kistler 4618A2 amplifier. Finally, injector electrical current profiles for the DI and PFI injectors are measured using a Fluke i30 AC/DC current clamp and two Trafag 8298 piezoresistive pressure transmitters are used for measuring common rail pressure before the DI injector.

3.1.9.3 Low Sampling Frequency Data

Low sampling frequency pressure and temperature signals from intake, exhaust, lubrication and cooling systems are acquired directly via a separate logger unit. K-type thermocouples are used in the test cell for temperature measurement, while pressures of different fluids is measured by Trafag 8298 piezoresistive transducers.

3.1.9.4 Flow Measurement

Air, natural gas and diesel fuel flows are logged using the low sampling frequency acquisition loop. Air flow is measured via a Coriolis mass flow meter Micro Motion 1700. Natural gas flow is measured before the pressure regulation valve with a Bronkhorst IN-Flow Series Thermal Mass Flow Meter F-106A. Finally, diesel fuel flow is estimated by means of a scale. The fuel tank weight is acquired continuously during operation, the data is buffered and a linear regression model is continuously fitted. Under steady-state conditions, the slope of the linear model represents the fuel consumption. For increased accuracy of this method, it is crucial to isolate the fuel tank from possible vibrations and to log fuel tank weight between 2 and 4 minutes, depending on signal-to-noise ratio.

3.1.9.5 Exhaust Gas Measurement

The exhaust gas flow is characterized by a Horiba MEXA-9400 motor exhaust gas analyzer. In this case, NO_x, CO, CO_2, O_2 and TUHC concentrations are acquired. As displayed in Figure 3.1, the exhaust gas is sampled after the back-pressure valves towards the measurement system through a heated line, where temperature is maintained over 190°C to avoid condensation.

Additionally, a lambda sensor LSU 4.9 coupled to an ETAS ES630.1 lambda module is installed next to the emission sampling location for fast estimation of fuel-air ratio. As presented in Chapter 4, exhaust gas composition is used for calculation of the global fuel-air ratio.

Table 3.3: Specification summary of sensors used in the Wärtsilä 20DF engine test cell

Sensor	Model	Measurement Range	Precision
CA Encoder	Kistler 2614CK	0-12000 rpm	±0.03 CA
Cylinder Pressure	Kistler 7061B Kistler 5011B10	0-250 bar	
Intake Port Pressure	Kistler 4075A10	0-10 bar	±0.3% FS
Exhaust Port Pressure	Kistler 4075A10	0-10 bar	±0.3% FS
Fuel Inj. Pressure	Kistler 4067C	0-3000 bar	±0.5% FS
Fuel Inj. Temperature		20-120	±0.5% FS
Generic Pressure	Trafag 8298	0-10 bar	±0.5% FS
Generic Temperature		0-1100℃	±2.5 ℃
Air Flow Meter	MicroMotion 1700	0-725 kg/min	±0.1% FS
NG Flow Meter	Bronkhorst F106A	0-54 kg/hr	±0.4% FS
Diesel Flow Meter	Vettek APP 25.R2	0-25000 gr	±0.1 gr
O_2	ETAS ES630.1	0-25%	
CO/CO_2	Horiba MEXA-9400	0-1/16%	±1% FS
NO_x		0-5000 ppm	±1% FS
TUHC		0-10000 ppm	±1% FS
O_2		0-25%	±1% FS

3.2 Volvo Light Duty Multi-Cylinder Engine

3.2.1 Specifications

Multi-cylinder metal engine experiments are performed in a light duty Volvo D4 diesel engine. The engine was originally equipped with a diesel direct injection common rail system and a natural gas port fuel injection system has been added for enabling dual fuel operation. Main engine specifications are presented in Table 3.4. Figure 3.3 shows a scheme of the different subsystems present in the test cell.

Table 3.4: Multi-cylinder Volvo D4 engine specifications

Bore x Stroke [mm]	82 x 93.2
Connecting Rod Length [mm]	147
Displacement per Cylinder [l]	0.492
Geometric Compression Ratio [-]	15.8:1
Number of Valves	4

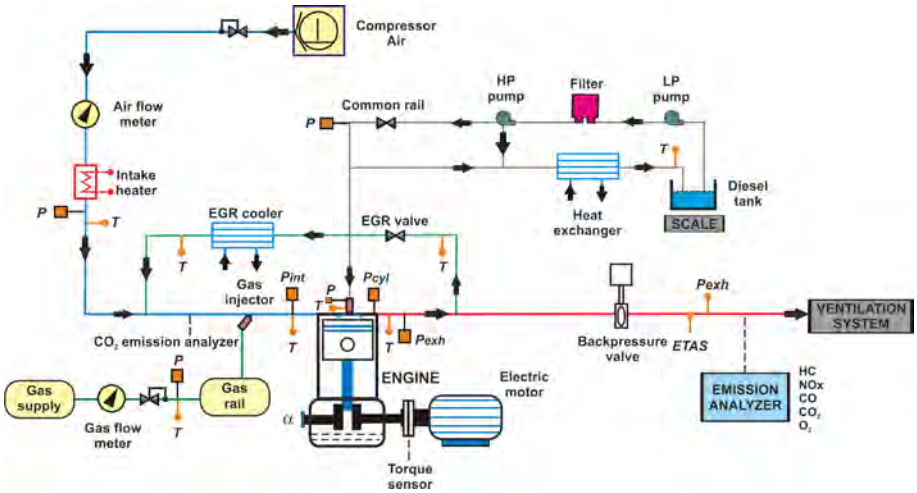

Figure 3.3: Volvo D4 engine test cell layout

3.2.2 Fuel Injection Systems

3.2.2.1 Common Rail Direct Injection System

The engine is provided with a Denso G4S common rail direct injection system. This system is equipped with four diesel direct injectors with integrated fuel pressure and temperature sensors. The main characteristics of the diesel injectors are depicted in Table 3.5.

The high-pressure pump receives diesel fuel from the fuel tank and it is enabled four times per engine cycle for controlling common rail pressure accurately. The engine control system receives rail pressure feedback from an extra pressure sensor installed in the rail volume and adjusts the high pressure pump timing accordingly via a PID controller. Maximum common rail injection pressure is limited to 2750 bar.

Table 3.5: Main characteristics of the Volvo D4 diesel injector

Type	Solenoid
Steady Flow Rate @ 100 bar [ml/min]	800
Number of Holes [-]	8
Hole Diameter [μm]	125
Spray Angle [°]	155

Figure 3.4: Volvo D4 adapter plate for port fuel injection system

3.2.2.2 Port Fuel Injection System

The original Volvo D4 engine is designed for diesel operation. Hence, a port fuel injection system has been installed for allowing natural gas port fuel injection. This system consists of 4 Keihin 73cc CNG injectors, which are connected to an adapter plate placed between the intake ports and the original intake manifold, as observed in Figure 3.4. Each connector of the adapter plate provides CNG to two different ports. The adapter plate is supplied by Westport, although slight modifications where required for fitting it into this diesel engine, since it is originally designed for SI gasoline engines converted to CNG-Gasoline bi-fuel operation.

Gas supply pressure is approximately 4.8 bar. After metering and filtering, the CNG supply line is connected to a common rail where the 4 injectors are installed. From here, four 25 cm hoses distribute the gas to the four different connecting points in the adapter plate. CNG has only been injected while the intake valve is open in order to minimize cylinder-to-cylinder variations [68].

3.2.3 Lubrication and Cooling Systems

The lubrication system of the engine is slightly modified for allowing measurement of piston oil flow and representative oil temperatures. In particular, K-type thermocouples are positioned in the common feed line to the piston cooling oil rail, while piston oil return temperatures are measured in the funnel-shaped collectors below pistons 2 and 3, as presented in Figure 3.5. These temperatures are assumed to be representative also of pistons 1 and 4. This solution allows calculation

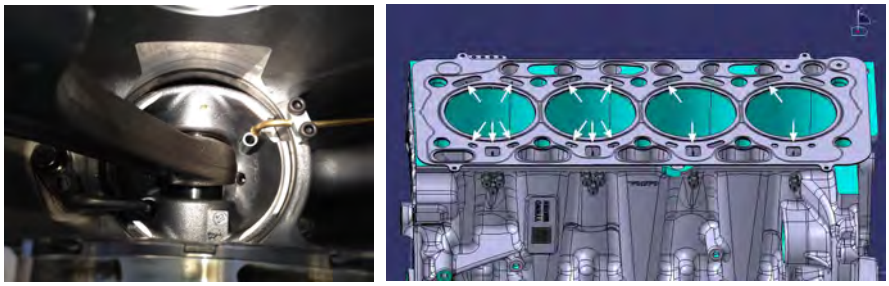

Figure 3.5: Position of temperature sensors installed in the piston oil return line (left) and cylinder head cooling channels (right) in the Volvo D4 engine

of steady-state piston oil cooling energy specifically, instead of global engine oil cooling energy. The stock engine oil cooler has not been altered.

Regarding the cooling water system, some modifications have been implemented for allowing individual measurement of cylinder head cooling and EGR cooling energy. The cylinder head is equipped with a series of T-type thermocouples which permit the estimation of cylinder head heat losses by measuring the temperature difference between intake side and exhaust side cooling channels. The position of the thermocouples is depicted in Figure 3.5. On the other hand, a separate heat exchanger and coolant circuit has been used for controlling EGR temperature before the intake manifold.

3.2.4 Air Supply System

As in the case of the Wärtsilä 20DF engine, the engine is not equipped with the original turbo-charging system. Instead, compressed air is used to provide the desired boosting levels. Intake pressure is regulated via a pilot operated Norgren R18-C00-RNXG pressure regulator coupled to a Norgren VP50 3-way proportional control valve which directly senses feedback pressure from the engine intake manifold. After pressure regulation, air flow is measured via a thermal mass flow meter. Then, air flow continues through a Malux electric process heater, which is controlled by an industrial PID controller, for adjusting intake temperature as desired via the test cell control system. In this case, no settling chamber is installed before the engine manifold since this effect has less importance in light duty multi-cylinder engines compared to medium speed single-cylinder engines. Intake pressure is monitored

at the intake manifold, while individual port temperatures are measured as close as possible to the intake ports.

3.2.5 Exhaust System

Firstly, individual exhaust temperatures are measured as close as possible to the exhaust ports. Secondly, the lack of turbo-charging system results in lower exhaust manifold pressure and different behavior of the pulsating flow generated every exhaust valve opening compared to the original solution. For this reason, an electronically controlled valve is installed after the exhaust manifold for generating a certain degree of back-pressure (generally around 0.2 bar over intake pressure), which resembles the effect of the original turbocharger and generates a positive pressure gradient between exhaust and intake manifold, which enables the use of short-route exhaust gas recirculation (EGR). EGR temperatures are measured before and after the EGR system, which remains unaltered from the stock engine. The EGR flow is controlled by the position of a valve governed by a servo-motor controlled by the test cell control system. Finally, measurement of emissions, soot and exhaust oxygen content takes place and the exhaust line is redirected towards the ventilation system of the test cell.

3.2.6 Engine Speed Regulation System

An electrical motor ABB M2BA-355-SMB-4 is used to maintain the engine at the desired rotational speed. Nominal power output and maximum speed are 355 kW and 2200 rpm respectively. The electrical motor is controlled via a dedicated ABB control system based on variable-frequency drive and regulator with a precision of ± 1 rpm. A remote is used for introducing stop and start commands and the desired engine speed. This solution allows cranking of the engine without fuel injection enabled, so characterization of the engine can be performed via motored tests.

3.2.7 Data Acquisition and Control System

A general diagram of the acquisition and control systems is presented in Figure 3.6. In this case, the target computer is based on a NI PXIe-8115 controller in a NI-PXIe-1078 chassis. The system is

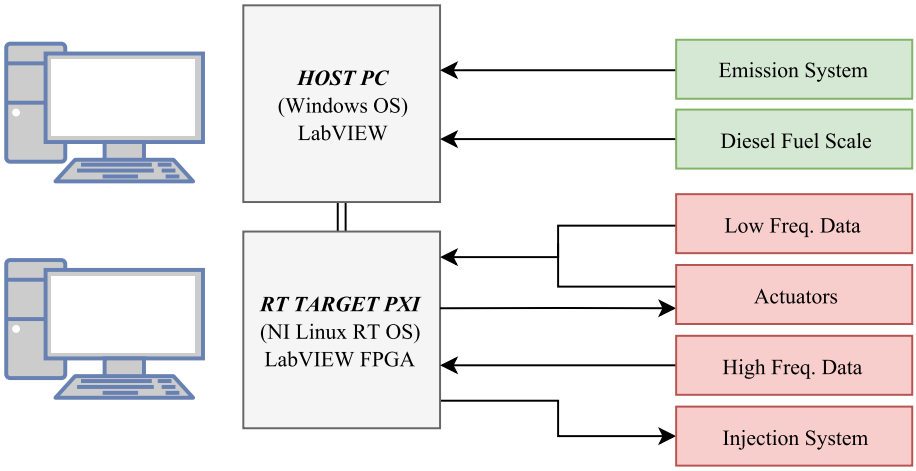

Figure 3.6: Description of Volvo D4 test cell acquisition and control system layout

equipped with two NI FPGA cards (7854R and 7851R) for fast I/O acquisition and control (both analog and digital I/O), a NI-TB4353 for temperature measurements and a NI PXI-6221 for low sampling frequency voltage inputs. Therefore, the different engine test cell components communicate directly with a single computer, which reduces complexity and enables easier error tracking.

Both host and target computers are part of an in-house developed LabVIEW control system for multi-cylinder engine operation, which manages all input and output paths, real-time calculations and safety and emergency shut-down procedures.

3.2.8 Instrumentation and Measurement Equipment

3.2.8.1 Piston Position and Speed

The high sampling frequency control system is based on a Leine & Linde RSI 503 crank angle incremental encoder located on the free end of the crankshaft. The encoder is based on optical scanning of a periodic structure, which results in two different digital output signals, as described in the Wärtsilä 20DF section. The resolution is 0.2 CAD and these signals are used for triggering the acquisition of fast sampling frequency sensor signals and calculating engine speed. The TDC signal is synched with the mechanical engine TDC position.

3.2.8.2 High Sampling Frequency Data

Individual in-cylinder pressure is acquired using 4 nearly flush mounted uncooled AVL GH14P piezoelectric pressure sensors in combination with a 4-channel AVL MicroIFEM piezo amplifier and M8 glow plug adapters AG04. The sensors have a measuring range between 0 and 250 bar.

Additionally, electrical current profiles from injectors (both DI and PFI) and high pressure diesel fuel pump are measured using LEM LTS25-NP current clamps and an OEM common rail pressure sensor is used for measuring common rail injection pressure.

Finally, a HBM T40B torque flange is installed in the shaft connecting the electrical motor and the engine for estimation of brake mean effective pressure, power, specific fuel consumption and efficiency.

3.2.8.3 Low Sampling Frequency Data

The control system in the Volvo D4 engine test cell is centralized in the PXI computer. All measurements except emission measurement data are connected directly to the different cards installed in the PXI computer. In particular, Pentronic K-type thermocouples installed in different locations of the intake, exhaust, cooling and lubrication systems are logged via the NI-TB4353 thermocouple input card. Some Pentronic T-type thermocouples are used for coolant temperature measurement in different cylinder head cooling channels. Each thermocouple input is configured for a specific thermocouple type and cold junction compensation is applied to all channels automatically.

At the same time, pressures of the different fluids are measured using Keller 23SY piezoresistive absolute pressure transmitters with a measuring range between 0 and 5 bar. These signals are sampled by the NI PXI-6221 card.

3.2.8.4 Flow Measurement

The test cell is equipped with 5 different sensors for flow metering. Firstly, air flow is measured using a Bronkhorst IN-Flow Series thermal mass flow meter F-106CI, while natural gas flow is measured before the natural gas common rail with a Bronkhorst IN-Flow Series thermal mass flow meter F-106AI. Then, a Macnaught MX12S-1SA oval meter

Table 3.6: Specification summary of sensors used in Volvo D4 engine test cell

Sensor	Model	Measurement Range	Precision
CA Encoder	Leine & Linde RSI503	0-6000 rpm	±0.02 CA
Cylinder Pressure	AVL GH14P AVL MicroFEIM	0-250 bar	
Fuel Inj. Pressure	OEM Sensor	0-2750 bar	
Torque	HBM T40B	0-10000 Nm	±0.05% FS
Generic Pressure	Keller 23SY	0-5 bar	±0.7% FS
Generic Temperature	Pentronic 8105000	0-1100℃	±2.5 ℃
Air Flow Meter	Bronkhorst F106CI	0-900 kg/hr	±0.1% FS
NG Flow Meter	Bronkhorst F106AI	0-50 kg/hr	±0.4% FS
Diesel Flow Meter	Sartorius MSE12201S	0-12200 gr	±0.1 gr
Oil Flow Meter	Macnaught MX12S-1SA	0-30 L/min	±0.5% FS
Coolant Flow Meter	GL LX-BSP	0-270 L/min	±0.5% FS
O_2	ETAS ES635 + LSU4.9	0-25%	
CO/CO_2	Horiba MEXA-9400	0-1/16%	±1% FS
CO_2 EGR		0-25%	±1% FS
NO_x		0-5000 ppm	±1% FS
TUHC		0-10000 ppm	±1% FS
O_2		0-25%	±1% FS
CH_4	AVL AMA i60	0-10000 ppm	
Soot	MSSPlus AVL MicroSoot	0-50 mg/m^3	±5 g/m^3

is installed for piston oil cooling flow measurement and a GL LX-BSP turbine flow meter is selected for engine coolant flow estimation. Finally, diesel fuel flow is calculated by means of a Sartorious scale in the same way as in the Wärtsilä 20DF test cell.

3.2.8.5 Exhaust Gas Measurement

The exhaust gas flow is characterized by an Horiba MEXA-9200F motor exhaust analyzer. Due to the use of EGR flow during some experiments, CO_2 concentration is also measured in the intake manifold. Additionally, the possibility of measuring CH_4 is available by means of an AVL AMA i60 exhaust measurement system which was installed in the last stages of the project. Finally, soot values are acquired using a MSSplus AVL Micro Soot sensor.

3.3 Baseline Fuel Properties

Both the Wärtsilä W20DF and Volvo D4 engines are run using diesel-like fuel as high reactivity fuel (HRF) and natural gas as low reactivity fuel (LRF). In this section, an overview of the characteristics of the fuels selected is presented.

- **Low Reactivity Fuel:** Compressed natural gas supply is pre-installed in all engine test cells present at the laboratories of the Division of Combustion Engines at Lund University and the pressure is reduced to 4.8 bar. The network is connected to the south-west Sweden's national grid, which is managed by the company Swedegas. Since the natural gas supply is sensitive to changes in composition over time, its specifications are updated monthly and the main characteristics are presented in Table 3.7. The values included in this table are calculated considering only the months when engine experiments have been performed.
- **High Reactivity Fuel:** Swedish diesel MK1, following SS-15 54 35 and EN590 diesel fuel standards, are used as pilot injection fuel for all experiments performed under metal engine conditions. Main specifications are presented in Table 3.7

Table 3.7: (Up) Composition and main properties of the low reactivity gas fuel used in this study. (Down) Main properties of the high reactivity fuel used in this study

LOW REACTIVITY FUEL

	Methane CH_4 mol-%	**Ethane** C_2H_6 mol-%	**Propane** C_3H_8 mol-%	**i-Butane** i-C_4H_10 mol-%	**n-Butane** n-C_4H_{10} mol-%	**i-Pentane** i-C_5H_{12} mol-%	**n-Pentane** i-C_5H_{12} mol-%	**Hexane** i-C_6H_{14} mol-%	**Nitrogen** N_2 mol-%	**Carbon Dioxide** CO_2 mol-%
Average	88.91	6.00	2.46	0.39	0.60	0.13	0.10	0.05	0.32	1.04
Standard Deviation	0.24	0.092	0.059	0.011	0.018	0.005	0.004	0.002	0.008	0.091

	Methane Number -	**LHV** MJ/kg	**Density** kg/m^3
Average	71.70	47.90	0.827
Standard Deviation	0.28	0.11	0.002

HIGH REACTIVITY FUEL

	Cetane Number -	**H/C** -	**Boiling Point** ℃	**Density** kg/m^3	**LHV** MJ/kg
Diesel MK1	51-54	1.87	160-380	810-820	43.15

CHAPTER 4

DIAGNOSTIC METHODS

4.1 Combustion Diagnostics

4.1.1 Heat Release Analysis

The heat release analysis consists of a theoretical formulation which describes the combustion process. It is based on the first law of thermodynamics applied to an open system where the combustion chamber is modelled as a single zone, where pressure, temperature and composition are homogeneous. Cylinder head, cylinder walls and piston form the control volume. Consequently, the first law of thermodynamics applied to that control volume results in:

$$\frac{dQ_{ch}}{dt} = \frac{dU_s}{dt} + \frac{dQ_{ht}}{dt} + \frac{dW}{dt} + \sum h_i m_i \tag{4.1}$$

The previous equation explains that the heat released during combustion (Q_{ch}) is linked to variations of the internal energy (U_s), the heat transfer through the chamber walls(Q_{ht}), the work performed by the piston (W) and the enthalpies (h_i) across the system boundary due to in and out flows (m_i). Depending on the degree of complexity and assumptions made, the specific weight of each term in equation 4.1 might differ. In this particular case, the heat transfer through the combustion chamber

walls and the mass term are neglected. These simplifications imply that:

$$\frac{dQ_{ch}}{dt} = \frac{dU_s}{dt} + \frac{dW}{dt} \tag{4.2}$$

Since mass flux over the control volume is neglected, internal energy can be expressed as a function of bulk gas temperature:

$$\frac{dU_s}{dt} = mC_v(T)\frac{dT}{dt} \tag{4.3}$$

The specific heat capacity at constant volume, C_v, is an index which depends on gas composition and temperature. Considering that the in-cylinder gas follows the ideal gas model:

$$p\frac{dV}{dt} + V\frac{dp}{dt} = mR\frac{dT}{dt} \tag{4.4}$$

The combination of equations 4.3 and 4.4 results in:

$$\frac{dU_s}{dt} = \frac{C_v}{R}\left(p\frac{dV}{dt} + V\frac{dp}{dt}\right) \tag{4.5}$$

On the other hand, the mechanical work produced by the gas inside the chamber is defined by:

$$\frac{dW}{dt} = p\frac{dV}{dt} \tag{4.6}$$

Inserting equations 4.5 and 4.6 into equation 4.2 leads to:

$$\frac{dQ_{ch}}{dt} = \frac{C_v}{R}\left(p\frac{dV}{dt} + V\frac{dp}{dt}\right) + p\frac{dV}{dt} \tag{4.7}$$

In an attempt to simplify expression 4.7, the specific gas constant R and the ratio of specific heats γ are expressed as:

$$R = C_p - C_v \tag{4.8}$$

$$\gamma = \frac{C_p}{C_v} \tag{4.9}$$

which in combination with equation 4.7:

$$\frac{dQ_{ch}}{dt} = \frac{\gamma}{\gamma - 1}p\frac{dV}{dt} + \frac{1}{\gamma - 1}V\frac{dp}{dt} \tag{4.10}$$

Traditionally, pressure and volume in the combustion chamber are expressed in terms of crank-angle θ:

$$\frac{dQ_{ch}}{d\theta} = \frac{\gamma}{\gamma - 1}p\frac{dV}{d\theta} + \frac{1}{\gamma - 1}V\frac{dp}{d\theta} \tag{4.11}$$

which finally correlates the heat release process during the combustion event with changes in volume and pressure in the combustion chamber. This expression is usually referred as *apparent rate of heat release* (aRoHR). Consequently, three different parameters must be known for computing the apparent heat release analysis.

- **In-cylinder pressure:** In most cases, in-cylinder pressure measurement is based in piezoelectric pressure sensors. Unfortunately, piezoelectric pressure sensors are relative pressure sensors which do not provide absolute pressure data. This fact introduces the need of referencing the pressure signal to an absolute level. This process is normally referred to as *pegging*. The method applied through this document is based on the assumption that in-cylinder pressure equals intake pressure during a short interval (typically 10 degrees CA) around intake valve closing. Other methods such as those based on exhaust pressure or those assuming polytropic compression are available in literature [69, 70].

$$p(ivc-5:ivc+5) = p_{intake} \tag{4.12}$$

- **In-cylinder volume:** In-cylinder volume as function of crank angle degrees is defined as:

$$V = V_c + \frac{V_d}{2}\left(r+1-\cos\theta-\left(r^2-\sin^2\theta\right)^{\frac{1}{2}}\right) \tag{4.13}$$

  where V_c is the clearance volume, V_d corresponds to the displacement volume, r is the ratio between the connecting rod and the crank radius. Two different aspects are important in order to evaluate volume in the combustion chamber V as function of engine crank angle θ. Firstly, the different forces present in the combustion chamber have an impact on the nominal dimensions of the engine structure. These forces cause deviations from the nominal volume trace and consequently they affect the heat release calculation. Secondly, there might exist an offset between the piston pin and the center of the crankshaft, which is not considered in equation 4.13.

  Additionally, since the volume calculation is not based on the encoder trigger signals which control the acquisition of in-cylinder pressure data, there might exist an offset between the in-cylinder pressure sensor data and the associated volume trace calculated.

This is normally referred as *TDC offset* and is caused by inaccurate calibration of the crank angle encoder signals. This offset is normally empirically adjusted so the peak in-cylinder pressure during motored conditions occurs at a certain fixed location (referred to as *themodynamic loss angle*; usually between 0.3 to 0.5 CAD bTDC) [71]. In this case, in-cylinder peak pressure during motored conditions is forced to be located at 0.4 CAD bTDC.

- **Specific heat ratio:** In this study, the specific heat ratio during intake and expansion strokes is calculated assuming isoentropic conditions in the combustion chamber during those processes. The transition between the two different zones during the combustion process is assumed to be linear. This is a strong simplification of the combustion process since the specific heat ratio varies simultaneously with temperature and composition [72].

The presented heat release method models a highly heterogeneous (in pressure, temperature and composition) multi-component system and, consequently, it should be understood as an approximation of reality rather than an exact method. Several improvements can be applied to the described method but the proposed approach captures the main characteristics of the combustion process.

4.1.2 Combustion Metrics

Several different parameters can be used to globally describe and understand the injection and combustion events. Therefore, a description of the combustion metrics used in the following chapters is provided below:

- **CAx**: Crank angle degree in which the x% of the total heat release has been released during the combustion process. The crank angle is referred to TDC
- **Start of combustion (SOC)**: Defined as the crank angle position referred to TDC when cumulative heat release reaches 5%.
- **Ignition delay (ID)**: Defined as the time elapsed from the HRF start of injection and SOC. It is normally expressed in crank angle degrees.

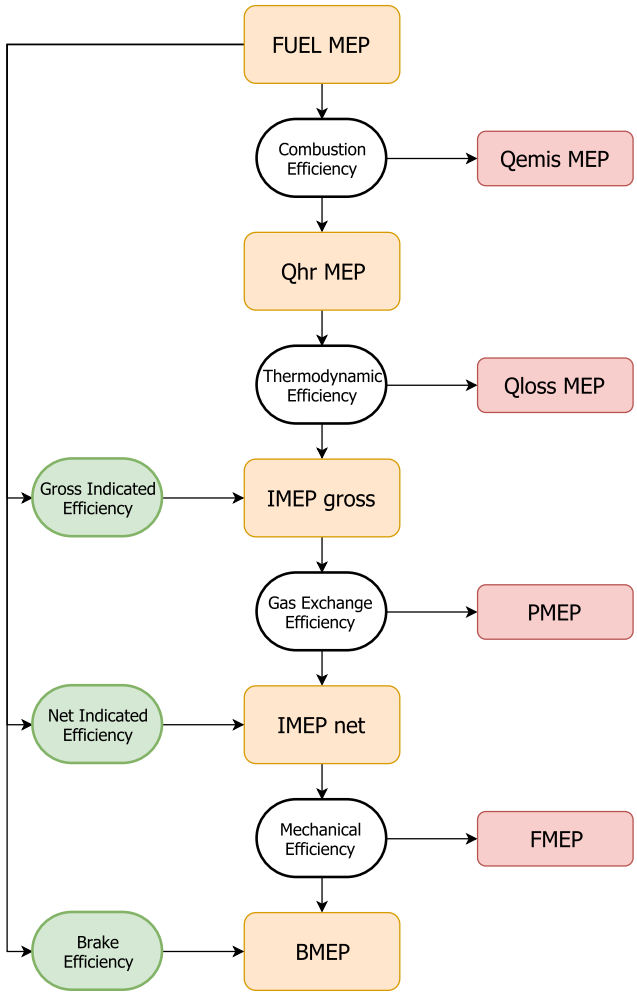

Figure 4.1: Energy flow from fuel to useful mechanical energy, expressed as mean effective pressures and efficiences

- **Combustion duration**: Defined as the time elapsed from SOC up to CA90. It is normally expressed in crank angle degrees.

The different energy or work levels representative of each engine cycle phase can be normalized using the displacement of the engine, resulting in the so called *mean effective pressures*. In this way, the complete engine cycle is defined in a series of energy steps from the fuel energy input to the final engine brake power output. This process is depicted in Figure 4.1 and it includes a definition of the relevant efficiency and energy losses of the system.

- The process starts with the energy contained by the fuel mass (FuelMEP), which results in chemical energy release in the form of heat in the combustion chamber (QhrMEP) after the combustion process. The energy loss associated with this stage (QemisMEP) is represented by partially or fully unburnt fuel, which is estimated through the measurement of exhaust emissions.

- Secondly, part of the heat is converted to actual work on the piston (IMEP gross), while the rest is lost as heat transfer losses (Qloss MEP). This last one includes both heat transfer to the surrounding walls and exhaust gas heat losses.

- The mechanical work transferred to the piston can be calculated via the in-cylinder pressure and volume traces discussed previously. If mechanical work is evaluated over compression and expansion strokes, it is normally referred to as *gross* indicated mean effective pressure, while *net* indicated mean effective pressure (IMEP net) is used over the entire four stroke engine cycle. The pumping losses (PMEP) inherent to the gas exchange process reflect the deviation from gross to net indicators.

- Finally, the efficiency over the entire engine process is represented by the *brake* efficiency. Brake mean effective pressure (BMEP) is estimated by measuring the torque on the engine output shaft. The mechanical losses (FMEP) associated with friction and some auxiliary devices cause the difference between net and brake values.

Regarding combustion stability, the main indicator used in the following chapters is the coefficient of variation of gross indicated mean effective pressure (COV_{IMEPg}), defined as:

$$COV_{IMEP_g}(\%) = \frac{\sigma_{IMEP_g}}{\mu_{IMEP_g}} \times 100 \tag{4.14}$$

where σ and μ correspond to the standard deviation and the mean value of IMEP_g over the measured cycles. The maximum acceptable COV_{IMEPg} during engine operation is set to 5%.

Finally, in-cylinder pressure oscillations and knock are evaluated using the integral modulus of pressure grandient (IMPG), which is defined as:

$$IMPG = \frac{1}{N}\sum_{n=1}^{N}\int_{\theta_0}^{\theta_0+\xi} |\frac{d\hat{p}}{d\theta}| d\theta \tag{4.15}$$

where $\hat{p}$ is the filtered in-cylinder pressure trace (bandpass filter) and θ_0 and $\theta_0+\xi$ define the beginning and the end of the crank angle window over which IMPG is evaluated. The proper filtering frequencies have been estimated using C.S Draper's acoustic pressure wave theory [73], where speed of sound was calculated under the assumption that the premixed charge behaved as an ideal gas. The IMPG knocking level is proportional to the ringing intensity estimator which is commonly used in CI combustion [74, 75, 76]. In this study, IMPG limit has been set at 50 bar.

4.1.3 Stoichiometry

Traditionally, equivalence ratio in single-fueled combustion engines is defined as:

$$\phi = \frac{\frac{m_{fuel}}{m_{air}}}{\left(\frac{m_{fuel}}{m_{air}}\right)_{ST}} = \frac{1}{\lambda} \tag{4.16}$$

where the actual mass flows m_i of fuel and air are compared to the reference mass ratio under stoichiometric conditions *ST*. This method is based on the measurement of air and fuel flows and the prior knowledge of fuel composition for determining the stoichiometric fuel-to-air ratio. However, a more advanced approach based on exhaust emission measurement analysis is used for determining λ in a more accurate way (only valid for non-oxygenated fuels):

$$\lambda = \frac{a}{2(a+\frac{b}{4})}\left(\frac{x_{H_2O}+(1-x_{H_2O})(2x^*_{CO_2}+x^*_{CO}+2x^*_{O_2}+x^*_{NO}+2x^*_{NO_2})}{ax_{C_aH_b}+(1-x_{H_2O})(x^*_{CO_2}+x^*_{CO})}\right) \tag{4.17}$$

where a and b correspond to carbon and hydrogen atoms per molecule of fuel, the wet concentrations of the different measured exhaust species are noted by x^* while the dry concentration of water is estimated using:

$$x_{H_2O} = \frac{b}{2a}\left(\frac{x^*_{CO_2}+x^*_{CO}}{1+\frac{x^*_{CO}}{x^*_{CO_2}K}+\frac{b}{2a}(x^*_{CO_2}+x^*_{CO})}\right) \tag{4.18}$$

where K is the equilibrium constant for the water/gas reaction and its standard value is 3.5 [77]. The previous equations allow the calculation of lambda if exhaust gas analysis is performed with an exhaust gas motor analyzer and the fuel composition is known. However, dual

fuel operation implies the simultaneous presence of two different fuels in the combustion chamber. This introduces uncertainty about which fuel composition to be used for lambda calculation. In this case, the carbon and hydrogen coefficients have been estimated as a function of the relative fuel mass of each individual fuel, as described in 4.19. The high reactivity fuel is assumed to be approximately $C_{12}H_{28}$ while the compressed natural gas is defined as $C_1H_{3.7}$ (due to the presence of multiple gases apart from methane).

$$\begin{aligned} a_{global} &= \frac{n_{HRF}}{n_{HRF}+n_{LRF}} a_{HRF} + \frac{n_{LRF}}{n_{HRF}+n_{LRF}} a_{LRF} \\ b_{global} &= \frac{n_{HRF}}{n_{HRF}+n_{LRF}} b_{HRF} + \frac{n_{LRF}}{n_{HRF}+n_{LRF}} b_{LRF} \end{aligned} \tag{4.19}$$

where n stands for number of moles per second. Before introducing equation 4.19 in 4.17, the fuel composition is re-written as:

$$\begin{aligned} a &= 1 \\ b &= \frac{b_{global}}{a_{global}} \end{aligned} \tag{4.20}$$

As a result, global lambda (or global equivalence ratio) can be estimated accurately under dual fuel mode if the individual fuel flows and compositions are known and exhaust gas measurement is performed. At the same time, single-fuel air-fuel ratio is estimated using equation 4.16 for the HRF and LRF separately.

Additionally to the lambda calculation, the analysis of the exhaust emission measurement allows the calculation of combustion efficiency using [78]:

$$\eta_{comb} = 1 - \frac{\sum \frac{M_i}{M_p} x_i^* (1 - x_{H_2O}) Q_{LHV,i}}{\frac{1}{1+A/F} Q_{LHV,f}} \tag{4.21}$$

where the subindexes p and i stand for products in the exhaust and the different measured exhaust species respectively, the wet concentrations of the different exhaust species are noted by x_i^*, the dry water concentration is given by equation 4.18, $Q_{LHV,i}$ and $Q_{LHV,f}$ represent the lower heating value of the exhaust species and fuel respectively and A/F corresponds to the actual air-to-fuel mass ratio.

4.2 1D Diesel Spray Modeling

The purpose of using 1D spray modeling in this study is to estimate HRF equivalence ratio distribution in the combustion chamber at the experimental SOC. This has been done by using DICOM software [79, 80, 81]. This tool is developed and widely validated at the research institute CMT-Motores Termicos in Valencia, Spain. A collaboration between the author of this thesis and a team of researchers from CMT Valencia has allowed its application to this study. In the next sections, an overview of the model and its simplifications and limitations are presented.

4.2.1 Model Description

The software is based on the model presented in Figure 4.2. The main assumption of the model is that the spray is injected into a quiescent volume which is large enough so the mixture conditions far away from the nozzle remain unaltered. Consequently, the model fits particularly well for diesel injection processes in large bore combustion engines. The velocity profile at the exit of the injector nozzle is uniform. This profile is changed along the spray axis as the flow exchanges momentum with the surrounding mixture, which leads to a cone shape which increases in width with the axial distance. This distance is defined by the variable x while the radial growth is explained by the spray cone angle θ. Consequently, the origin of the spray is defined as:

$$x_0 = \frac{d_0/2}{\tan(\theta/2)} \tag{4.22}$$

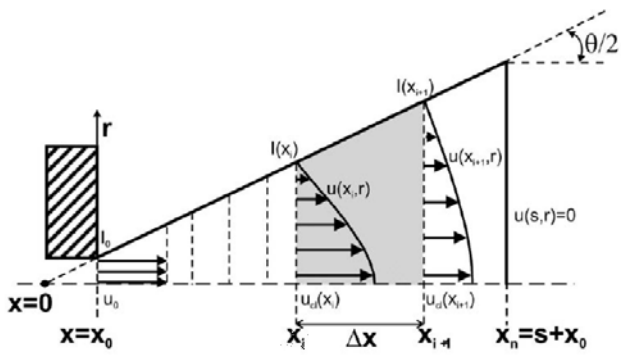

Figure 4.2: 1D Spray model description used in DICOM [79, 80, 81]

The spray domain is divided into cells of thickness Δx along its axial length. Each cell is therefore limited by inlet and outlet sections where $x_{i+1} = x_i + \Delta x$. Required inputs for the model are the spray cone angle (θ), spray momentum (I_0) and mass flux (M_0) at the nozzle exit. In addition, the thermodynamic conditions acquired during engine experiments are also necessary, in terms of fuel injection pressure, density and temperature at the nozzle and surrounding mixture. With this information, the 1D model solves the general conservation equations for axial momentum and fuel mass in terms of the on-axis (i.e., center line) referred to instantaneous values of velocity and species mass fractions. Then, assuming self-similar conditions, the conservative properties are extrapolated radially through a radial Gaussian profile. Local temperature, density and composition can also be calculated through state relationships. The instantaneous spray penetration (S) is defined as the axial position of the cell which satisfies that inlet and outlet velocities are non-zero and zero, respectively. An extensive explanation of the calculation process and the hypotheses assumed by the model can be found in [79, 80, 81].

Despite the reduction in computational cost, the simplifications of geometry and process description imply that the results from the model should only be analyzed qualitatively. The main limitations of the model are:

- The 1-D spray model assumes no swirling conditions and no wall-spray interaction.
- No axial diffusion is considered and injection pressure is assumed constant during the injection process.
- Inert and non-vaporizing spray conditions are selected. This is the reason why the experimental SOC is an input for analyzing the results from the software.
- Only mixed HRF fuel mass distribution is considered, which translates into HRF equivalence ratios from 0.2 to 9.

This tool provides a basic approach to the problem and does not aim to replace complex CFD calculations in real engine geometries. However, it provides useful information to understand pilot spray behavior in engine conditions.

4.2.2 Dual Fuel Model Set-up

Two additional inputs to the software are required for using DICOM in a dual fuel combustion context. In an attempt of resembling real ambient conditions and considering the entrainment of air and natural gas into the diesel spray, the oxygen mass fraction at IVC and the stoichiometric pilot fuel-to-air ratio defined as in Equation 4.23 are required.

$$\left(\frac{m_{HRF}}{m_{air}}\right)_{ST} = \frac{1-\phi_{LRF}}{a_{HRF}+\frac{b_{HRF}}{4}} \frac{12a_{HRF}+b_{HRF}}{32} \frac{1}{1+\frac{Y_{N_2}}{Y_{O_2}}+\phi_{LRF}\frac{1}{a_{LRF}+\frac{b_{LRF}}{4}}\frac{12a_{LRF}+b_{LRF}}{32}} \tag{4.23}$$

The previous equation provides the required HRF-to-air ratio required for reaching stoichiometric conditions when a LRF is present in the surrounding mixture. Apart, the oxygen content at IVC is estimated with the hypothesis that no residual gas remains in the combustion chamber during the gas exchange process.

4.2.3 Model Output

In the context of dual fuel pilot ignited natural gas combustion, the model has mainly been used for estimation of HRF equivalence ratio distribution in the combustion chamber at the experimental SOC. This information is highly important for analyzing the combustion process since it is a key parameter that controls HRF ignition and consequently affects LRF combustion, engine out emissions and combustion efficiency. An example of the results provided by the model is presented in Figure 4.3. For each condition analyzed, the mixing process calculations are initialized at the start of HRF injection timing while the output data is analyzed at the SOC obtained from experimental data. The equivalence ratio distribution is presented in the form of histograms. For the sake of clarity, only the envelope curve is presented and the data is also grouped in 4 different equivalence ratio groups: very lean ($\phi < 0.2$), lean ($0.2 < \phi < 0.8$), reactive ($0.8 < \phi < 1.2$) and rich conditions ($\phi > 1.2$).

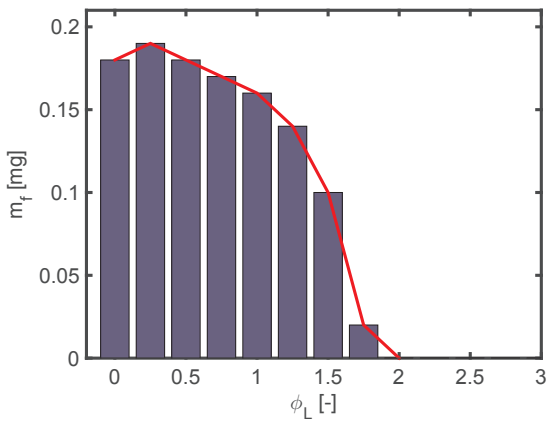

Figure 4.3: 1D Spray model output results describing HRF equivalence ratio distribution at the experimental SOC

CHAPTER 5

RESULTS - LIGHT DUTY APPLICATION

The results presented in this section are focused on high gas fraction low and mid load operation in a light duty diesel engine retrofitted for dual fuel operation. As described in Chapter 2, low load is the most challenging area of operation for automotive applications due to the lean nature of the mixture resulting from unthrottled operation. Consequently, the flammability of the air-gas mixture greatly depends on the equivalence ratio and thermodynamic conditions of the mixture present in the combustion chamber. These conditions can be categorized into those dependent on pilot injection, such as pilot timing, and those which are mainly associated with premixed mixture conditions, such as gas equivalence ratio or mixture temperature.

5.1 Low Load Operation

The maximization of combustion efficiency and consequently, minimization of TUHC emissions directly depends on the thermodynamic conditions of the premixed mixture, i.e temperature, pressure, composition and motion. The mixture should be within its flammability limit for assuring acceptable combustion efficiency. In the next section, a sensibility analysis of the combustion process and flammability and, consequently, combustion efficiency, to different settings affecting in-cylinder reactivity is presented.

Firstly, the isolated effects of gas equivalence ratio (via gas injector energizing time), combustion phasing (via pilot injection timing) and intake temperature (via air heating) are presented, followed by an analysis of their effects on combustion duration and ignition delay for promoting a better understanding of the interaction effects.

Lastly, the consequences on emissions, efficiency and after-treatment considerations are discussed. In this section, combustion efficiency is considered "acceptable" if TUHC are below a hypothetical engine-out TUHC emission level of 4 g/kWh (assuming 0.5 g/kWh legislated limit, 85% oxidation catalyst efficiency and 0.66 g/kWh safety margin). This section is mainly based on discussions included in Paper II.

5.1.1 Combustion Analysis

The effect of gas equivalence ratio on the heat release process is described in Figure 5.1. In this case, it also represents the changes in engine load by adjusting the amount of gas admitted during the intake stroke, given a certain intake pressure. It is observed that the leanest case basically consists of a premixed first peak and there is no evidence of a sustained high intensity flame propagation process immediately after. In the other two cases, there is evidence of flame propagation and even self-

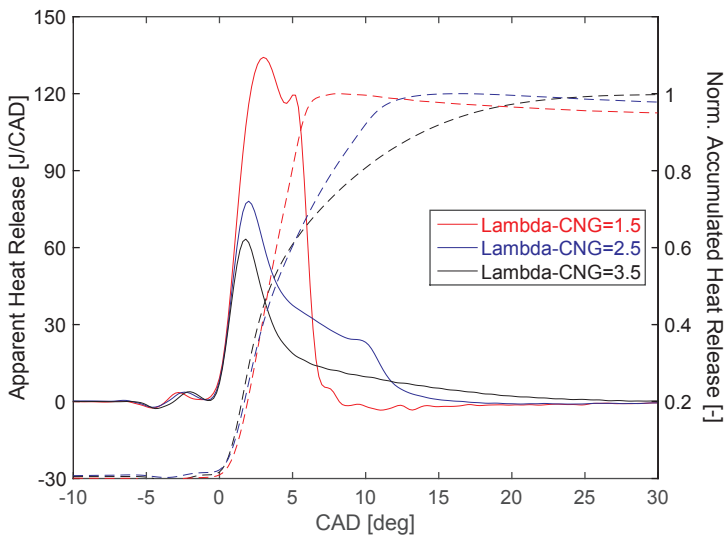

Figure 5.1: Apparent rate of heat release for different gas equivalence ratios. Conditions: 1500 rpm, Diesel single injection: 2.7 mg/st/cyl, $IMEP_g$=8/5.5/3 bar, GF=87/81/76%, EGR=0%, CA50=4 CAD aTDC, T_{in}=90°C

ignition of the gas charge. This suggests that the combustion is beyond the flammability limits in the first case and combustion efficiency is improved as the charge is enriched. It is important to mention how insensitive the cold flame processes and start of ignition associated with the pilot fuel are to different air-gas lambda conditions since pilot injection timing and ignition delay are unaltered between the different cases. In this particular case, this suggests that the pilot fuel ignition is mainly dominated by the mixing rate and thermodynamic effects rather than by the interaction with the surrounding gas mixture.

Secondly, the effect of combustion phasing on the heat release process under late pilot injection conditions is presented in Figure 5.2. As expected, pilot injection timing controls combustion phasing. Therefore, it can be expected that the average in-cylinder temperature during combustion increases for advanced combustion phasing. This causes a reduction of ignition delay and consequently a reduction of the pilot premixing time. This effect combined with the higher in-cylinder temperature results in a staged combustion process, while later combustion phasing results in an HCCI-like combustion event (absence of initial premixed peak)

Finally, in an attempt to enhance combustion efficiency at highly diluted conditions, intake temperature effects have been investigated. An

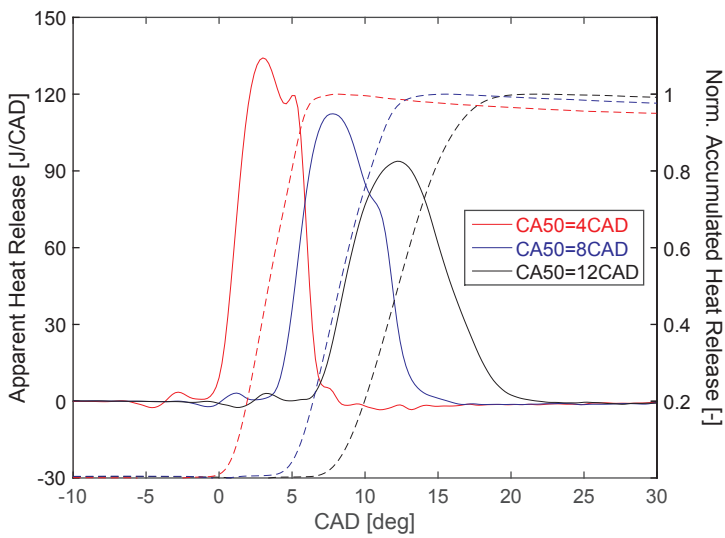

Figure 5.2: Rate of heat release for different combustion phasing. Conditions: 1500 rpm, Diesel single injection: 2.7 mg/st/cyl, $IMEP_g$=5.5 bar, GF=81%, EGR=0%, T_{in}=90°C, λ_{gas}=1.5

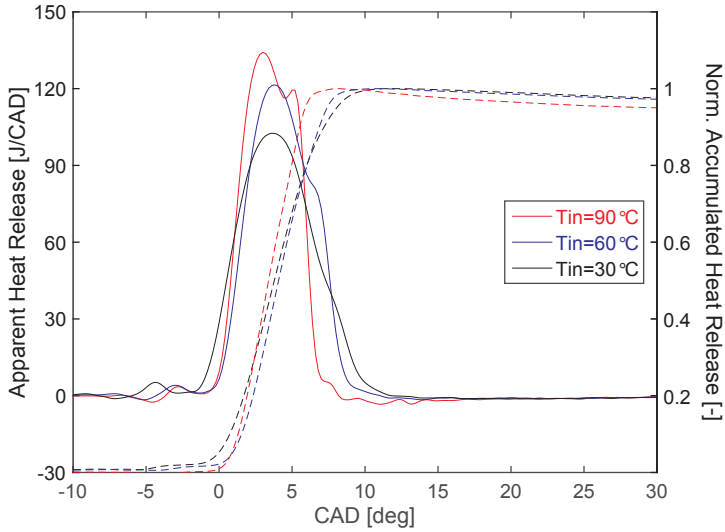

Figure 5.3: Rate of heat release for different intake temperatures. Conditions: 1500 rpm, Diesel single injection: 2.7 mg/st/cyl, $IMEP_g$=5.5 bar, GF=81%, EGR=0%, CA50=4 CAD aTDC, λ_{gas}=1.5

example of this analysis is depicted in Figure 5.3. The results show how the nature of the heat release process is altered. For the lowest temperature case, there is an absence of the traditional premixed heat release peak associated with pilot combustion. This can be due to the lower mixture temperature during pilot injection, which promotes longer ignition delay and, consequently, longer mixing time of the pilot fuel with the main charge, which might cause excessive dilution of the pilot fuel and a reduction of its reactivity. On the contrary, high temperature causes an increase of mixture temperature before SOC, which reduces ignition delay and, therefore, premixed pilot fuel combustion is enhanced.

In summary, these individual results show the importance of appropriate mixture thermodynamic conditions in pilot-ignited dual fuel combustion. Ignition delay, air-gas lambda and overall combustion duration play key roles in the assessment of the combustion process. These parameters are represented in Figure 5.4. Accordingly, ignition delay is mainly governed by temperature effects, while the influence of the gas equivalence ratio on the combustion of the pilot fuel is limited. This suggests that the ignition of the pilot fuel is not clearly influenced by pilot spray entrainment effects. On the other hand, combustion duration is greatly dominated by the gas equivalence ratio when the mixture approaches stoichiometric conditions. Near the lean limit, the variation of combustion duration

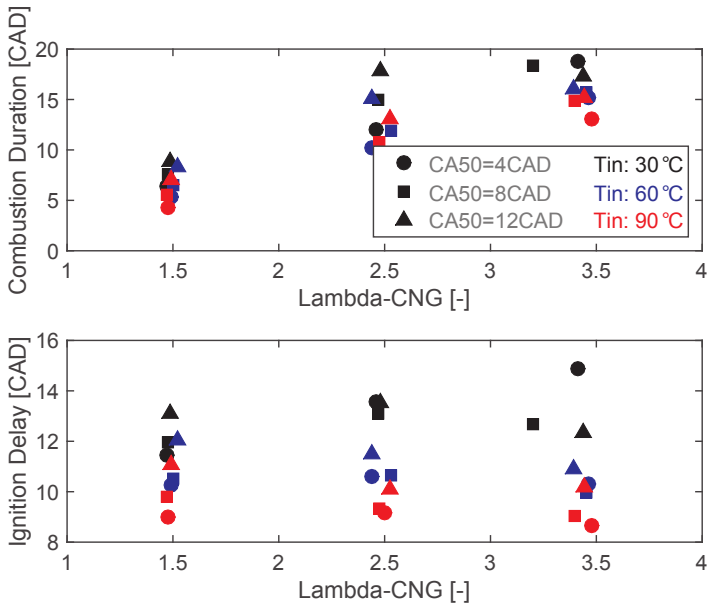

Figure 5.4: Ignition delay and combustion duration sensitivity for the different operating settings. Conditions: 1500 rpm, Diesel single injection: 2.7 mg/st/cyl, $IMEP_g$=8/5.5/3 bar, GF=87/81/76%, EGR=0%

is dominated by temperature effects, since the dispersion of the data increases as the mixture temperature is altered.

All previous information provides a general description of the natural gas-diesel dual fuel combustion process under late pilot injection conditions in a light duty engine operated at low loads. In the following sections, the impact of the combustion process on emissions, efficiency and exhaust temperature is presented.

5.1.2 Performance Analysis

The effects of the previously described control parameters on TUHC are presented in Figure 5.5. The reduction of TUHC when the mixture becomes richer points out that combustion quality is severely improved. For the leanest case, intake air temperature and combustion phasing play a more important role. This suggests that bulk flame quenching dominates since the mixture is beyond its flammability limits. This introduces a limitation of how lean the engine can be operated. On the other hand, the dispersion of the data is reduced as mixture approaches richer conditions, which implies that the trends in TUHC emissions

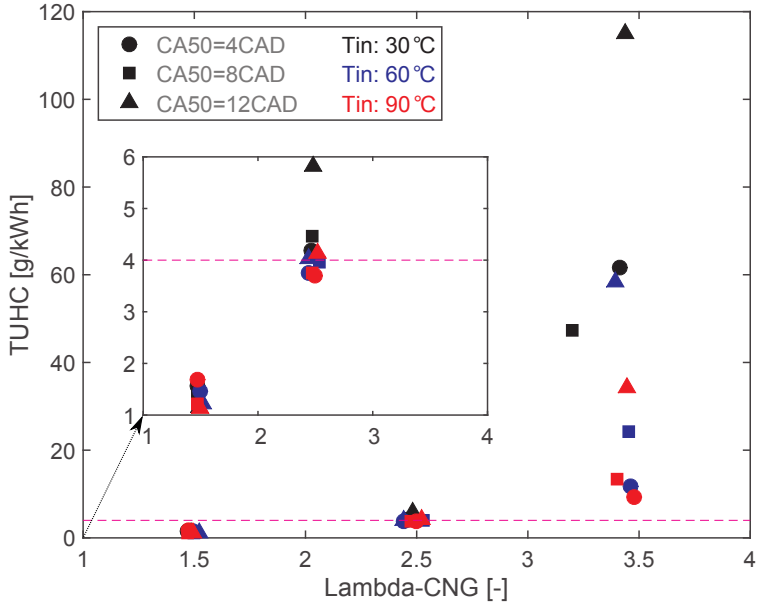

Figure 5.5: TUHC emissions as a function of the different operating settings. Conditions: 1500 rpm, Diesel single injection: 2.7 mg/st/cyl, $IMEP_g$=8/5.5/3 bar, GF=87/81/76%, EGR=0%

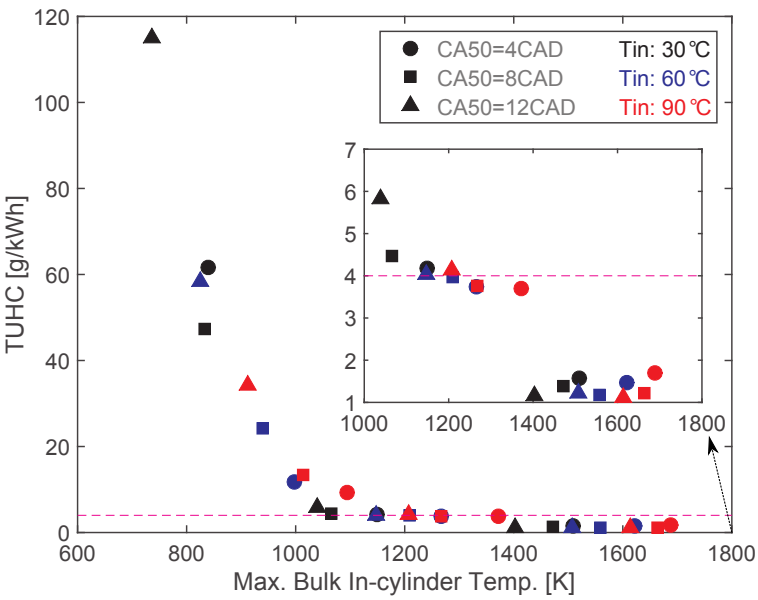

Figure 5.6: TUHC emissions as a function of maximum bulk in-cylinder temperature (ideal gas law) for different operating settings. Conditions: 1500 rpm, Diesel single injection: 2.7 mg/st/cyl, EGR=0%

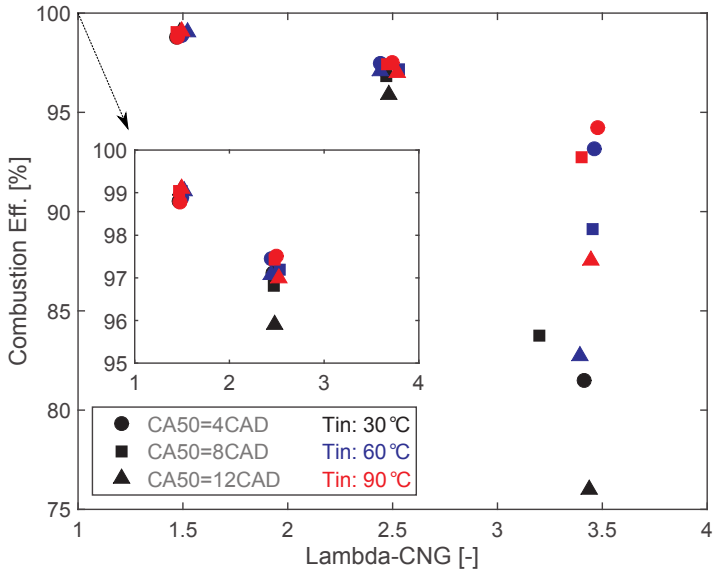

Figure 5.7: Combustion efficiency sensitivity for the different operating settings. Conditions: 1500 rpm, Diesel single injection: 2.7 mg/st/cyl, $IMEP_g$=8/5.5/3 bar, GF=87/81/76%, EGR=0%

cannot be further explained only by bulk flame quenching processes when mixture equivalence ratio is closer to stoichiometric conditions. This is represented in Figure 5.6, where an asymptotic TUHC lower limit of 1 g/kWh is observed. At these conditions, combustion efficiency is close to 99% and there is no clear difference caused by intake temperature. However, earlier combustion phasing does not result in lower TUHC anymore beyond 1400K maximum bulk in-cylinder temperature. In fact, the trend is inverted and later combustion phasing results in slightly poorer combustion efficiency. These facts can be explained by the availability of hydrocarbons released from crevices during the expansion stroke.

Part of the trapped premixed fuel in crevices is released during the expansion stroke. As depicted in Figure 5.4, combustion duration is greatly reduced when the gas-air mixture is enriched. Consequently, combustion phasing should be then selected for enabling the combustion of the released fuel from crevices and, therefore, obtain higher combustion efficiency. However, the use of standard diesel engine pistons probably introduces a limitation in the minimum TUHC emissions achievable due to their large crevice volume and high compression ratio.

In order to quantify the sensitivity of hydrocarbon emissions to intake temperature and combustion phasing variations, a polynomial analysis of the data included in Figure 5.5 results in an operating interval for the maximum gas-lambda value from which TUHC below 4 g/kWh can be achieved via adjustments of in-cylinder reactivity defined as:

$$\lambda_{gas_{max}}(TUHC < 4g/kWh) < 2.32 \pm 0.23 \tag{5.1}$$

Regarding emission after-treatment, the light-off temperature of oxidation catalysts for methane is considerably higher than for oxidation catalysts used for diesel and gasoline after-treatment systems, as described in Chapter 2. This introduces a heavy requirement on the operation of natural gas dual fuel CI engines. As depicted in Figure 5.8, exhaust temperatures are highly dependent on equivalence ratio. Results show that roughly a maximum gas-lambda value of 2 is required for obtaining exhaust temperatures over 400°C. However, exhaust temperature levels can be influenced to some extent by combustion phasing and mixture temperature. For high combustion efficiency cases, retarded combustion results in higher exhaust temperatures. However, under highly diluted conditions, late combustion phasing does

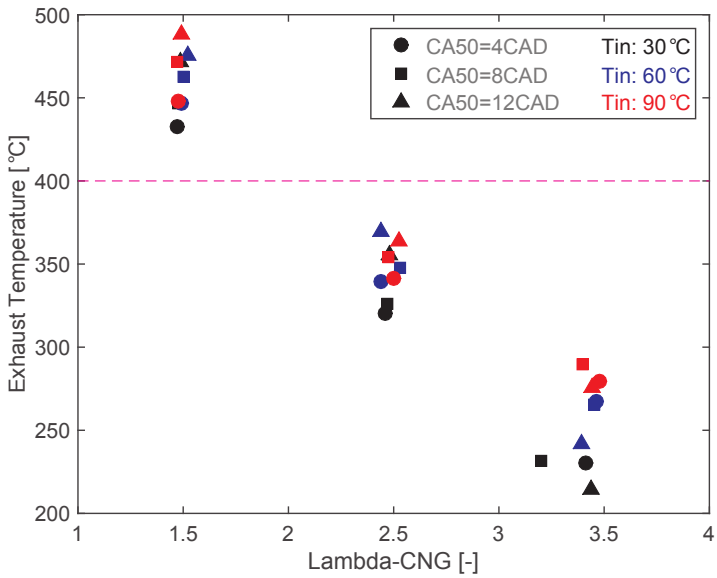

Figure 5.8: Exhaust temperature for the different operating setting. Conditions: 1500 rpm, Diesel single injection: 2.7 mg/st/cyl, $IMEP_g$=8/5.5/3 bar, GF=87/81/76%, EGR=0%

not directly translate into higher exhaust temperatures due to the deterioration of combustion efficiency. Under these conditions, intake air heating stands as a more effective solution than combustion phasing optimization.

In order to quantify the sensitivity of exhaust temperature to intake temperature and combustion phasing variations, a polynomial analysis of the data included in Figure 5.8 results in a maximum gas-lambda value from which acceptable exhaust temperature can be achieved via adjustments of in-cylinder reactivity defined as:

$$\lambda_{gas_{max}}(T_{exh} > 400°\mathrm{C}) < 2.01 \pm 0.25 \tag{5.2}$$

The combination of the relationships 5.1 and 5.2 results in an *average* limit for gas-lambda value of 2.01 (ϕ=0.49) in order to fulfill TUHC emissions and exhaust temperature requirements simultaneously. This also means that an upper *maximum* gas-lambda value of 2.26 (ϕ=0.44) limits engine operation under CDF mode.

Regarding efficiency aspects, it has been shown how combustion efficiency plays a key role at highly diluted conditions. Obviously,

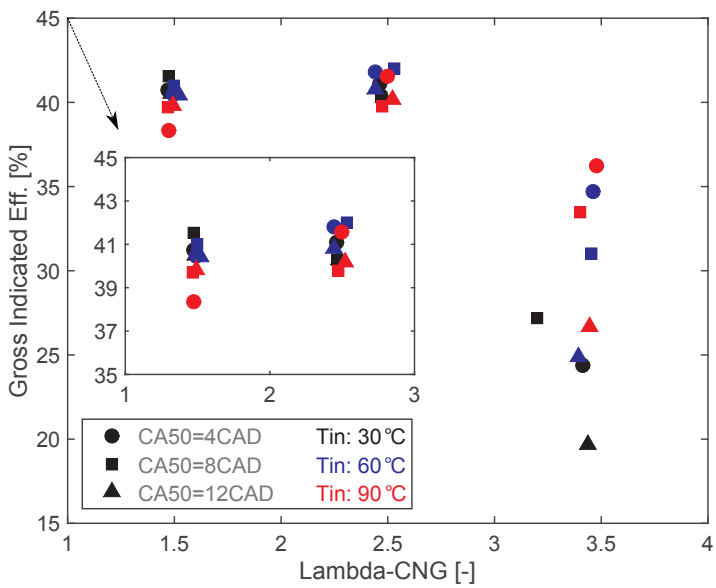

Figure 5.9: Gross indicated efficiency sensitivity for the different operating settings. Conditions: 1500 rpm, Diesel single injection: 2.7 mg/st/cyl, $IMEP_g$=8/5.5/3 bar, GF=87/81/76%, EGR=0%

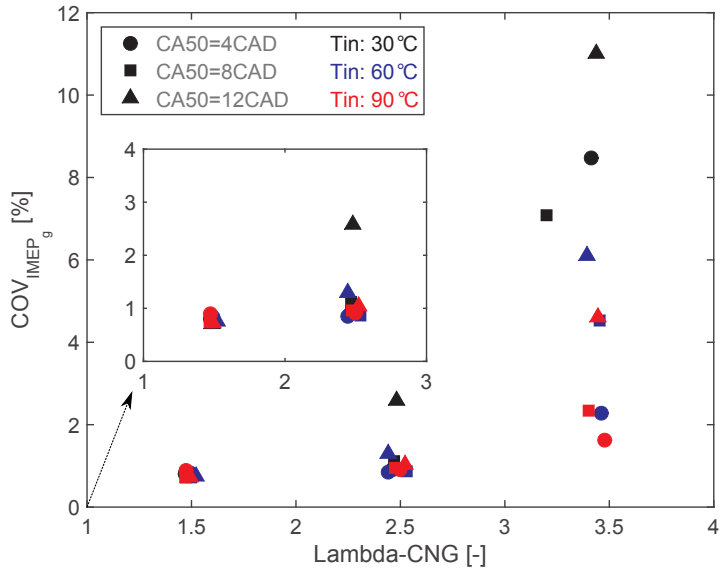

Figure 5.10: COV IMEP$_g$ for the different operating settings. Conditions: 1500 rpm, Diesel single injection: 2.7 mg/st/cyl, IMEP$_g$=8/5.5/3 bar, GF=87/81/76%, EGR=0%

this has a direct effect on the gross indicated efficiency. Figure 5.9 shows that gross indicated efficiency over 40% can be achieved under high gas fraction conditions beyond 5 bar IMEP$_g$, with reasonable TUHC emissions and high combustion stability (see Figure 5.10). These numbers are remarkably higher than those for traditional natural gas spark ignition combustion engines, where throttling losses at low and part loads limit brake engine efficiency. Besides, the use of throttling in dual fuel combustion results in benefits under highly diluted conditions due to the larger increment of combustion efficiency despite increased heat transfer and pumping losses. Therefore, gross indicated efficiency can be further improved at the lowest load tests which results in a minimum indicated efficiency of 40% beyond 3 bar IMEP$_g$ (see Paper II).

5.2 Part Load Operation

The previous section has shown the dominant role of combustion efficiency at low load operation. However, improved combustion efficiency results in an increase of NO_x emissions (Papers I and II). This represents the typical trade-off present in pilot-ignited lean dual

fuel applications between TUHC and NO_x emissions, since combustion temperature should be kept as low as possible for limiting NO_x formation but, at the same time, high enough for robust pilot autoignition and efficient natural gas lean combustion.

At those regions where combustion efficiency is not the main limiting constraint, the number of possible pilot injection strategies increases. Consequently, different combustion modes, which depend on the degree of premixing and quantity of the pilot fuel, are possible. In this context, NO_x reduction stands as a more limiting factor and strategies for its minimization are investigated. The ones here presented are pilot fuel dilution (over-mixing) and EGR. This section is mainly based on discussions included in Paper III.

5.2.1 Combustion Analysis

As introduced in Chapter 2, RCCI combustion requires prior long mixing of the two fuels and low enough combustion temperatures to achieve simultaneous reduction of NO_x and soot. Similarly, the pilot fuel ignition delay can be prolonged to achieve lower combustion temperatures. For that reason, the pilot injection timing has been advanced until excessive pilot dilution results in combustion instabilities under different EGR levels, resulting in a transition from CDF, through partially premixed mode and finally, RCCI conditions. The maximum achievable GF is limited by the EGR levels selected. This is the consequence of the deterioration of pilot fuel combustion efficiency as EGR level is increased. Consequently, high GF under high EGR levels and advanced pilot injection strategy might result in unstable operation. The results presented in this section corresponds to a GF=70% case, enabling in this particular case pilot injection targets outside of the piston bowl.

As expected, advancing *pilot injection timing* results in earlier SOC. This is only valid for those pilot injection timings within 10 and 30 CAD bTDC, as depicted in Figure 5.11. Under these conditions, ignition delay does not show high sensitivity to pilot timing, which suggests that pilot injection globally controls combustion phasing but no substantial change is introduced in the heat release characteristics apart from those related to temperature effects. From this point, the relationship between combustion phasing and pilot injection timing is inverted and the combustion mode shifts towards kinetically controlled processes, which largely depend on thermodynamic conditions in the combustion

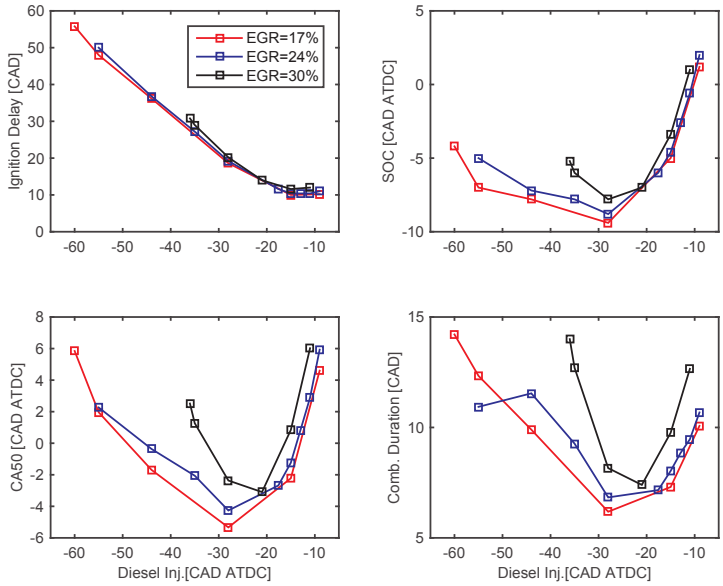

Figure 5.11: Heat release parameters during transition from CDF to RCCI. Conditions: 1500 rpm, Diesel single injection: 7 mg/st/cyl, $IMEP_g$=10 bar, GF=70%, λ_{gas}=2.1/2/1.9, T_{in}=35°C

chamber. Under advanced pilot injection timing conditions, advancing pilot injection results in retarded SOC and a linear relationship between ignition delay and pilot injection timing is established.

EGR levels severely affect the pilot injection window for stable operation. 17% EGR level allows a pilot injection timing window of 60 CAD approximately, while this range is reduced roughly by half for the 30% EGR level. According to Figure 5.11, ignition delay is not heavily affected by EGR levels. However, combustion duration is highly influenced by EGR levels, which suggests a high impact on natural gas combustion. This is particularly true for early pilot injection timings, where flame propagation is likely to dominate the combustion process. Under late pilot injection conditions, pilot autoignition is heavily dominated by the mixing process of the pilot fuel with the premixed charge and consequently, EGR has a lower impact on ignition. Besides, the combustion process under highly premixed pilot conditions is dependent mainly on the characteristics of the main charge due to the over-dilution of the pilot fuel and therefore, the heat release process is relatively more influenced by EGR levels.

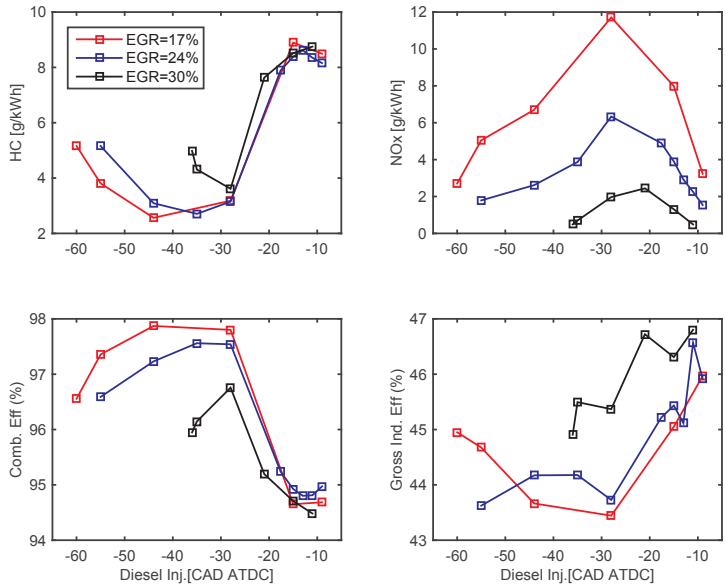

Figure 5.12: Emission and efficiency analysis during transition from CDF to RCCI. Conditions: 1500 rpm, Diesel single injection: 7 mg/st/cyl, $IMEP_g$=10 bar, GF=70%, λ_{gas}=2.1/2/1.9, T_{in}=35°C

5.2.2 Performance Analysis

Emission and efficiency results are presented in Figure 5.12. Regarding TUHC and NO_x engine-out emission, late pilot injection conditions result in the trade-off introduced in the low load operation section. However, the transition towards RCCI conditions offers potential for simultaneous reduction of TUHC and NO_x due to the maximization of combustion efficiency and reduction of engine cooling and exhaust losses. These combined effects are achieved only during a narrow pilot injection window from 30 to 45 CAD bTDC. Further advancements, although offering potential for improved efficiency due to lower heat losses and more optimal combustion phasing, result in a decrease of combustion efficiency and therefore, increased TUHC emissions. This change of behavior might be linked to insufficient pilot ignition energy due to over-dilution of the pilot fuel and wall-jet interaction effects.

It is important to highlight that the global equivalence ratio selected for these tests results in exhaust port temperatures over 400°C for all operating points presented in this section and consequently, after proper optimization work, hydrocarbon emissions could be lowered until hypothetical legislation limits.

It is well known that EGR has a huge influence on NO_x emissions levels due to its impact on specific heat ratio and combustion temperature. These effects greatly reduce heat transfer and exhaust energy losses and those enable high gross efficiency operation. However, as explained in the combustion analysis section, the pilot timing window is severely reduced and consequently, this high efficiency operation cannot be extrapolated to early pilot injection conditions.

5.2.3 Other Considerations

The *mass of pilot fuel* in pilot-ignited dual fuel applications is a key setting from different points of view. Economically, the minimization of pilot enhances vehicle driving range and customer savings. Moreover, maximization of GF could result in lower combustion temperatures due to the lean nature of the gas-air mixture. Simultaneously, NO_x emission levels increase rapidly with pilot mass. Consequently, there should be an optimal pilot mass for the robust ignition of gas-air mixtures for each specific in-cylinder condition. Figure 5.13 shows an example of heat release parameters when pilot fuel mass is minimized.

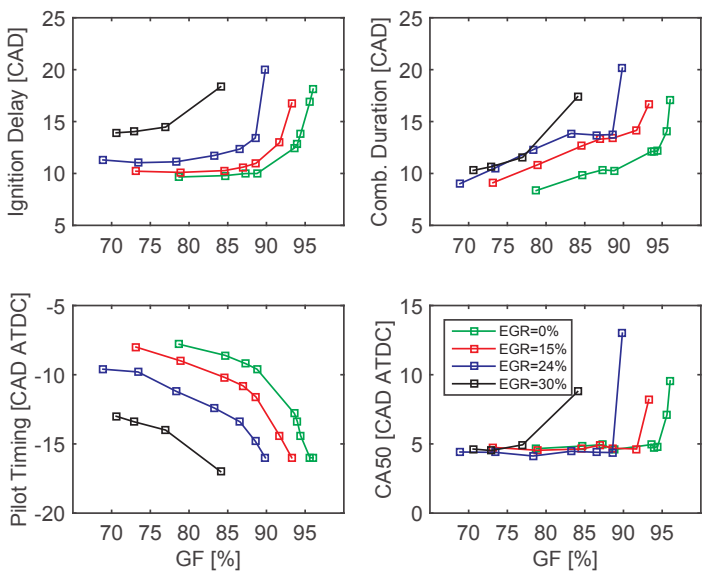

Figure 5.13: Heat release parameters during pilot mass minimization sweep. Conditions: 1500 rpm, λ_{gas}=2.2/2.1/2/1.9, T_{in}=35°C, CA50=5 CAD aTDC

As pilot mass is decreased, pilot timing is corrected for phasing combustion at the desired CA50. That strategy guarantees combustion phasing control until the point that ignition delay is sufficiently long for causing excessive dilution of the pilot fuel prior to SOC. That causes a significant increase of combustion duration due to the reduced ignition energy release from pilot combustion, which eventually results in unstable combustion.

In relation to EGR effects, the maximum GF under stable conditions is reduced as EGR percentage increases. Given a certain mixture temperature and oxygen concentration in the combustion chamber, the pilot fuel will ignite as soon as mixing results in a fuel-air mixture under reactive equivalence ratio. Consequently, if the mixture temperature and oxygen concentration are reduced, such as with the use of higher cooled EGR levels, longer mixing time would be required to achieve ignition. In that case, pilot fuel equivalence ratio distribution will lean out and eventually, ignition energy will decrease causing excessive combustion duration or even misfiring. That appears to be the reason for the upper limits on GF imposed by higher EGR levels.

Engine operation over 95% GF conditions could require excessively short injection durations, which might cause instabilities linked to injector non-linear behavior and shot-to-shot variations in delivered mass. In this case, all points tested which included EGR resulted in stable conditions if EGR was removed. Consequently, it is not likely that instabilities appeared due to the injector shot-to-shot variations. The maximum GF achieved is 96.5% together with a pilot mass of 0.7 mg per cycle and cylinder corresponding to 170us injection duration at 1250 bar injection pressure. In fact, it is likely that this is near the limit of injector needle opening for the given rail pressure and injector. It is unclear which spray pattern appears under these micro pilot conditions and this topic should be further examined in future investigations.

Another aspect which plays an important role in dual fuel operation is air motion. While dual fuel combustion is insensitive to tumble [82], swirl is expected to highly influence the pilot fuel distribution before SOC. In the case of late pilot injection conditions, ignition delay is reduced as swirl is increased, as depicted in Figure 5.14. Charge motion not only affects pilot fuel combustion but also natural gas combustion. Previous research showed how moderate levels of swirl directly (flame propagation velocity) and indirectly (pilot fuel distribution) increase combustion velocity and further improve oxidation of hydrocarbons from crevices in dual fuel

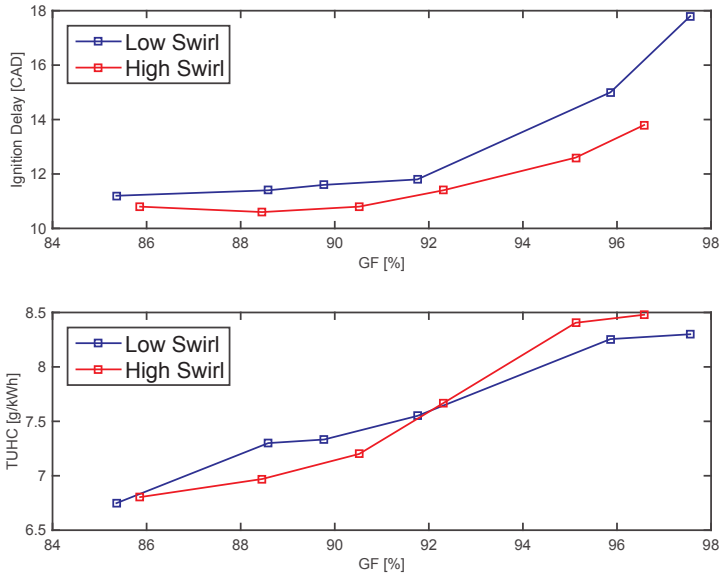

Figure 5.14: Ignition delay and TUHC evolution during pilot mass reduction under different swirl levels. Conditions: 1500 rpm, λ_{gas}=1.5, T_{in}=50°C, CA50=7 CAD aTDC

applications [82]. However, results show that excessive swirl levels under micro-pilot conditions could affect TUHC negatively, most likely due to fuel distribution effects prior SOC.

5.3 Summary Light Duty Application

The two focus areas investigated in the previous sections can be summarized as follows:

- **Low Load Operation**: It has been demonstrated that engine settings combination can be used for improving combustion efficiency at low load operation under highly diluted conditions. Both gas equivalence ratio and mixture temperature are key parameters for dual fuel operation.
  - The main lower boundary limit for low load operation is linked to exhaust temperature and its effect on methane oxidation catalyst efficiency. This severely limits the low load range of pilot-ignited dual fuel engines operated under high GF.

  - Efficient lean operation requires a maximum premixed mixture lambda value of 2.26 (ϕ=0.44) due to after-treatment limitations, together with accurate control of mixture temperature and combustion phasing.
  - Engine operation within project boundaries has been possible only beyond 5 bar $IMEP_g$. Below that level, insufficient exhaust energy and poor combustion efficiency limit natural gas-diesel dual fuel operation under lean and high gas fraction conditions.

- **Part Load Operation**: In those operating points where conditions allow efficient combustion of natural gas, different pilot injection strategies in combination with different EGR levels have been evaluated in an attempt of controlling NO_x emissions.

  - Low NO_x emissions and high efficiency operation can be achieved with lean CDF via the use of large quantities of EGR due to the high ignition energy that diesel combustion provides. The main drawback of this combustion mode is linked to TUHC emissions.
  - The results show how alternative combustion modes, such as RCCI combustion, offer great benefits in terms of simultaneous reduction of TUHC and NO_x, although it requires more advanced combustion control strategies. Due to the nature of the combustion process, exhaust temperature controllability under high pilot premixing conditions is reduced and it mainly depends on global equivalence ratio. Moreover, EGR severely limits the possibility of highly premixed combustion modes due to the deterioration of pilot fuel combustion efficiency.

CHAPTER 6

RESULTS - MEDIUM SPEED APPLICATION

The results presented in Chapter 5 point out the importance of pilot fuel distribution in the combustion chamber for appropriate assessment of the general characteristics of dual fuel combustion. Consequently, this chapter provides deeper insights on the links between pilot combustion characteristics and the ignition process of the gas-air mixture and how pilot autoignition affects the main combustion process in a medium speed dual fuel combustion engine.

The main hypothesis is based on the idea that CDF combustion relies on pilot fuel stratification for combustion stability. However, higher local combustion temperatures and increased knocking probability cause poor performance in terms of emissions and maximum gas fraction at high load. For that reason, reduced stratification of the pilot fuel in the combustion chamber could reduce combustion temperatures and therefore, decrease emissions levels and the risk of knocking.

All test points presented in this chapter were run at 0.5 global equivalence ratio, which resulted in 85% and 95% gas fractions for part and high load operation respectively. Detailed operating conditions can be found in Paper IV.

6.1 Part Load Operation

6.1.1 Combustion Analysis

6.1.1.1 Effects of pilot injection pattern

As described in Figure 6.1 and introduced in Chapter 5, combustion phasing in pilot-ignited natural engines operated under CDF mode is directly controlled via pilot injection timing. However, highly premixed combustion modes result in a linear and inverse relationship between pilot timing and SOC where advancing pilot timing results in later combustion phasing. In addition, the impact of pilot injection pressure on SOC is also depicted in Figure 6.1. While increments in injection pressure under late pilot injection conditions cause earlier combustion phasing, this trend is inverted for early pilot injection timings.

Given constant thermodynamic conditions in the combustion chamber during the compression stroke, the variation of pilot injection pattern results in different pilot fuel mass spatial distribution. Representative cases (15, 30 and 40 CAD bTDC pilot injection timing) have been simulated using the model described in Chapter 4. Results are depicted

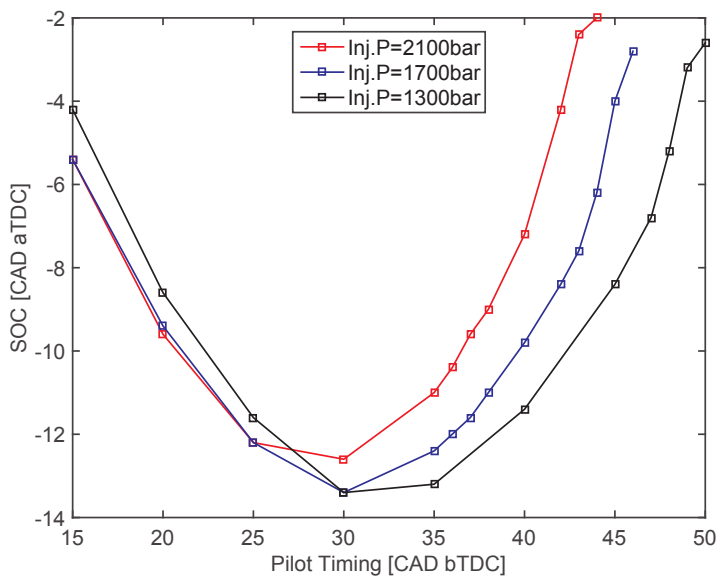

Figure 6.1: SOC versus pilot injection timing for different pilot injection pressure. Conditions: 1000 rpm, Diesel single injection: 50 mg/st, $IMEP_g$=10 bar, GF=88%, EGR=0%, T_{in}=47°C, λ_{global}=2

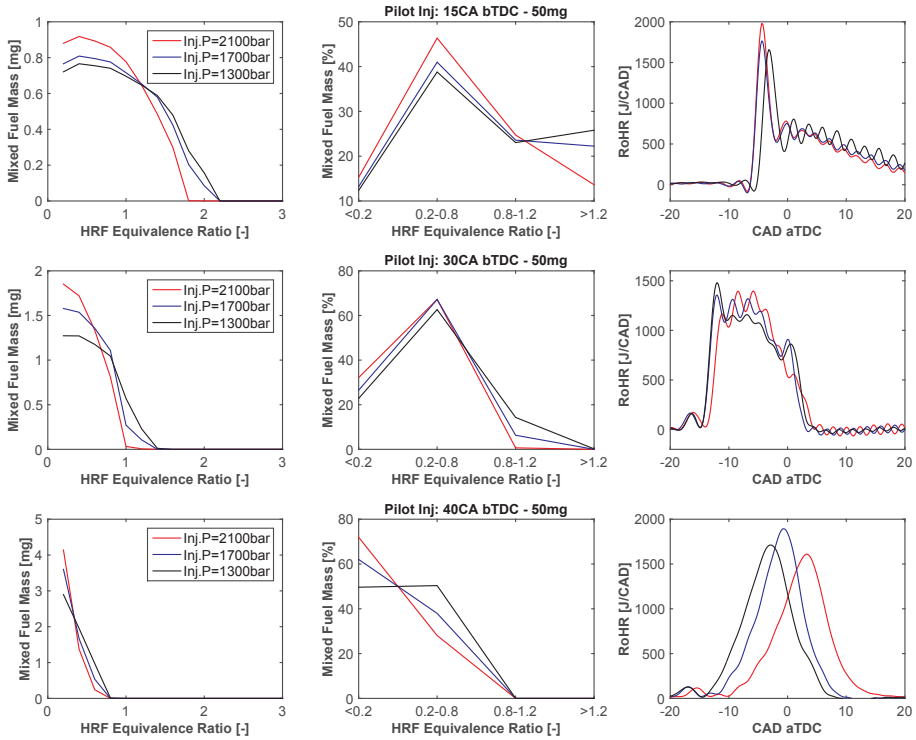

Figure 6.2: RoHR and pilot equivalence ratio distribution at SOC comparison between late and early pilot injection timings. Conditions: 1000 rpm, Diesel single injection: 50 mg/st, $IMEP_g$=10 bar, GF=88%, EGR=0%, T_{in}=47°C, λ_{global}=2

in Figure 6.2, where left and center plots describe the estimated pilot fuel equivalence ratio distribution at SOC and the right plot corresponds to the associated rate of heat release.

In the case of late pilot injection timing (15 CAD bTDC), there is a significant amount of pilot fuel under reactive equivalence ratios at SOC (approximately 25%). This high degree of pilot fuel stratification, in combination with the high pressure and temperature present in the combustion chamber during the injection process, results in short ignition delay. Under these circumstances, given a fixed pilot injection timing, increased pilot injection pressure causes an increment of the pilot fuel mixing rate with the surrounding mixture and, consequently, more pilot mass under reactive equivalence ratio is present at SOC. This is the reason why combustion phasing is advanced compared to cases with lower injection pressure. Moreover, the pilot fuel stratification level is responsible for the high premixed peaks observed during the first stage of the combustion process. However, injection pressure has no

significant impact on combustion rates. Consequently, pilot injection pressure under late pilot injection conditions affect ignition delay but the general combustion characteristics prevail.

On the other hand, the pilot fuel equivalence ratio distribution at SOC for the early pilot injection case (40 CAD bTDC) strongly differs from the previously described scenario. In this case, pilot injection occurs while thermodynamic conditions in the combustion chamber do not result in pilot fuel autoignition. Consequently, longer ignition delay causes an increment of pilot fuel mixing time and most pilot fuel is under lean conditions at SOC. Therefore, the higher the injection pressure, the leaner the pilot fuel distribution, which extends the ignition delay. However, in this case the heat release process is highly affected by the changes in pilot injection pressure and consequently, the resulting pilot fuel equivalence ratio distribution at SOC. The rate at which combustion develops is reduced as injection pressure is increased, which suggests that the longer pilot fuel mixing time reduces the overall reactivity of the mixture. Simultaneously, this leaning process causes the relative effect of thermodynamic conditions in the combustion chamber to be increased, which explains the sensitivity of highly premixed modes to in-cylinder thermodynamic conditions.

The hypothesis that the amount of pilot fuel mass under reactive equivalence ratio at SOC controls the impact of pilot injection pressure on combustion phasing is supported by the results of the transition case. As observed in Figure 6.1, the turning point is located at 30 CAD bTDC pilot injection timing. In this case, simulations suggests that combustion phasing is delayed as soon as there is no presence of pilot fuel stoichiometric areas in the combustion chamber. From this point, any measure towards higher mixing rate results in delayed combustion phasing. This reduced stratification and absence of highly reactive pilot fuel areas in the combustion chamber at SOC cause the Gaussian-shape heat release traces observed in Figure 6.2. This suggests that the mixture reactivity is severely affected by the spatial distribution of pilot fuel since it basically alters the equivalence ratio at which natural gas is burnt. Therefore, as depicted in Figure 6.2, the effects of injection pressure on the heat release process are more intense for early than for late pilot injection conditions.

Besides, the spatial location of the fuel in the combustion chamber plays a key role in the pilot ignition process. Pilot fuel equivalence ratio distributions for the cases 15 and 40 CAD bTDC injection timing are

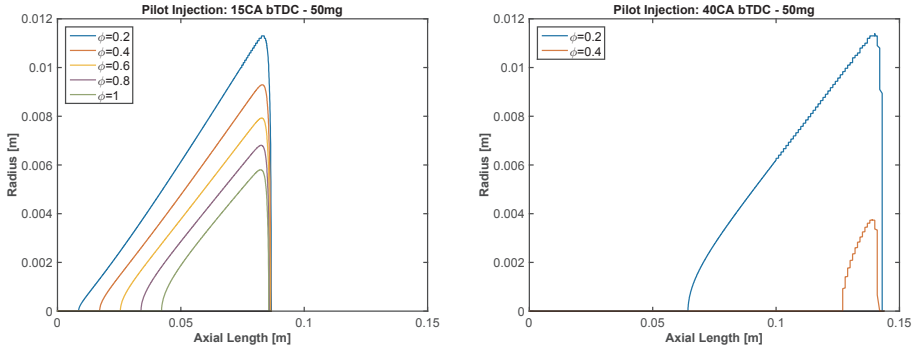

Figure 6.3: Pilot fuel equivalence ratio spatial distribution at SOC for 15 and 40 CAD bTDC pilot injection timing and 1700 bar injection pressure. Conditions: 1000 rpm, Diesel single injection: 50 mg/st, $IMEP_g$=10 bar, GF=88%, EGR=0%, T_{in}=47°C, λ_{global}=2

depicted in Figure 6.3. Under late pilot injection conditions, the pilot fuel with reactive equivalence ratio is expected to be closer to the injector nozzle and at a smaller radius from the center line. This means that only gas and air is present outside the pilot spray area and it explains the low reactivity of the second RoHR phase observed in Figure 6.2. By contrast, early pilot injection conditions result in fuel dispersed more homogeneously over the entire combustion chamber, which causes a more volumetric combustion event, as described previously.

6.1.1.2 Effects of effective compression ratio

One of the drawbacks of controlling combustion phasing only with pilot injection parameters is that acceptable combustion phasing requires high dilution of the pilot fuel as load increases. This is challenging from a control perspective since the ignition process becomes sensitive to little variations in the pilot fuel distribution. For that reason, control of in-cylinder thermodynamic conditions has a role in the ignition process together with pilot fuel distribution. Consequently, under those conditions where pilot fuel distribution results in unacceptable combustion phasing, in-cylinder conditions can be tuned to prolong the ignition delay. One of these techniques consists of variable compression ratio via variable valve timings. Obviously, the reduced compression temperature and pressure causes an overall reduction of combustion temperatures. Consequently and despite the narrower pilot injection timing window, combustion phasing can be adjusted after TDC without further dilution of the pilot fuel distribution at SOC. Details about this analysis can be found in Paper IV.

6.1.2 Performance Analysis

The degree of pilot fuel stratification in the combustion chamber at SOC has a key impact on combustion stability, as depicted in Figure 6.4. High degree of stratification combined with short ignition delay results in robust auto-ignition of pilot fuel. However, those conditions also limit the degree of mixing between the pilot fuel and its surrounding mixture. Therefore, the mixture around the pilot fuel cloud is basically gas and air close to the lean limit. After ignition, the heat release process associated with this mixture is long and slow, which combined with lower cylinder pressure and temperature during the expansion stroke, reduces combustion stability due to end-gas flame quenching.

Intermediate pilot injection timings result in longer ignition delay and increased mixing of pilot fuel within the premixed charge. This increases the overall reactivity of the mixture and combustion stability is maximized. However, excessive ignition delay results in excessive dilution of the pilot fuel and consequently, a reduction of the ignition energy which leads to combustion instability. This can be partially solved by the use of lower injection pressures since pilot fuel premixing is reduced and that maximizes the combustion stability window.

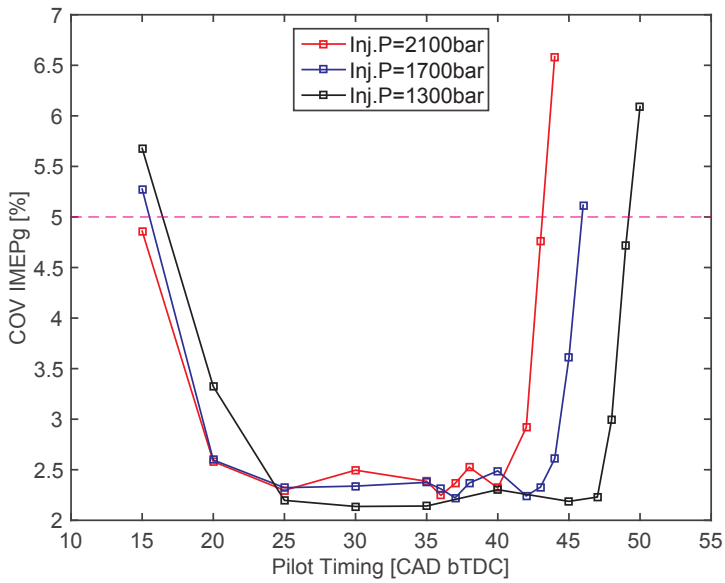

Figure 6.4: COV $IMEP_g$ versus pilot injection timing for different pilot injection pressure. Conditions: 1000 rpm, Diesel single injection: 50 mg/st, $IMEP_g$=10 bar, GF=88%, EGR=0%, T_{in}=47°C, λ_{global}=2

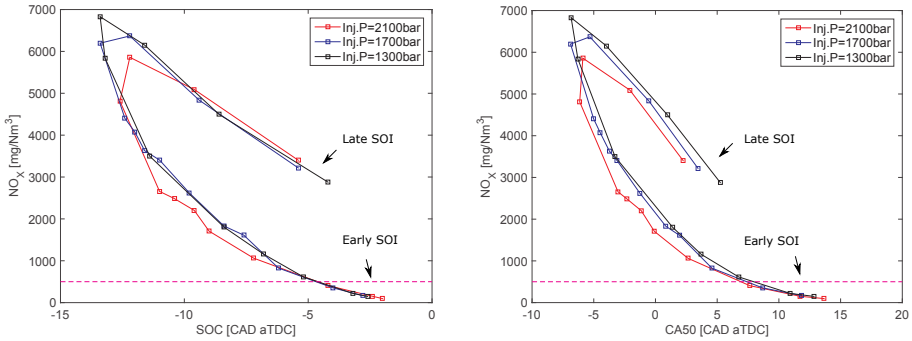

Figure 6.5: NO_x versus SOC and CA50 timings for different pilot injection pressure. Conditions: 1000 rpm, Diesel single injection: 50 mg/st, $IMEP_g$=10 bar, GF=88%, EGR=0%, T_{in}=47°C, λ_{global}=2

Regarding NO_x emissions, the improved mixing of pilot fuel with the surrounding mixture under late pilot injection conditions results in an increase of NO_x emissions. As introduced in Figure 6.2, advancements of pilot injection timing result in a larger mass of pilot fuel at reactive equivalence ratio, which causes earlier combustion phasing and higher heat release peak. For those reasons, CA50 timing occurs earlier in the cycle and NO_x emissions increase due to higher combustion temperatures. However, the increase of pilot fuel premixing as pilot injection timing is further advanced provoke lower engine-out NO_x levels. As depicted in Figure 6.5, pilot injection pressure does not have a clear effect on NO_x emissions at constant SOC or CA50 under early pilot conditions, which suggests that NO_x emissions are mainly dominated by pilot fuel combustion for late pilot injection conditions, while combustion phasing governs this process as mixture reactivity is altered by early pilot injection timings. Therefore, the lowest possible NO_x emissions would be obtained for the longest possible ignition delay where combustion stability is maintained. This means that engine operation around the combustion stability limit is required for NO_x emission minimization under high GF lean operation.

As summary, while short ignition delay conditions cause excessive NO_x emissions, early pilot injection conditions provide potential for stable operation with engine-out NO_x levels below the legislated limit without dedicated NO_x after-treatment system at part load. Due to the lean nature of the mixture, combustion phasing controls NO_x emissions under long ignition delay conditions, while the high degree of stratification of the pilot fuel under late pilot injection conditions strongly contributes to overall NO_x levels despite high GF lean operation.

6.2 High Load Operation

Operation at high load differs from part load conditions due to the limitations in peak cylinder pressure and increased knock probability. Since higher load levels are obtained via higher boosting level and gas flow rate, pilot fuel distribution at SOC is overall more diluted compared to part load operation. Consequently, thermodynamic conditions play an even more important role under high load operation. The next sections briefly described the most important aspects of ignition under high load operation. The strategy implemented included Miller timings for achieving a lower compression ratio at high load. More detailed information is available in Paper IV.

6.2.1 Combustion Analysis

The pilot injection window is delimited by combustion instability for excessively early pilot injection timing and by maximum peak cylinder pressure for less diluted conditions. This range is depicted in Figure 6.6, where SOC is analyzed for two different pilot injection pressures and intake temperatures versus pilot injection timing. As

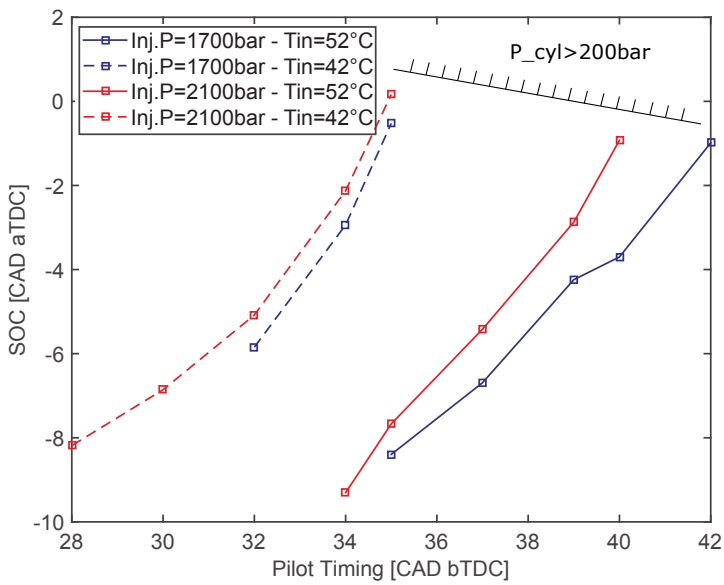

Figure 6.6: SOC versus pilot injection timing for different pilot injection pressure. Conditions: 1000 rpm, Diesel single injection: 45 mg/st, $IMEP_g$=19 bar, GF=95%, EGR=0%, λ_{global}=2

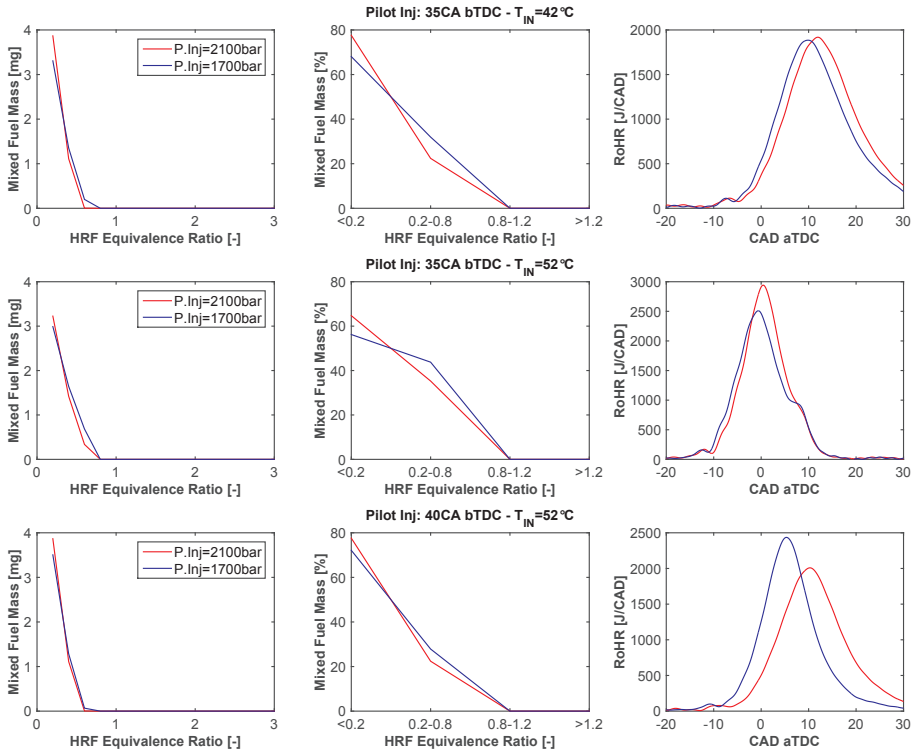

Figure 6.7: RoHR and pilot equivalence ratio distribution at SOC comparison between late and early pilot injection timings. Conditions: 1000 rpm, Diesel single injection: 45 mg/st, $IMEP_g$=19 bar, GF=95%, EGR=0%, λ_{global}=2

observed in Figure 6.6, the pilot injection timing window is severely affected by intake temperature conditions. Given a fixed pilot fuel timing, a variation of 10°C in intake temperature can cause a transition from operation near the limit of peak cylinder pressure to combustion instability. Since SOC is heavily altered by temperature, it can be assumed that the problem of instability at low intake temperature conditions is linked to poor pilot fuel auto-ignition. Once intake temperature is at the high level, pilot injection timing should be further advanced until pilot fuel is again excessively lean. Simulations of pilot fuel equivalence ratio distribution are presented in Figure 6.7, where left and center plots describe the estimated pilot fuel equivalence ratio distribution at SOC and the right plot corresponds to the associated rate of heat release traces.

In the case of low intake temperature conditions, the stability limit is located around 35 CAD bTDC pilot injection timing. This point is

simulated and depicted in the upper row of Figure 6.7. In this particular case, almost 70% of the pilot fuel mass is equivalence ratios below 0.2 at SOC. This translates into low ignition energy and therefore, combustion stability depends mostly on the reactivity of the premixed mixture. For that reason, higher injection pressure results in longer ignition delay, as explained for part load operation.

From these points, higher intake temperature conditions result in unacceptable combustion phasing, since most of the combustion takes place before TDC. This suggests that pilot injection timing should be further advanced and this strategy is presented in the bottom row of Figure 6.7. However, in this case, despite really similar pilot fuel equivalence ratio distributions, the magnitude of the impact of injection pressure is increased. This motivates how sensitive the combustion process becomes to variations of the thermodynamic state and pilot fuel distribution for early pilot injection conditions at high load operation. Therefore, it can be concluded that mixture characteristics have a higher impact on the main combustion process as the fuel stratification is decreased.

6.2.2 Performance Analysis

Under these high load operating conditions, the legislated NO_x emission value corresponds to approximately 0.9 g/kWh. The results presented in Figure 6.8 suggest that high load operation under high GF without the need of NO_x after-treatment system is possible. However, further investigations regarding the controllability of the combustion process are

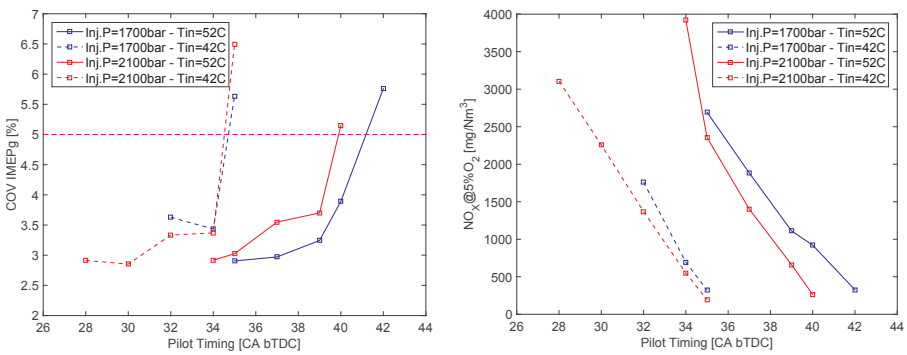

Figure 6.8: COV $IMEP_g$ and NO_x emissions versus pilot injection timing for different injection pressure and intake temperature. Conditions: 1000 rpm, Diesel single injection: 45 mg/st, $IMEP_g$=19 bar, GF=95%, EGR=0%, λ_{global}=2

required since operation around the stability limit is required. Moreover, given fixed thermodynamic conditions in the combustion chamber before SOC, the pilot injection timing window between excessive instability and maximum peak cylinder pressure is in the range of a few crank angle degrees, which introduces even more challenges from a control perspective.

6.3 Summary Large Bore Application

The previous results are part of a set of experiments which was designed to support optical investigations. Experimental results are supported by pilot spray simulations in order to provide an estimation of pilot fuel equivalence ratio distribution in the combustion chamber at the experimental SOC. The goal was to further understand how to control pilot injection characteristics under both CDF and highly premixed combustion modes and to provide initial insights into the ignition characteristics for pilot-ignited dual fuel combustion.

The two focus areas investigated in the previous sections can be summarized as follows:

- **Part Load Operation**: It has been demonstrated that extremely low NO_x emission levels can be achieved without the need of an after-treatment system (marine and stationary applications) under part load conditions via adjustments on pilot fuel equivalence ratio distribution.
  - Pilot fuel distribution in the combustion chamber before SOC highly affects not only start of combustion but also mixture reactivity and consequently, premixed mixture combustion characteristics.
  - Pilot fuel injection pressure has a larger impact on NO_x for early injection timings. For late pilot timing conditions, this effect has a lower weight on the start of combustion timing since thermodynamic conditions result in short ignition delay (presence of pilot fuel under stoichiometric equivalence ratio). However, early pilot injection timings cause an increase of the ignition delay, which enhances the mixing process and results in a well mixed overall lean mixture prior to start of

combustion. This is responsible for the absence of a premixed heat release peak and the HCCI-like heat release process.

  - Excessively lean conditions will lead to poor ignition characteristics, which combined with lean natural gas conditions, will deteriorate combustion stability. On the other hand, excessively rich areas will contribute significantly to NO_x emissions and, despite robust ignition, flame propagation throughout the premixed mixture will be poor due to its reduced reactivity.

- **High Load Operation**: It has been demonstrated that extremely low NO_x emission levels can be achieved without the need for an after-treatment system (marine and stationary applications) even at high load conditions via adjustments of pilot fuel equivalence ratio distribution. However, the operating range is severly limited by maximum peak in-cylinder pressure and combustion instabilities.

  - Late pilot injection settings result in excessive in-cylinder pressure and therefore, this combustion mode is not suitable for high load operation.
  - Over-dilution of pilot fuel is an effective way of expanding the load range. However, the operating range is really narrow (in the range of few crank angle degrees).
  - Miller timing operation (late IVC) allows high load operation with reduced mixture temperature and pressure after the compression stroke and therefore, reduced knocking probability.
  - Operation near the lean limit at high load implies a high sensitivity of the combustion process to mixture thermodynamic conditions. Consequently, cycle-to-cycle control strategies should be further investigated for assuring robust operation.

CHAPTER 7

SUMMARY AND CONCLUSIONS

This chapter contains a brief summary of the main observations and contributions of the work presented in this thesis. An overall overview of the topics investigated in this thesis is provided in Figure 7.1.

Different studies have been conducted to evaluate the performance of pilot-ignited natural gas dual fuel combustion as an alternative to conventional spark ignition natural gas combustion. The main objective of the work is to contribute to the understanding of how the pilot ignited natural gas dual fuel combustion process should be optimized for its implementation in the different fields of application.

The literature review performed on natural gas-diesel dual fuel combustion provided a description of the general challenges. The ones considered in this thesis are the trade-off between TUHC and NO_x under lean conditions, combustion efficiency at low loads, the oxidation of CH_4 in the after-treatment system and the possibility of knock during high load operation.

These issues have been addressed by modifications of in-cylinder reactivity. Two different approaches have been presented. The first one is related to the premixed mixture characteristics and it involves intake conditions, EGR, gas fraction and valve timing strategies. The second one is linked to pilot injection settings, so advanced injection strategies, pilot injection pressure and combustion phasing optimization

have been evaluated. These two ways determine the characteristics of the premixed mixture and pilot fuel distribution just before the start of combustion and, consequently, they greatly influence its characteristics. The main assessment parameter is the ignition delay.

- **Low Pilot Premixing**: This can be roughly defined as the range where the ratio between ignition delay and pilot injection duration is lower than 5. It results in 2-phase rate of heat release due to the presence of highly reactive pilot fuel areas in the combustion chamber just before the start of combustion. Consequently, pilot injection controls the start of combustion and ignition of natural gas takes place mainly in the surroundings of the pilot fuel clouds. Regarding its performance, this mode is characterized by high NO_x emissions and poor combustion efficiency under lean conditions. However, controllability is improved and robust ignition is achieved.
- **High Pilot Premixing**: This can be roughly defined as the range where the ratio between ignition delay and pilot injection duration is greater than 5. The pilot fuel combustion process cannot be distinguished from the main combustion process via the rate of heat release since the pilot fuel distribution at start of combustion is overall lean or very lean. Consequently, pilot injection does not control the start of combustion directly and ignition is expected to happen a at longer radial distance from the pilot injector nozzle. Under these circumstances, extremely low NO_x emissions can be achieved and TUHC are also reduced due to the larger area covered by pilot fuel. The lean nature of the pilot fuel distribution reduces the risk of abnormal combustion but controllability and poor ignition can limit the operating range.

As a result, it can be concluded that ignition delay controls the overall combustion mode. While conventional dual fuel combustion relies on pilot fuel stratification and consequently, low pilot premixing conditions, alternative combustion strategies are based on high pilot premixing via longer ignition delay. For this reason, accurate pilot fuel injection control is a key feature in dual fuel combustion. It has been demonstrated that operation near the lean-limit for the premixed mixture implies that most NO_x emissions are caused by the pilot fuel stratification. This is also the reason why high pilot premixing results in simultaneous reduction of NO_x and TUHC emissions compared to low premixing conditions.

Under low premixing conditions, high load operation is very limited by excessive peak cylinder pressure and the possibility of knocking behavior. For that reason, this mode is mostly valid at low and mid load ranges. Under these circumstances, experimental evaluations of the natural gas dilution limit under the context of strict CH_4 emission levels have pointed out that a maximum premixed mixture lambda value of approximately 2.26 (ϕ=0.44) due to methane after-treatment considerations is required. Under these conditions, the simultaneous optimization of intake manifold conditions, such as intake temperature or pressure, and combustion phasing can result in acceptable operation via improvements of combustion efficiency. In this particular case, a modern multi-cylinder CI light duty engine has been effectively operated under dual fuel high gas fraction conditions beyond 5 bar $IMEP_g$. At part load conditions, where combustion efficiency is not the main limiting factor, NO_x emissions can be controlled via moderated EGR rates and, together with increased ignition delay, simultaneous reduction of TUHC and NO_x emissions can be achieved via high pilot premixing conditions.

Advanced pilot injection timing has been proved as an effective way to decrease NO_x emissions due to the highly lean nature of the premixed mixture. Apart from the benefits in terms of TUHC and combustion efficiency, it has been shown as an effective way of controlling peak cylinder pressure and knock probability due to the reduced ignition energy. In this particular case, experiments performed in a medium speed marine engine has shown that part and high load operation under high gas fraction conditions is possible without the need of an NO_x after-treatment system. However, due the overall lean nature of the pilot distribution at the start of combustion, thermodynamic conditions in the combustion chamber have a higher relative impact on overall performance than in low premixing conditions. For that reason, accurate control of intake manifold conditions is crucial for maintaining high pilot fuel combustion efficiency and combustion stability without increasing the risk of knocking cycles.

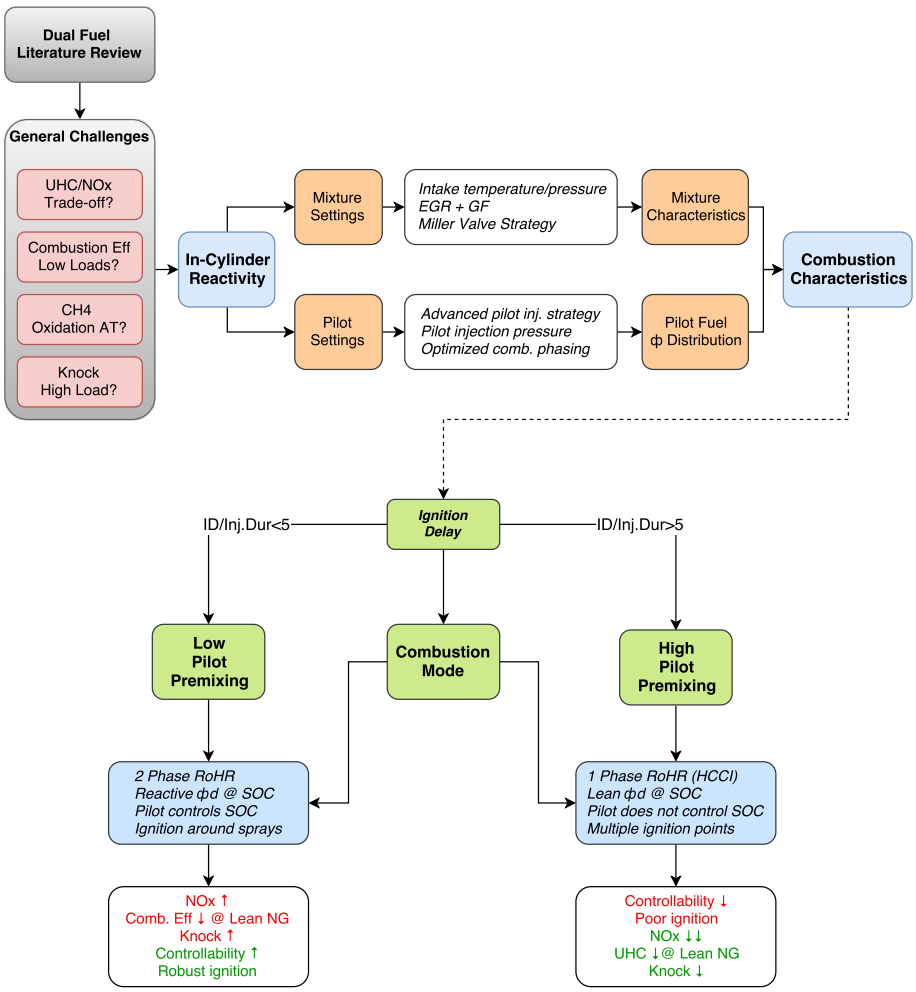

Figure 7.1: General view of the different studies presented in this thesis

CHAPTER 8

FUTURE WORK

Some suggestions for future pilot-ignited dual fuel combustion research are:

- The ignition process is a complex process in dual fuel combustion. The spatial location of the initial ignition spots and how those locations are affected by the pilot fuel distribution and thermodynamic conditions in the combustion chamber remain unclear. Consequently, optical investigations should be applied to further investigate this question.
- The use of micro-pilot injections for ignition purposes implies the use of really short injection durations. This might cause the pilot injector to operate only under transient conditions so it might never reach a steady needle opening. Therefore, most likely traditional spray models for diesel sprays do not apply for pilot-ignited dual fuel operation. Then, a specific pilot fuel "plume" definition for micro-pilot conditions and how it is affected by different injector specifications should be analyzed.
- Related to the previous suggestion, it would be highly relevant for high gas fraction operation to clarify which parameters limit the minimum pilot fuel mass delivered by a DI system.
- All previous suggestions are required to improve the validation of current models for dual fuel combustion simulations since the

availability of optical investigations is more limited than in other fields, particularly for medium speed combustion engines.

Some of the previous areas for future work were initially planned as part of the work to be presented in this thesis. The single-cylinder Wärtsilä 20DF engine described in Chapter 3 and used for the investigations presented in Chapter 6 was converted to optical configuration. Unfortunately, different technical problems limited the amount of investigations carried out and therefore, results have not been included in this thesis. However, information about this novel setup and a few preliminary results are provided in Appendix A as a complement to this section.

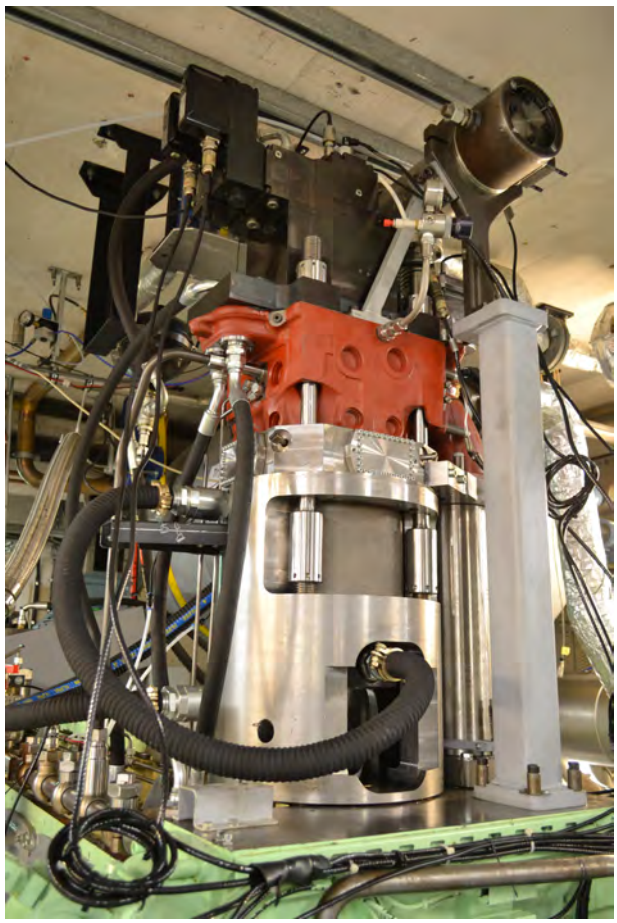

Figure 8.1: Wärtsilä 20DF optical engine

APPENDIX A

WÄRTSILÄ 20DF OPTICAL ENGINE

A.1 Introduction to Optical Engines

Combustion engine research is carried out by means of many different techniques. In general, ordinary combustion engines are used, where the combustion chamber is made of steel, aluminium or other metallic elements. Typically, these engines are instrumented with in-cylinder pressure sensors and, in some cases, other sensor-based techniques might be applied. The knowledge that this experimental technique offers is consequently based on these sensors. However, it is extremely useful to actively visualize the phenomena that occurs inside the combustion chamber. For this purpose, optical engines are designed to provide optical access and, by means of high speed cameras and other tools, record and analyze the processes that take place inside the combustion chamber.

Already back in 1872, Nikolaus Otto used optical diagnostics to develop his famous 4-stroke cycle. He designed a model with a transparent cylinder to observe the motion of smoke entering the cylinder during the intake stroke [83]. Other researchers and inventors kept developing combustion engines by using optical access in certain areas of the combustion chamber, but it was not until 1961 when Fred Bowditch created a breakthrough in optical engine design by introducing the quartz piston engine [84]. Nowadays generally called Bowditch design,

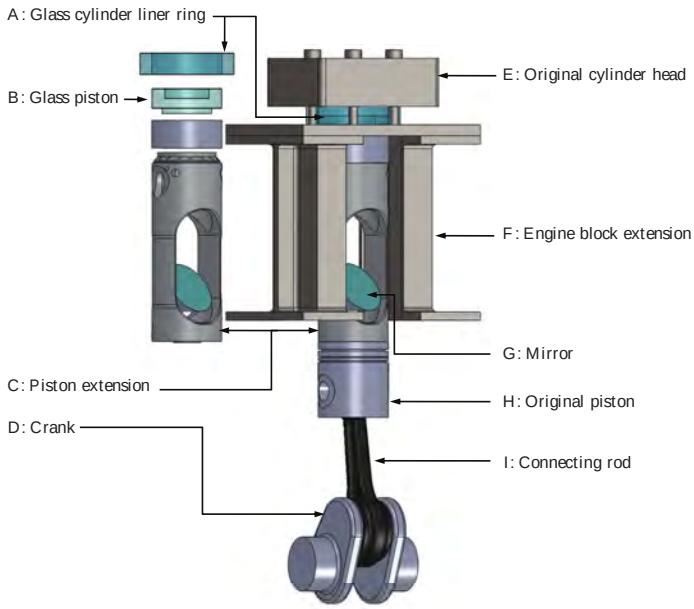

Figure A.1: Example of optical engine of Bowditch design. Reproduced from [8]

it consists of a hollow piston extension where a transparent piston is mounted at the top. This extension is coupled to the original piston, located inside the engine block. This layout allows a 45° mirror to be mounted inside the hollow extension, gaining access to a view from beneath the combustion chamber. This solution implies that the cylinder head must be separated from the cylinder block and a new optical piston liner is placed to complete the assembly. An example of an Bowditch design optical engine is depicted in Figure A.1. This technique has been applied to light and heavy-duty research engines. To best of the author's knowledge, the optical engine here described is unique due to the size of the optical piston (20 cm bore diameter).

A.2 Design

In this case, the single-cylinder metal Wärtsilä 20DF research engine has been converted to optical configuration using a Bowditch design. The design of this optical engine has been mainly done by Wärtsilä. Optical access to the combustion chamber is provided from the sides via transparent windows and from beneath through a transparent piston.

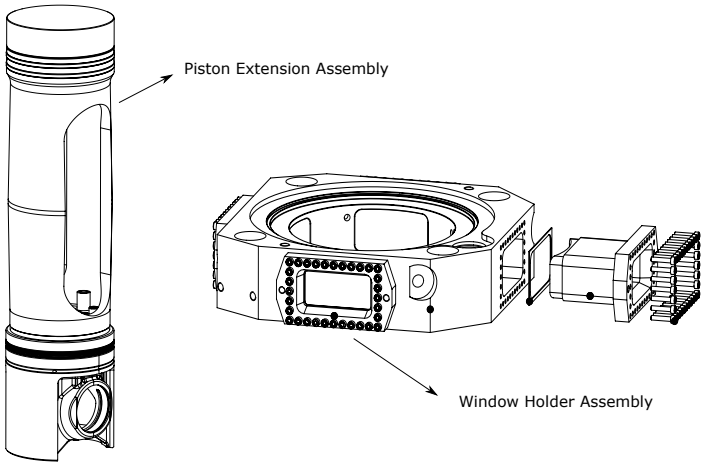

Figure A.2: Wärtsilä 20DF optical piston and window assemblies

The same cylinder as in metal configuration has been maintained as the firing cylinder, while the other 5 pistons have been replaced by new pistons with tungsten weights for balancing the extra mass of the piston extension assembly. Both DI and PFI injection systems and the EHVA system have remained unaltered from the metal engine version. Drawings of the optical piston and window holder assemblies are presented in Figure A.2. The optical piston has the same diameter as the original metal piston and it is made of one single piece of quartz. The length of the optical piston assembly is roughly 73 cm.

Unfortunately, excessive amounts of oil on the mirror and base of the optical piston prevented the author from performing quality experimental campaigns on this setup. A re-design of some components have been performed by Wärtsilä and new tests are planned.

A.3 Preliminary Tests

In this case, a Photron Fascam SA-X2 high speed CMOS camera was used to acquire high speed images from the natural chemiluminescence of the combustion process. This camera was controlled via triggering signals every 0.2 CAD from the test cell control system, which results in a 24 kHz frame rate at 800 rpm engine speed. The parameter *bitshift* is specified for each figure and it can be understood as an indicator of how much the intensity of the images is artificially increased.

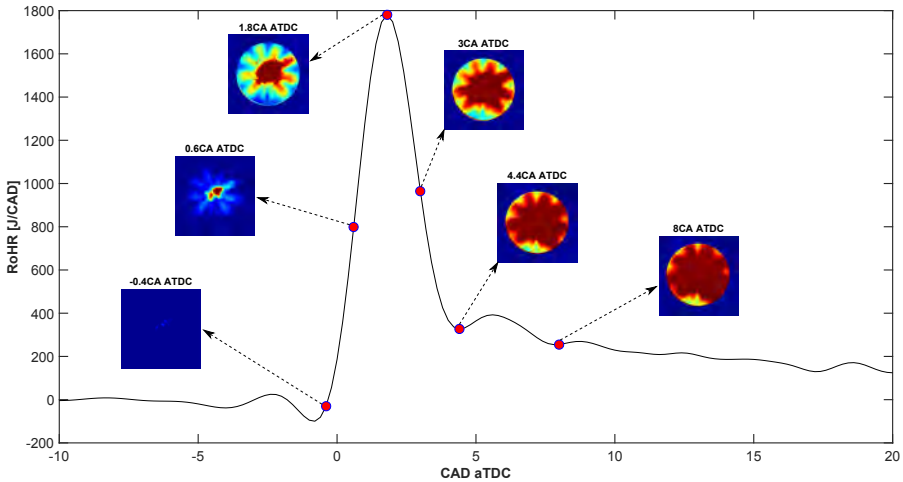

Figure A.3: Example of mean RoHR and mean optical images from raw natural luminosity under CDF conditions (50 fired cycles , *bitshift=2*). Conditions: Pilot timing: 10 CAD BTDC, Load: 7 bar IMEP*g*, λ_{gas}=2.28

Several different test runs were performed in this setup but just few of them provided data with sufficient image quality. Figure A.3 includes an example of averaged combustion images coupled to the rate of heat release under CDF conditions. Although this is only a small part of the planned tests, it already provided insights about the *real* combustion process.

As observed in Figure A.3, the ignition location appears rather towards the center of the combustion chamber and the flame propagates from this point towards the areas where diesel fuel is dispersed. In this case, 9 flame fronts are generated following the pilot fuel path. The process can be separated into the high intensity phase, corresponding to the premixed peak associated with pilot combustion, and the low intensity phase associated with the last stage of the combustion process.

Firstly, detailed focus on the first part of the rate of heat release is presented in Figure A.4, based on combustion images from a representative combustion cycle. The crank angles presented in Figure A.4 range from SOC to the timing of maximum RoHR. The color intensity of the images has been adjusted for improving the detection of SOC according to the analysis of the heat release rate. The first high color intensity zone detected is located near the center of the combustion chamber, on three different fuel clouds. Different ignition locations appear sequentially after the first ignition in all those areas where pilot

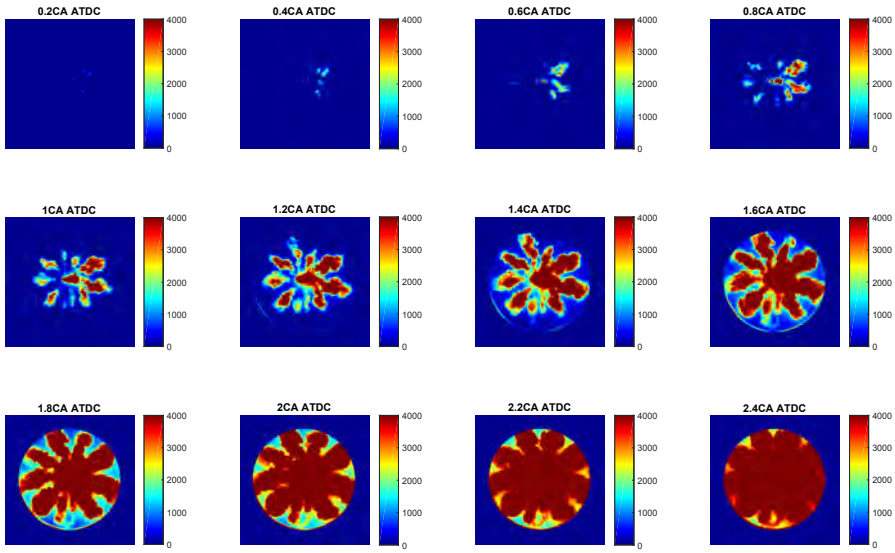

Figure A.4: Example of optical images from raw natural luminosity under CDF conditions (single cycle, *bitshift=4*). Conditions: Pilot timing: 10 CAD BTDC, Load: 7 bar IMEP$_g$, λ_{gas}=2.28

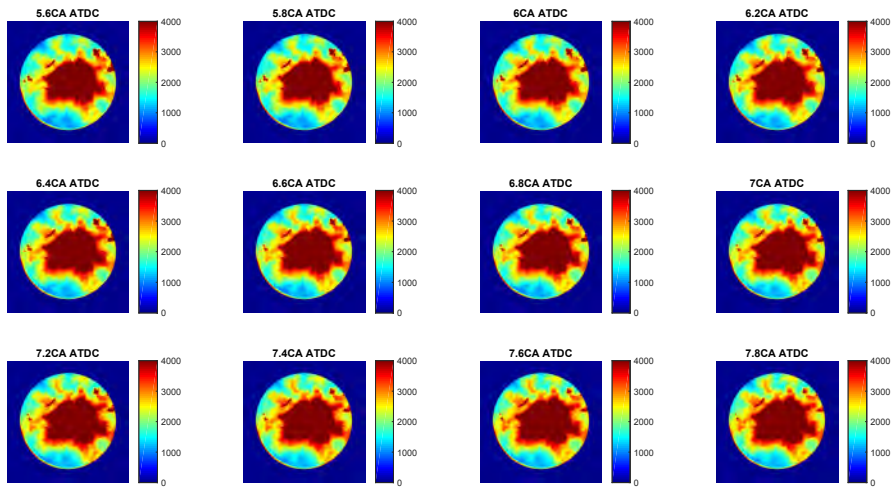

Figure A.5: Example of optical images from raw natural luminosity under CDF conditions (single cycle, *bitshift=1*). Conditions: Pilot timing: 10 CAD BTDC, Load: 7 bar IMEP$_g$, λ_{gas}=2.28

fuel is dispersed. After that, evidence of on-going combustion is detected along those areas with pilot fuel presence. This occurs from the center of the combustion chamber towards the periphery following the pilot fuel cloud. As combustion continues, the area covered by high color intensity around the pilot fuel clouds is enlarged. This might be linked to combustion of the natural gas around the pilot fuel zones.

During the second part of the premixed peak, combustion progresses at a lower rate around the pilot fuel cloud, as depicted in Figure A.3. An example of cycle images of this phase is presented in Figure A.5. After the premixed peak, the areas with the lowest image intensity are located in the periphery of the combustion chamber and between the pilot fuel areas. As observed in Figure A.5, the image intensity does not vary substantially from 5.6 to 7.8 CAD aTDC. This could be linked to the lower reaction rates associated with lean natural gas combustion after all diesel fuel has been oxidized. This also suggests that natural gas molecules not burnt during the highly premixed stage of the combustion process are unlikely to be oxidized later during the expansion stroke, which could explain the high TUHC emissions associated with this combustion mode.

Another aspect that has been identified during this preliminary test is the potential impact of injector dribble on the ignition process. It is possible to observe in Figure A.4 that high luminosity is detected

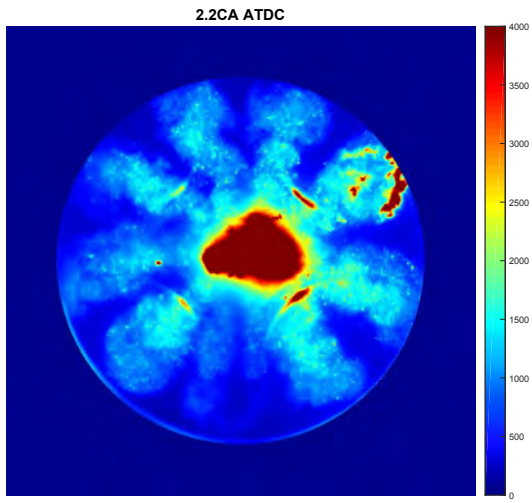

Figure A.6: Single optical image from raw natural luminosity under CDF conditions (single cycle, *bitshift=1*). Conditions: Pilot timing: 10 CAD BTDC, Load: 7 bar IMEP$_g$, λ_{gas}=2.28

in the very center of the combustion chamber. If image intensity is not artificially increased via the post-processing of the raw images, the brightest area is in fact located in the center, as observed in Figure A.6. This suggests a possible impact of injector dribble on the ignition process under CDF combustion. If the pilot fuel is burnt in premixed mode and excessive injector dribble exists, it might be possible that highly reactive pilot fuel located in the center triggers the onset of combustion and represents a large fraction of the energy released. This fact should be further explored in future studies.

The previous statements are just hypothesized from the initial commissioning of the optical setup. As mentioned in Chapter 8, further test will be performed for better understanding of the ignition process in dual fuel combustion processes.

BIBLIOGRAPHY

[1] US Energy Information Administration. International Energy Outlook 2017. Report. September 2017.

[2] International Energy Agency. CO_2 Emissions from Fuel Combustion 2017. Report. 2017.

[3] McKinsey and Company. Electric Vehicles in Europe: Gearing up for a new phase?. Technical report. 2014.

[4] Robert Edwards, Heinz Hass, Jean-Francois Larive, Laura Lonza, Heiko Mass, and David Rickeard. JEC Well-to-Wheels Analysis. European Commission. Report. 2014.

[5] International Group of Liquefied Natural Gas Importers. The LNG Industry. Annual report. 2017.

[6] US Environmental Protection Agency. Methane and Nitrous Oxide Emissions from Natural Sources. Report. 2012.

[7] Demirbas Ayhan. Fuel properties of hydrogen, liquefied petroleum gas (LPG), and compressed natural gas (CNG) for transportation. *Energy Sources*, 24(7):601–610, 2002.

[8] Ulf Aronsson. *Processes in Optical Diesel Engines - Emissions Formation and Heat Release*. PhD thesis, Lund University, 2011.

[9] John E. Dec. A conceptual model of DI diesel combustion based on laser-sheet imaging. In *International Congress and Exposition*, number 970873. SAE International, feb 1997.

[10] Takeyuki Kamimoto and Myurng-Hoan Bae. High combustion temperature for the reduction of particulate in diesel engines. In *SAE Technical Paper*, number 880423. SAE International, feb 1988.

[11] Tie Li and Hideyuki Ogawa. Analysis of the trade-off between soot and nitrogen oxides in diesel-like combustion by chemical kinetic calculation. *SAE Int. J. Engines*, 5(2):94–101, aug 2011.

[12] Gary D. Neely, Shizuo Sasaki, Yiqun Huang, Jeffrey A. Leet, and Daniel W. Stewart. New diesel emission control strategy to meet US Tier 2 emissions regulations. In *SAE 2005 World Congress and Exhibition*, number 2005-01-1091. SAE International, apr 2005.

[13] Simon K. Chen and N. John Beck. Gas engine combustion principles and applications. In *SAE Technical Paper*, number 2001-01-2489. SAE International, aug 2001.

[14] Patrik Einewall, Per Tunestål, and Bengt Johansson. Lean burn natural gas operation vs. stoichiometric operation with EGR and a three way catalyst. In *SAE 2005 World Congress and Exhibition*, number 2005-01-0250. SAE International, apr 2005.

[15] R. L. Evans and J. Blaszczyk. A comparative study of the performance and exhaust emissions of a spark ignition engine fuelled by natural gas and gasoline. *Proceedings of the Institution of Mechanical Engineers, Part D: Journal of Automobile Engineering*, 211(1):39–47, 1997.

[16] M. Davy, R.L. Evans, and A. Mezo. The ultra lean burn partially stratified charge natural gas engine. In *9th International Conference on Engines and Vehicles*. Consiglio Nazionale delle Ricerche, sep 2009.

[17] A Das and H C Watson. Development of a natural gas spark ignition engine for optimum performance. *Proceedings of the Institution of Mechanical Engineers, Part D: Journal of Automobile Engineering*, 211(5):361–378, 1997.

[18] A. Ramesh, O. Le Corre, and M. Tazerout. Experimental investigation on cycle by cycle variations in a natural gas fueled spark ignition engine. In *SIAT 2001*, number 2001-28-0021. The Automotive Research Association of India, nov 2001.

[19] J.D. Dale, M.D. Checkel, and P.R. Smy. Application of high energy ignition systems to engines. *Progress in Energy and Combustion Science*, 23(5-6):379–398, 1997.

[20] Masaki Tsunekane, Takayuki Inohara, Kenji Kanehara, and Takunori Taira. Micro-solid-state laser for ignition of automobile engines. In *Advances in Solid State Lasers Development and Applications*, chapter 10. InTech, Rijeka, 2010.

[21] Tran X Phuoc. Single-point versus multi-point laser ignition: experimental measurements of combustion times and pressures. *Combustion and Flame*, 122(4):508–510, 2000.

[22] P. D. Ronney. Laser versus conventional ignition of flames. *Optical Engineering*, 33, feb 1994.

[23] J. R. Wilson F. J. Weinberg. A preliminary investigation of the use of focused laser beams for minimum ignition energy studies. *Proceedings of the Royal Society of London A: Mathematical, Physical and Engineering Sciences*, 321(1544):41–52, 1971.

[24] Ashish Shah, Per Tunestal, and Bengt Johansson. Effect of relative mixture strength on performance of divided chamber 'avalanche activated combustion' ignition technique in a heavy duty natural gas engine. In *SAE Technical Paper*, number 2014-01-1327. SAE International, apr 2014.

[25] Ashish Shah. *Improving the Efficiency of Gas Engines using Pre-chamber Ignition.* PhD thesis, Lund University, 2015.

[26] William P. Attard, Neil Fraser, Patrick Parsons, and Elisa Toulson. A turbulent jet ignition pre-chamber combustion system for large fuel economy improvements in a modern vehicle powertrain. *SAE International Journal of Engines*, 3(2):20–37, may 2010.

[27] Philip Zoldak, Joel John Joseph, William Shelley, Jaclyn Johnson, and Jeffrey Naber. Characterization of partially stratified direct injection of natural gas for spark-ignited engines. In *SAE 2015 World Congress and Exhibition*, number 2015-01-0937. SAE International, apr 2015.

[28] James Sevik, Michael Pamminger, Thomas Wallner, Riccardo Scarcelli, Ronald Reese, Asim Iqbal, Brad Boyer, Steven Wooldridge, Carrie Hall, and Scott Miers. Performance, efficiency

and emissions assessment of natural gas direct injection compared to gasoline and natural gas port-fuel injection in an automotive engine. *SAE International Journal of Engines*, 9(2):1130–1142, apr 2016.

[29] R. Diesel. Method of igniting and regulating combustion for internal-combustion engines., April 30 1901. US Patent 673,160.

[30] D.B. Lata and Ashok Misra. Analysis of ignition delay period of a dual fuel diesel engine with hydrogen and LPG as secondary fuels. *International Journal of Hydrogen Energy*, 36(5):3746–3756, 2011.

[31] Antonio P. Carlucci, Domenico Laforgia, Roberto Saracino, and Giuseppe Toto. Combustion and emissions control in diesel–methane dual fuel engines: The effects of methane supply method combined with variable in-cylinder charge bulk motion. *Energy Conversion and Management*, 52(8):3004–3017, 2011.

[32] Erwan Salaun, Julien Apeloig, Frédéric Grisch, Charles-Edouard Yvonnet, Baptiste Nicolas, and Frederic Dionnet. Optical investigation of ignition timing and equivalence ratio in dual-fuel CNG/diesel combustion. In *SAE Technical Paper*, number 2016-01-0772. SAE International, apr 2016.

[33] O. Badr, G.A. Karim, and B. Liu. An examination of the flame spread limits in a dual fuel engine. *Applied Thermal Engineering*, 19(10):1071–1080, 1999.

[34] Z.Liu and G.A.Karim. Knock in dual fuel engines. In *International Syluposium COMODIA 94*. COMODIA, jul 1994.

[35] G.A. Karim. *Dual-Fuel Diesel Engines*. CRC Press, 2015.

[36] Marc C. Besch, Joshua Israel, Arvind Thiruvengadam, Hemanth Kappanna, and Daniel Carder. Emissions characterization from different technology heavy-duty engines retrofitted for CNG/diesel dual-fuel operation. *SAE International Journal of Engines*, 8(3):1342–1358, apr 2015.

[37] Fredrik Königsson, Johannes Kuyper, Per Stalhammar, and Hans-Erik Angstrom. The influence of crevices on hydrocarbon emissions from a diesel-methane dual fuel engine. *SAE Int. J. Engines*, 6:751–765, apr 2013.

[38] Radu Florea, Gary D. Neely, Zainal Abidin, and Jason Miwa. Efficiency and emissions characteristics of partially premixed dual-fuel combustion by co-direct injection of NG and diesel fuel (DI2). In *SAE Technical Paper*, number 2016-01-0779. SAE International, apr 2016.

[39] Jennifer Wheeler, Joshua Stein, and Gary Hunter. Effects of charge motion, compression ratio, and dilution on a medium duty natural gas single cylinder research engine. *SAE International Journal of Engines*, 7(4):1650–1664, sep 2014.

[40] Gary D. Neely, Radu Florea, Jason Miwa, and Zainal Abidin. Efficiency and emissions characteristics of partially premixed dual-fuel combustion by co-direct injection of NG and diesel fuel (DI2) - part 2. In *WCX™ 17: SAE World Congress Experience*, number 2017-01-0766. SAE International, mar 2017.

[41] Takuji Ishiyama, Jeongho Kang, Yutaka Ozawa, and Takahiro Sako. Improvement of performance and reduction of exhaust emissions by pilot-fuel-injection control in a lean-burning natural-gas dual-fuel engine. *SAE Int. J. Fuels Lubr.*, 5:243–253, aug 2011.

[42] Tanet Aroonsrisopon, Mongkol Salad, Ekathai Wirojsakunchai, Krisada Wannatong, Somchai Siangsanorh, and Nirod Akarapanjavit. Injection strategies for operational improvement of diesel dual fuel engines under low load conditions. In *SAE Technical Paper*, number 2009-01-1855. SAE International, jun 2009.

[43] Bo Yang, Long Wang, Le Ning, and Ke Zeng. Effects of pilot injection timing on the combustion noise and particle emissions of a diesel/natural gas dual-fuel engine at low load. *Applied Thermal Engineering*, 102:822–828, 2016.

[44] Zhongshu Wang, Zhongxiang Zhao, Dan Wang, Manzhi Tan, Yongqiang Han, Zhongchang Liu, and Huili Dou. Impact of pilot diesel ignition mode on combustion and emissions characteristics of a diesel/natural gas dual fuel heavy-duty engine. *Fuel*, 167:248–256, 2016.

[45] Sebastian Zirngibl and Georg Wachtmeister. Extensive investigation of a common rail diesel injector regarding injection characteristics and the resulting influences on the dual fuel pilot

injection combustion process. In *SAE 2016 World Congress and Exhibition*, number 2016-01-0780. SAE International, apr 2016.

[46] Zhiqiang Lin and Wanhua Su. A study on the determination of the amount of pilot injection and rich and lean boundaries of the pre-mixed CNG/air mixture for a CNG/diesel dual-fuel engine. In *SAE 2003 World Congress and Exhibition*, number 2003-01-0765. SAE International, mar 2003.

[47] Fredrik Königsson, Per Stalhammar, and Hans-Erik Angstrom. Controlling the injector tip temperature in a diesel dual fuel engine. In *SAE 2012 World Congress and Exhibition*, number 2012-01-0826. SAE International, apr 2012.

[48] Jeremy Rochussen, Jeff Yeo, and Patrick Kirchen. Effect of fueling control parameters on combustion and emissions characteristics of diesel-ignited methane dual-fuel combustion. In *SAE 2016 World Congress and Exhibition*, number 2016-01-0792. SAE International, apr 2016.

[49] Nicolas Dronniou, Julian Kashdan, Bertrand Lecointe, Kyle Sauve, and Dominique Soleri. Optical investigation of dual-fuel CNG/diesel combustion strategies to reduce CO2 emissions. *SAE International Journal of Engines*, 7(2):873–887, apr 2014.

[50] P. Stalhammer, L. Erlandsson, K. Willner, and S. Johannesson. Assessment of Dual Fuel Technology. Report 233. SGC. June 2011.

[51] Sage L. Kokjohn, Reed M. Hanson, Derek A. Splitter, and Rolf D. Reitz. Experiments and modeling of dual-fuel HCCI and PCCI combustion using in-cylinder fuel blending. *SAE International Journal of Engines*, 2(2):24–39, nov 2009.

[52] Kazuhisa Inagaki, Takayuki Fuyuto, Kazuaki Nishikawa, Kiyomi Nakakita, and Ichiro Sakata. Dual-fuel PCI combustion controlled by in-cylinder stratification of ignitability. In *SAE 2006 World Congress and Exhibition*, number 2006-01-0028. SAE International, apr 2006.

[53] Derek E. Nieman, Adam B. Dempsey, and Rolf D. Reitz. Heavy-duty RCCI operation using natural gas and diesel. *SAE International Journal of Engines*, 5(2):270–285, apr 2012.

[54] Mufaddel Dahodwala, Satyum Joshi, Erik W. Koehler, and Michael Franke. Investigation of diesel and CNG combustion in a dual fuel regime and as an enabler to achieve RCCI combustion. In *SAE 2014 World Congress and Exhibition*, number 2014-01-1308. SAE International, apr 2014.

[55] Erik Doosje, Frank Willems, and Rik Baert. Experimental demonstration of rcci in heavy-duty engines using diesel and natural gas. In *SAE 2014 World Congress and Exhibition*, number 2014-01-1308. SAE International, apr 2014.

[56] Emission standards. `https://www.dieselnet.com/`. Accessed: February 2018.

[57] International Maritime Organization. Studies on the feasibility and use of LNG as a fuel for shipping. Report. 2016.

[58] Regulation (EC) No 595/2009 of the European Parliament. *OJ*, L 188:1–13, 2009-07-18.

[59] Commission regulation (EU) No 582/2011 of 25 may 2011 implementing and amending regulation (EC) no 595/2009 of the European Parliament. *OJ*, L 167:1–168, 2011-06-25.

[60] Commission regulation (EU) No 133/2014 of 31 january 2014 amending directive 2007/46/ec, regulation (EC) no 595/2009 and commission regulation (EU) no 582/2011. *OJ*, L 47:1–57, 2014-02-18.

[61] Input for a revision of the THC and methane (CH_4) emission limits for vehicles equipped with engines running on natural gas euro 6 light duty vehicles. *GRPE Informal Group on Gaseous Fuelled Vehicles*, Discussion draft v.12, 2012-05-08.

[62] Davide Ferri, Martin Elsener, and Oliver Kröcher. Methane oxidation over a honeycomb Pd-only three-way catalyst under static and periodic operation. *Applied Catalysis B: Environmental*, 220:67–77, 2018.

[63] Yuanzhou Xi, Nathan Ottinger, and Z. Gerald Liu. Development of a lab reactor system for the evaluation of aftertreatment catalysts for stoichiometric natural gas engines. In *WCX™ 17: SAE World Congress Experience*, number 2017-01-0999. SAE International, mar 2017.

[64] Nathan Ottinger, Rebecca Veele, Yuanzhou Xi, and Z. Gerald Liu. Desulfation of Pd-based oxidation catalysts for lean-burn natural gas and dual-fuel applications. *SAE International Journal of Engines*, 8(4):1472–1477, apr 2015.

[65] Göran Hellén, Lars Ola Liavåg, and Antonino Di Miceli. Development of exhaust gas aftertreatment systems applied to modern high efficiency four-stroke medium-speed engines. In *28th CIMAC World Congress 2016*, June 2016.

[66] Donnie J. Worth, Marc E. J. Stettler, Paul Dickinson, Kieran Hegarty, and Adam M. Boies. Characterization and evaluation of methane oxidation catalysts for dual-fuel diesel and natural gas engines. *Emission Control Science and Technology*, 2(4):204–214, Oct 2016.

[67] Mika Herranen, Kalevi Huhtala, Matti Vilenius, and Gösta Liljenfeldt. The electro-hydraulic valve actuation EHVA for medium speed diesel engines - development steps with simulations and measurements. In *SAE Technical Paper*, number 2007-01-1289. SAE International, apr 2007.

[68] David Sancho Casarrubios. Modelling and CNG distribution study of a natural gas-diesel dual fuel engine, 2015. MSc Thesis.

[69] Kangyoon Lee, Minsu Kwon, Myoungho Sunwoo, and Maru Yoon. An in-cylinder pressure referencing method based on a variable polytropic coefficient. In *Asia Pacific Automotive Engineering Conference*, number 2007-01-3535. SAE International, aug 2007.

[70] Richard Davis and Gary Patterson. Cylinder pressure data quality checks and procedures to maximize data accuracy. In *SAE 2006 World Congress and Exhibition*, number 2006-01-1346. SAE International, apr 2006.

[71] Per Tunestål. Model based TDC offset estimation from motored cylinder pressure data. *IFAC Proceedings Volumes*, 42(26):241 – 247, 2009. 2nd IFAC Workshop on Engine and Powertrain Control, Simulation and Modeling.

[72] Marcus Klein and Lars Eriksson. A specific heat ratio model for single-zone heat release models. In *SAE 2004 World Congress and Exhibition*, number 2004-01-1464. SAE International, mar 2004.

[73] Draper C.S. Pressure waves accompanying detonation in the internal combustion engine. *Journal of the Aeronautical Sciences*, 5(6):219–226, 1938.

[74] Jesús Benajes, Santiago Molina, Antonio García, Javier Monsalve-Serrano, and Russell Durrett. Performance and engine-out emissions evaluation of the double injection strategy applied to the gasoline partially premixed compression ignition spark assisted combustion concept. *Applied Energy*, 134:90–101, 2014.

[75] G. Brecq and O. Le Corre. Modeling of in-cylinder pressure oscillations under knocking conditions: Introduction to pressure envelope curve. In *SAE Technical Paper*, number 2005-01-1126. SAE International, apr 2005.

[76] J. A. Eng. Characterization of pressure waves in HCCI combustion. In *SAE Technical Paper*, number 2002-01-2859. SAE International, oct 2002.

[77] Jeff Koncsol and Julia Buckland. Comparison of methodologies for chemical measurement of air to fuel ratio at very lean conditions. In *SAE 2003 World Congress and Exhibition*, number 2003-01-0566. SAE International, mar 2003.

[78] Bengt Johansson, Öivind Andersson, Per Tunestal, and Martin Tuner. *Combustion engines. Vol. 1.* Department of Energy Sciences, Lund University, Lund, 2014.

[79] J.M. Desantes, J.V. Pastor, J.M. García-Oliver, and J.M. Pastor. A 1D model for the description of mixing-controlled reacting diesel sprays. *Combustion and Flame*, 156(1):234–249, 2009.

[80] José V. Pastor, J. Javier López, José M. García, and José M. Pastor. A 1D model for the description of mixing-controlled inert diesel sprays. *Fuel*, 87(13–14):2871–2885, 2008.

[81] Jose V. Pastor, Jose M. Garcia-Oliver, Jose M. Pastor, and W. Vera-Tudela. One-dimensional diesel spray modeling of multicomponent fuels. *Atomization and Sprays*, 25(6):485–517, 2015.

[82] Fredrik Königsson, Henrik Dembinski, and Hans-Erik Angstrom. The influence of in-cylinder flows on emissions and heat transfer from methane-diesel dual fuel combustion. *SAE International Journal of Engines*, 6(4):1877–1887, oct 2013.

[83] Paul Miles. The history and evolution of optically accessible research engines and their impact on our understanding of engine combustion. In *ASME 2014 Internal Combustion Engine Division Fall Technical Conference, ICEF 2014*, volume 2, 2014.

[84] Fred Bowditch. A new tool for combustion research a quartz piston engine. In *SAE Technical Paper*, number 610002. SAE International, jan 1961.

SUMMARY OF PAPERS

Paper I

Experimental Investigation on CNG-Diesel Combustion Modes under Highly Diluted Conditions on a Light Duty Diesel Engine with Focus on Injection Strategy

P. García, P. Tunestål

SAE Int. J. Engines 8(5):2177-2187, 2015, 2015-24-2439

This paper presents an initial study of how combustion characteristics in a multi-cylinder dual fuel methane-diesel light duty engine are altered by the injection control strategy adopted (CDF, PPCI and RCCI) on different high substitution ratio operating points under highly diluted conditions at low and part load operation. This investigation does not aim for an optimization of the injection parameters in dual fuel combustion mode, but it aims to point out and understand the most relevant characteristics and behaviors of a light duty dual fuel CNG-Diesel engine operating under high substitution ratios.

I designed and performed the experiments, post-processed the data and wrote the article together with Per Tunestål. I had the main responsibility for writing the paper.

Paper II

Effects of Intake Manifold Conditions on Dual Fuel CNG-Diesel Combustion in a Light Duty Diesel Engine Operated at Low Loads

P. García, P. Tunestål

SAE Technical Paper 2016-01-0805, 2016

In this paper, an experimental investigation of the effects of different intake manifold conditions on the pilot-ignited dual fuel combustion process is presented, based on performance and emissions of a light duty diesel engine rebuilt for dual-fuel operation operated at low loads and lean conditions. The main goal is to understand how intake temperature and pressure affects the combustion process and to identify possible control strategies for those parameters over the low load range of operation.

I designed and performed the experiments, post-processed the data and wrote the article together with Per Tunestål. I had the main responsibility for writing the paper.

Paper III

Analysis of Dual-Fuel CNG-Diesel Combustion Modes Towards High Efficiency and Low Emissions at Part Load

P. García, P. Tunestål

Proc. 36th FISITA World Automotive Congress, 2016, Busan, South Korea

Conventional dual fuel (CDF) pilot ignition and reactivity controlled compression ignition (RCCI) combustion are evaluated and compared based on emissions, heat transfer and efficiency under part load conditions. The goal of the study is to analyze how pilot fuel dilution and pilot fuel mass minimization strategies alter the combustion process in dual fuel operation with a focus on NO_x emissions. For that reason, the impact of different EGR levels is also analyzed.

I designed and performed the experiments, post-processed the data and wrote the article together with Per Tunestål. I had the main responsibility for writing the paper.

Paper IV

Impact of Diesel Pilot Distribution on the Ignition Process of a Dual Fuel Medium Speed Marine Engine

P. García, P. Tunestål, J. Monsalve-Serrano, A. García, J. Hyvönen

Energy Conversion and Management, 149:192-205, 2017

An experimental study is carried out in an 8.8 l dual fuel single cylinder Wärtsilä 20DF engine in order to evaluate different diesel equivalence ratio distributions in the combustion chamber and to get a deeper insight into the interaction between the high reactivity (diesel) and the low reactivity (natural gas) fuels during the ignition process. Engine testing is complemented with diesel spray pattern simulations for a better understanding of local combustion conditions.

I designed and performed the metal engine experiments. Simulations of diesel sprays were performed by Javier Monsalve-Serrano and Antonio García. I post-processed the experimental data. I post-processed the simulation data together with Javier Monsalve-Serrano. I wrote the article together with Per Tunestål, Javier Monsalve-Serrano, Antonio García and Jari Hyvönen. I had the main responsibility for writing the paper.